Impacts of Collateral Effects and Spatial Heterogeneity on the Evolution of Resistance in Enterococcus

by

Anh Huynh

A dissertation submitted in partial fulfillment
of the requirements for the degree of
Doctor of Philosophy
(Biophysics)
in the University of Michigan
2023

Doctoral Committee:

Associate Professor Kevin Wood, Chair
Professor Jinsang Kim
Associate Professor Robert Woods
Associate Professor Qiong Yang

Anh Huynh
anhhuynh@umich.edu
ORCID iD: 0000-0001-8891-4234

ACKNOWLEDGMENTS

To all the people who contributed to, and helped me with this thesis, I will never be able to properly express my gratitude, never say thank you enough. But, to summarize a thousand appreciation notes, I'm deeply grateful for your mentorship, friendship, encouragement, guidance, and patience that you have given me. I want you to know that the positive impact you've had on my life is immeasurable. You are amazing and phenomenal!

To Benjamin Nash, I feel very fortunate to have met you. I'll never forget how you sat with me during my first class of college to calm my fears. (As I felt like an outsider that somehow snuck my way into a world I didn't belong in.) You have shown me how to embark on a journey that led to many incredible and fortunate experiences, far beyond what I could have ever imagined. Your support, help, and belief in me over the years has had a tremendous positive impact. I am so grateful for your friendship!

To Dr. Matthew Ferguson at Boise State University, thank you for giving me my first experience doing research. It was an invaluable experience, given the excellent training you provided with patience and thoughtfulness. I am incredibly thankful for the opportunity to work in your lab and all the guidance and support you gave me.

To the bestest and most amazing mentor at the University of Michigan, Dr. Kevin Wood, thank you for making the impossible possible. This thesis exists because of you! From day one as your student, whether in your class or working in your lab, you've shown that you deeply care about your students' needs and well-being. Thank you for allowing me to be myself, even when I'm at my worst, for offering no judgment, only kindness, genuineness, compassion and support. Perhaps everyone knows how challenging it is to push a wheel that won't turn, or helping someone who is struggling with doubts and uncertainties. You've constantly refused to give up on me, even when I lost my "wheels" and I was difficult to deal with. You have consistently shown empathy, understanding, optimism, and patience throughout our research. Thank you for being you, for helping me every step of the way, for encouraging me, and for creating this chapter of my life full of wonderful lessons about science and life. Thank you for accepting me into your lab. Not only you are an amazing and incredible scientist, but also an exceptional and insightful educator. Thank you for everything. I'm so lucky and eternally grateful to be your student.

I am also grateful to Dr. Qiong Yang, Dr. Robert Woods, and professor Jinsang Kim for serving on my committee. I deeply appreciate your support, understanding, advice, and wisdom. To the

past and present members of the Wood Lab, thank you for welcoming me into the lab and for always taking the time to listen and help me. To my awesome collaborators: Anupama Sharma, Max De Jong and Jeff Maltas, I feel very lucky to have crossed paths with you, to have had the opportunity to learn from you, and to be inspired by you.

Thank you to Sarah Veatch for being an awesome cheerleader, thank you for your encouragement and the care you have for your students. Thank you to Sara Grosky for being the best administrator and coordinator! I deeply appreciate all your help!

To my family, thank you for loving me unconditionally and always caring about my happiness. To my late, beloved dad and brother! I am always thinking about you!

Lastly, I am grateful for being another example of how, with the right person, even in the wrong circumstance or at the wrong time, even if one is unequipped or feels like an outsider, with unwavering support and guidance, one is still able to achieve great things: such as receiving a degree from a prestigious institution. This is beyond my wildest dreams. Thank you all and thanks to the Biophysics department and the staff at the University of Michigan for this surreal experience.

TABLE OF CONTENTS

LIST OF FIGURES

FIGURE

LIST OF TABLES

TABLE

ABSTRACT

Antibiotics are used to treat bacterial infections, as they can kill or inhibit the growth of bacterial populations. However, the misuse of antibiotics may also promote the evolution of drug resistance, reducing the efficacy of many treatments. The rapid rise of antibiotic resistance continues to outpace the development of new drugs and is becoming one of the most significant global health challenges. The mechanisms of antibiotic resistance are increasingly understood at the molecular level. But understanding how the dynamics of bacterial communities shape the emergence of resistance in microbial populations is an ongoing challenge. In this thesis, we combine quantitative experiments on bacteria with simple mathematical models to investigate how resistance to antibiotic emerges in communities of *E. faecalis*, a Gram positive bacterial species and opportunistic human pathogen. Our focus is not on identifying new mechanisms of drug resistance; instead, our goal is to gain a deeper understanding of how mutants harboring known resistance mechanisms rise to dominance in microbial populations characterized by temporal and spatial heterogeneity.

This thesis can be divided into two primary themes: time dependent effects of collateral evolution (Part I) and effects of multi-strain interactions in heterogeneous communities (Part II). Collateral effects refer to an increase (collateral resistance) or decrease (collateral sensitivity) in resistance to one drug that occurs during adaptation to a second drug. In Part I of this work, we use laboratory evolution experiments to investigate how collateral sensitivity profiles change over time as *E. faecalis* undergoes adaptation to a diverse library of antibiotics. We describe a rich collection of dynamics that exhibit global trends–for example, collateral resistance often arises in early stages of adaptation, while sensitivity tends to increase in later stages–but also reveal a number of drug- and population-specific dynamics that we characterize using a combination of genome sequencing and phenotype measurements.

In Part II, we investigate how interactions between cells and the surrounding spatial environment influence the evolution of resistance. Our work focuses on two aspects of these interactions: the role of 1) spatial heterogeneity and 2) inter-cellular competition in modulating the evolution of resistance. We investigate these issues in laboratory populations using customized, computer-controlled bioreactors, which allow us to experimentally simulate both migration dynamics between spatially distinct populations and adaptive antibiotic treatments that depend on cell density. Our findings reveal a complex interplay between migration, spatial heterogeneity, and population

density, demonstrating how different features of the environment can accelerate, or impede, the evolution of resistance.

As a whole, this thesis highlights both the simplicity and complexity of evolutionary dynamics leading to resistance. On one hand, Part I highlights how collateral effects and evolution can be remarkably diverse even in simple laboratory settings. Part II underscores the important role that spatial heterogeneity can play in modulating resistance, yet also highlights how initially counter-intuitive dynamics can–at least sometimes–be understood with simple mathematical models. We hope these results motivate continued explorations of resistance evolution, both in the lab and the clinic.

CHAPTER 1

Introduction

The discovery of antibiotics has tremendously transformed the field of medicine and improved public health [2]. However, multiple factors–including the overuse and misuse of antibiotics–have promoted the rapid spread of antibiotic resistance ([3]). Unfortunately, the development of new drugs is an arduous and time-consuming endeavor, and the emergence of resistance appears to be outpacing the advent of new drugs, making antibiotic resistance an increasing threat to global health [4, 5, 6, 7, 8, 9, 10].

Because of the slow pace of drug development, there has been renewed focus on strategies for using currently available drugs to slow down the emergence of resistance. Doing so requires an understanding of resistance on multiple levels–from molecular and genetic to the epidemiological and ecological scales. With the increasing recognition that bacterial communities play an integral in human health and physiology–not merely for infections, but also as part of the natural ecosystems in human hosts–there is continued need to develop a quantitative and predictive understanding of microbial dynamics. Rapid breakthroughs in genetics, molecular biology, and biophysics have led to a detailed, if still incomplete, picture of antibiotic resistance at the molecular level. However, much less is known about how those molecular details give rise to population behavior that shapes the survival, adaptation, and potential extinction of microbial communities. Over the past decade, an increasing body of work suggests that antibiotic resistance is a community phenomena–one that depends not only on the behavior of single cells, but on how those cells interact in larger communities [11, 12, 13].

As traditional maximum tolerable dose treatments fail at increasing rates, evolution-based treatments have emerged as a promising method to prolong the efficacy of current drugs or even reverse resistance. Evolution-based treatments are designed to minimize drug-resistance by leveraging common, but sometimes neglected, features of population dynamics–for example, competitive interactions between different cells. These strategies include drug cycling [14, 15, 16, 17], harnessing spatial dynamics [18, 19, 20, 21], cooperation [22, 23, 24, 25], adaptive therapy [26, 27, 28], and judicious use of drug combinations [29, 30, 31, 32, 33, 34, 35, 36]. More recently there has been a

growing focus on exploiting collateral sensitivity–which occurs when a population evolves resistance to a selecting drug and as a direct result exhibits decreased resistance to a different drug–to slow or reverse evolution in bacteria and cancer [37, 38, 39, 40, 41, 42, 43, 44, 45, 46].

In this thesis, we combine quantitative experiments on bacteria with simple mathematical models to investigate how resistance to antibiotic emerges in microbial communities. One aim for this work is to investigate the use of evolutionary-based strategies to slow down the emergence of resistance–or to steer evolution more generally [47]. Antibiotics are a good model system because they create strong selection pressures by killing or inhibiting the growth of susceptible cells–effects that are relatively easy to measure with light scattering (optical density) and classical microbiological methods. Our goals are grounded in basic science, not clinical application; while the experiments described here are vast over simplifications of the complex dynamics that take place within and between human hosts, the experiments also take place under relatively well controlled conditions, allowing us to tease apart factors that contribute to the evolution of resistance in a simple setting. This thesis can be divided into two primary themes: time dependent effects of collateral evolution (Part I) and effects of multi-strain interactions in heterogeneous communities, particularly those that are spatially non-uniform (Part II). In what follows, we briefly describe our choice of model system, give a short overview of these two themes, and then outline the structure of the thesis.

1.1 Model system

E. faecalis is a Gram positive bacterial species and opportunistic human pathogen associated with a variety of nosocomial infections, such as endocarditis, bacteremia, urinary tract infections, and wound and medical device infections [48, 49, 50, 51, 52, 53]. Our choice of *E. faecalis* as a model system is motivated in part by its clinical relevance, but also because common strains–including those we use–are fully sequenced and well characterized [48, 54], there are an increasing collection of tools available for genetic manipulation of enterococci, they are intrinsically resistant to many antibiotics and rapidly acquire new resistance, and because–at the molecular level–there is evidence that enterococci frequently engage in collective behavior, including horizontal gene transfer, biofilm formation, and pheromone-based signaling [48]. *E. faecalis* are particularly relevant for the study of spatial dynamics, as they are frequently found in the human gut, where different subpopulations may exist under different environmental conditions and contribute to emergence of resistance in the clinic [55].

1.2 Collateral effects of antibiotics

Collateral effects refer to an increase (collateral resistance) or decrease (collateral sensitivity) in resistance to one drug that occurs during adaptation to a second drug. While collateral sensitivity is a promising approach for designing evolutionary therapies, a number of factors make its application to the clinic challenging; for example, collateral effects exhibit a high degree of heterogeneity [56, 57], distinct collateral profiles arise from different selection pressures [58], collateral effects are often not repeatable [59], and many non-antibiotic environments can confer collateral sensitivity [60, 61, 62, 63, 64, 65]. Despite these challenges, theoretical and laboratory studies have shown that control theoretic approaches may be used to counter, and even leverage, stochastic features of the evolutionary process to shape population outcomes [56, 66].

Still, many fundamental questions about collateral sensitivity remain unanswered and are the focus of ongoing work. For example, the molecular mechanisms behind collateral sensitivity are known in relatively few cases [43, 67], and it is unclear the extent to which collateral profiles are conserved across diverse species [68]. In addition, collateral drug pairs are difficult to identify in clinical settings, despite notable recent progress [69, 70], and somewhat surprisingly, little is known about how collateral profiles change under continued selection, with much of the work performed only recently in other organisms such as cancer [44, 71]. Many studies of collateral sensitivity in bacteria focus on endpoint measurements that quantify resistance or sensitivity at a single point in time–for example, at the end of a lab evolution experiment. In the work reported here, we use laboratory evolution experiments to investigate how collateral sensitivity profiles change over time as *E. faecalis* undergoes adaptation to a diverse library of antibiotics. We describe a rich collection of dynamics that are characterized by global trends–for example, collateral resistance arises in early stages of adaptation, while sensitivity tends to increase in later stages–but a number of drug- and population-specific dynamics that we characterize using a combination of genome sequencing and phenotype measurements.

1.3 Interactions between cells and their spatial environment

In Part II, we investigate a second important aspect of evolutionary dynamics: interactions between cells and the surrounding spatial environment. Research has shown that bacterial interact with other cells and with their environment in many ways, ranging from metabolic cooperation between cells to competition for space and nutrients. Our work investigates two aspects of these interactions: the role of 1) spatial heterogeneity and 2) inter-cellular competition in modulating the evolution of resistance. A large of body of theoretical work indicates that spatial heterogeneity can dramatically impact evolution in different contexts, from range expansions in microbes [72, 73, 74] to host

heterogeneity in infectious disease models [75, 76, 77]. In the context of drug resistance, theory suggests that the presence of spatial gradients of drug tends to accelerate resistance evolution [78, 79, 80, 81, 82], though it can be slowed down by tuning the drug profiles [20] or in cases where the fitness landscape is non-monotonic [83].

While experiments in spatially-extended communities are notoriously difficult, experiments using innovative approaches–for example, microfluidics devices [18] and large "mega" agar plates [19]–have shown that spatial drug concentration gradients can promote resistance, even in cases where adaptation does not occur when drug is distributed uniformly [18]. Such spatial effects could be particularly important for *E. faecalis* in the gut, which is a potentially heterogeneous environment. Recent work on gut microbes in simple organisms (zebrafish) has indeed shown that spatial effects, such as cell-cell clustering, can contribute to clearance and extinction of microbial communities [84, 85]. In addition, ecological theory predicts that the diversity of gut microbes depends on spatial dimensions, a predictions recently borne out in samples from human digestive tracts [86]. Nevertheless, these within-host dynamics remain difficult to study quantitatively, and the complexity of the *in vivo* environment makes it difficult to disentangle effects of spatial structure from other host effects.

Our work uses a different approach: we investigate these issues in laboratory populations using customized, computer-controlled bioreactors [87, 88], which allow us to experimentally simulate migration dynamics between spatially distinct populations and adaptive antibiotic treatments that depend on cell density. These experiments do not fully capture the complexity of clinical and natural environments; on the other hand, they take place under well controlled conditions that allow us to modulate different environmental factors–such as drug concentration–in a simple setting.

In addition to spatial structure, the emergence of resistance potentially depends on interactions between different cells in the community [13]. These interactions can potentially be leveraged to slow resistance. For example, recent studies propose that we could leverage competition for resources to slow down the spread of resistance [89, 90, 28], a concept that also underlies adaptive therapies for cancer, where the treatment is adapted in real time to account for the size (or other features) of a tumor [91]. In the context of bacteria, recent work in *E. coli* showed that a mixed population containing a large number of sensitive cells can be contained below a threshold density longer than matched populations without the sensitive cells [28]. The experimental setup involves adapting treatment to minimize the use of drug–adding drug only when population size eclipses some threshold–allowing the sensitive cells to compete with resistant strains for resources. The results show that the mixed population can contain the treatment for a longer time compared to the resistance population alone, but only when populations can be maintained at a sufficiently high density [90, 28]. Similar findings in cancer and parasites, as well as in mathematical models [92], suggest potential generality of this phenomena, but more work is needed to characterize these

adaptive therapies for a wide range of microbes and environmental conditions.

1.4 Organization of thesis

The thesis is organized as follows. In chapter 2, we investigate how collateral effects change over time in bacteria exposed to increasing antibiotic selection and, in turn, how these potentially dynamic collateral sensitivity profiles may influence the design of drug scheduling. Using laboratory evolution in *Enterococcus faecalis*, we measure collateral sensitivity and resistance profiles over time for 20 populations exposed to increasing concentrations of five drugs for a total of 400 strain-antibiotic susceptibility measurement combinations. These collateral profiles reveal a global trend: collateral resistance appears more frequently in early stages of adaptation–when resistance to the selecting drug is lower–while further evolution increasingly favors collateral sensitivity. Despite this global trend, collateral profiles are temporally dynamic and difficult to predict at the level of single drugs or single populations, which themselves can be comprised of multiple competing phenotypes, even after short-term adaptation for tens of generations. Finally, we show experimentally that optimal drug scheduling may require exploitation of specific time windows where collateral sensitivity is most likely to occur.

In Chapter 3, we narrow our focus to collateral effects that arise in populations adapted to daptomycin, a cyclic lipopeptide antibiotic that targets the cell membrane [93, 94, 95, 96]and an important therapeutic option for treating multi-drug-resistant infections [97, 98, 99, 100, 101], including vancomycin-resistant enterococci (VRE). Previous work (including that in Chapter 2) has shown that isolates selected in daptomycin are characterized by particularly heterogeneous collateral profiles [102, 103]. To examine how these collateral effects arise during daptomycin adaptation, we phenotypically and genetically characterized dozens of individual isolates selected from each of the four daptomycin-selected populations described in Chapter 2. In all populations, we identified isolates with mutations in one or more genes previously associated with DAP resistance, and these isolates are characterized by divergent phenotypic properties–including different levels of DAP resistance and different growth rates (i.e. fitness costs) in drug-free media. Interestingly, we also observed strongly divergent collateral responses to different antibiotics, particularly CRO, with collateral resistance arising in mutants harboring DAP-resistance mutations in cardiolipin synthetase (*cls*) or in genes linked to the two-component signaling system YxdJK (*becR* or *ycvR*) [104]. By contrast, mutations in *liaX*, a component of a LiaFSR two-component signaling system, arose in two of the four populations, with point mutations associated with CRO-sensitivity and a larger, IS256-mediated insertion associated with extreme CRO-sensitivity and a dramatically reduced growth rate. Our results reveal considerable phenotypic differences in mutations targeting the LiaSFR system and highlight trade-offs between resistance to daptomycin, collateral profiles

(most notably to CRO), and drug-free growth rates (fitness costs) in evolving lineages. As a whole, Part I underscores how rich–and remarkably diverse–evolutionary dynamics can emerge even in parallel populations adapting to simple drug escalation protocols.

Part II begins with Chapter 4, where we investigate whether drug (doxycycline) concentrations in heterogeneous meta-communities (collections of well-mixed individual populations that are linked to one another by migration) can be tuned to modulate the emergence of drug resistance. By measuring real-time growth rate in these meta-communities,we show that migration accelerates total population growth in mixed populations of drug-sensitive and drug-resistant cells. These results are consistent with a simple mathematical model and can be explained by the homogenizing effect of migration on the initial distribution of mutants. In addition, we investigate the emergence of resistance in initially sensitive populations on longer timescales in both single- and multi-habitat communities; on these timescales, we find that migration tends to delay adaptation when the concentration of drug is not uniform across habitats. Genome sequencing and phenotypic characterization of adapted isolates indicates that migration does not select for fundamentally new mutations but instead reshapes the distribution of sensitive and resistant populations across habitats. By contrast, we also observe cases where migration has little impact on growth adaptation, even when drug heterogeneity across habitats is substantial. These trends can be partially explained by changes in selection pressure across different habitats, which we show is correlated with the observed shift in adaptation times. Overall, these results show that migration and spatial structure can have substantial impacts on adaptation in microbial communities, even in simple scenarios where resistance is dominated by a selective sweeps of a single type of mutant.

Chapter 5 describes ongoing preliminary work on the effects of population density on the emergence of resistant populations in well-mixed communities. By performing parallel laboratory evolution experiments in populations fixed at different densities, we show that resistance arises more rapidly at lower cell densities, an effect that is captured by simple competition-based models of population dynamics. Surprisingly, however, we observe the opposite trend at low drug concentrations when populations are seeded, up-front, with low frequency mutant populations: growth increases are accelerated in the high-density populations. Finally, we describe a series of preliminary experiments that use adaptive drug dosing in mixed populations of sensitive and resistant cells in an attempt to maintain populations below a threshold "tolerable" density, which we refer to as "containment". These experiments extend previous studies in *E. coli* [28] to populations of *E. faecalis*. In most cases, these adaptive dosing schedules prolong containment for longer times in low-density populations, though the dynamics that follow the loss of containment are complex, with initially escaping populations sometimes reaching their maximum density more slowly than later-escaping populations.

As a whole, the thesis highlights both the simplicity and complexity of evolutionary dynamics

leading to resistance. On one hand, Part I highlights how collateral effects and evolution can be remarkably diverse even in simple laboratory settings where side-by-side populations in well-mixed communities undergo similar drug escalation protocols. Part II underscores the important role that spatial heterogeneity can play in modulating resistance, yet also highlights how initially counter-intuitive dynamics can–at least sometimes–be understood with simple mathematical models. We hope these results motivate continue explorations of resistance evolution, both in the lab and the clinic.

Part I

Dynamic Collateral Effects of Antibiotic Resistance

CHAPTER 2

Dynamic Collateral Sensitivity Profiles Highlight Challenges and Opportunities for Optimizing Antibiotic Sequences

This chapter was reproduced, in part, from the following manuscript, which has been submitted for publication: *J. Maltas, **A. Huynh**, and KB Wood, bioRxiv, 2022. doi: 10.1101/2021.12.19.473361*. The initial lab evolution experiments and collateral measurements (Figures 2.1-2.2) were performed by J. Maltas. I (AH) performed all experiments to characterize heterogeneity and time-depend effects in single populations (e.g. Figure 2.3, Figure 2.8). All authors contributed to experimental design, data analysis, figure design, and manuscript drafts/revisions.

2.1 Introduction

As discussed in Chapter 1, collateral effects have been proposed as a strategy to help design resistance-slowing combinations or cycles of antibiotics [105, 106, 102, 67, 107, 108]. Many studies of collateral sensitivity in bacteria have quantified collateral effects at a single point in time, but considerably less is known about how those collateral effects change over time.

In this Chapter, we sought out to understand how collateral effects change over time in bacteria exposed to increasing antibiotic selection and, in turn, how these potentially dynamic collateral sensitivity profiles may influence the design of drug scheduling. Using laboratory evolution in *Enterococcus faecalis*, a gram-positive opportunistic bacterial pathogen typically found in the gastrointestinal tracts of humans[48, 109, 50, 51, 52, 53], we measure collateral sensitivity and resistance profiles over time for 20 populations exposed to increasing concentrations of five drugs, yielding 400 strain-antibiotic susceptibility measurement combinations. These collateral profiles reveal a complex story. When data from all drugs are combined, a clear trend emerges: collateral resistance appears more frequently in early stages of adaptation–when resistance to the selecting drug is lower–while further evolution increasingly favors collateral sensitivity. At the same time,

collateral profiles are temporally dynamic and difficult to predict at the level of single drugs or single populations. Finally, we show experimentally that optimal drug scheduling may require exploitation of specific time windows where collateral sensitivity is most likely to occur. Taken together, our results underscore the importance of measuring temporal collateral profiles not only to better understand collateral evolution, but for any future work that hopes to harness collateral effects as a therapeutic option.

2.2 Results

2.2.1 Collateral effects are temporally dynamic

To investigate how collateral effects change over time in *E. faecalis*, we exposed four independent evolutionary replicates of strain V583 to escalating concentrations of a single drug over 8 days (approximately 60 generations) via serial-passage laboratory evolution (Fig 2.1, Materials and methods). In a previous study, we characterized collateral effects at the final endpoint of these evolutionary experiments [56]. In this work, we investigate the temporal progression of these collateral effects in a subset of five antibiotics chosen to represent a broad collection of mechanisms of action (Table 2.1). To do so, we isolated a single colony from each population at 2-day intervals and measured dose-response curves to each of the antibiotics (Fig 2.1A).

Table 2.1: **Antibiotics used in chapter 2.**

Drug Name (Abbreviation)	**Drug Class**	**Mechanism of Action**
Ceftriaxone (CRO)	β-Lactam	Cell wall synthesis inhibitor
Ciprofloxacin (CIP)	Quinolone	DNA gyrase inhibitor
Daptomycin (DAP)	Lipopeptide	Cell membrane insertion
Doxycycline (DOX)	Tetracycline	30S protein synthesis inhibitor
Linezolid (LZD)	Oxazolidinone	50S protein synthesis inhibitor

We quantified resistance and sensitivity by estimating the half-maximum inhibitory dose (IC_{50}) for each strain-antibiotic combination (Materials and Methods). In total, we estimated the IC_{50} for 400 strain-antibiotic combinations (20 evolving populations, measured against 5 antibiotics, at 4 evolutionary time points), each in (technical) replicates of three. For each measurement, we then calculated the collateral response $c \equiv \log_2 (IC_{50,Mut}/IC_{50,WT})$, the $\log_2$-scaled fold change in IC_{50} of the evolved strain relative to the ancestral V583 (Fig 2.1B). Resistance (direct or collateral) corresponds to $c > 0$ while sensitivity corresponds to $c < 0$ ($c = 0$ is indicated by the black dashed line). As in previous work [56, 60], we defined collateral resistance or sensitivity to occur when the

measured IC_{50} is at least 3 times the standard error of the mean of the wild-type ($|c| > 3\sigma_{WT}$, where σ_{WT} refers to standard error of the mean in the wild type; see Methods). While other definitions are possible, particularly in cases where a large number of technical replicates are available, we will see (below) that the qualitative trends we observe do not depend sensitively on the threshold for defining sensitivity or resistance.

Our results indicate that resistance to both the drug used for selection and the "unseen" testing drugs varies considerably over time. As expected, resistance to the selecting drug (diagonal entries, Fig 1B) tend to increase approximately (though not exclusively) monotonically over time and, in many cases, plateau after several days of selection. However, the temporal trends in collateral effects–the off-diagonal entries–are variable. In some cases, the population exhibits only collateral resistance (e.g. ciprofloxacin (CIP)-selected populations tested against ceftriaxone (CRO)) at all time points. In other cases, the same population exhibits collateral resistance at one time point and collateral sensitivity at another (e.g. ceftrixaone (CRO)-selected strains tested against doxycycline (DOX); Linezolid (LZD)-selected strains tested against CRO). Additionally, the variance in outcome across the 4 populations, and over time, depends on the testing drug. For example, resistance to DOX in all isolates varies over a relatively small range (fold-change in IC_{50} varies from a minimum of 0.4 to a maximum of almost 8), while resistance to CRO in the same strains varies substantially more (fold-change in IC_{50} varies from a minimum of 0.007 to a maximum of over 100). We also observe varying levels of induced collateral sensitivity between tested drugs. For example, at no point do any of the 20 evolved strains become collaterally sensitive to LZD, and collateral sensitivity to DAP is rare at all evolutionary time points. This is particularly notable because LZD and DAP are frequently used as last line of defense antibiotics in the treatment of multidrug resistant gram-positive infections[110, 111, 112, 113].

2.2.2 Collateral effects are initially dominated by resistance but shift toward sensitivity with further adaptation.

To quantify how the propensity for collateral resistance changes over time, we calculated the "instantaneous" collateral resistance (or sensitivity), which measures collateral effects at each time point *relative to the previous time-point*, rather than relative to the ancestral strain (Fig 2.2). For example, to investigate how the population changed between days 4 and 6 we calculate: $c_{\text{inst}} \equiv \log_2 \left(IC_{50,\text{D6Mut}}/IC_{50,\text{D4Mut}}\right)$, where the IC_{50}'s are calculated at days 6 and 4. This analysis reveals that the first two days of evolution are dominated by collateral resistance effects (91.25%), while the subsequent 6 days of evolution confer collateral resistance at considerably reduced frequencies (33.75%, 38.75%, and 32.50% respectively). Further, after the first two days of evolution, the last 6 days also share a similar frequency of collateral sensitivity (52.5%, 55.0%, and 57.5%

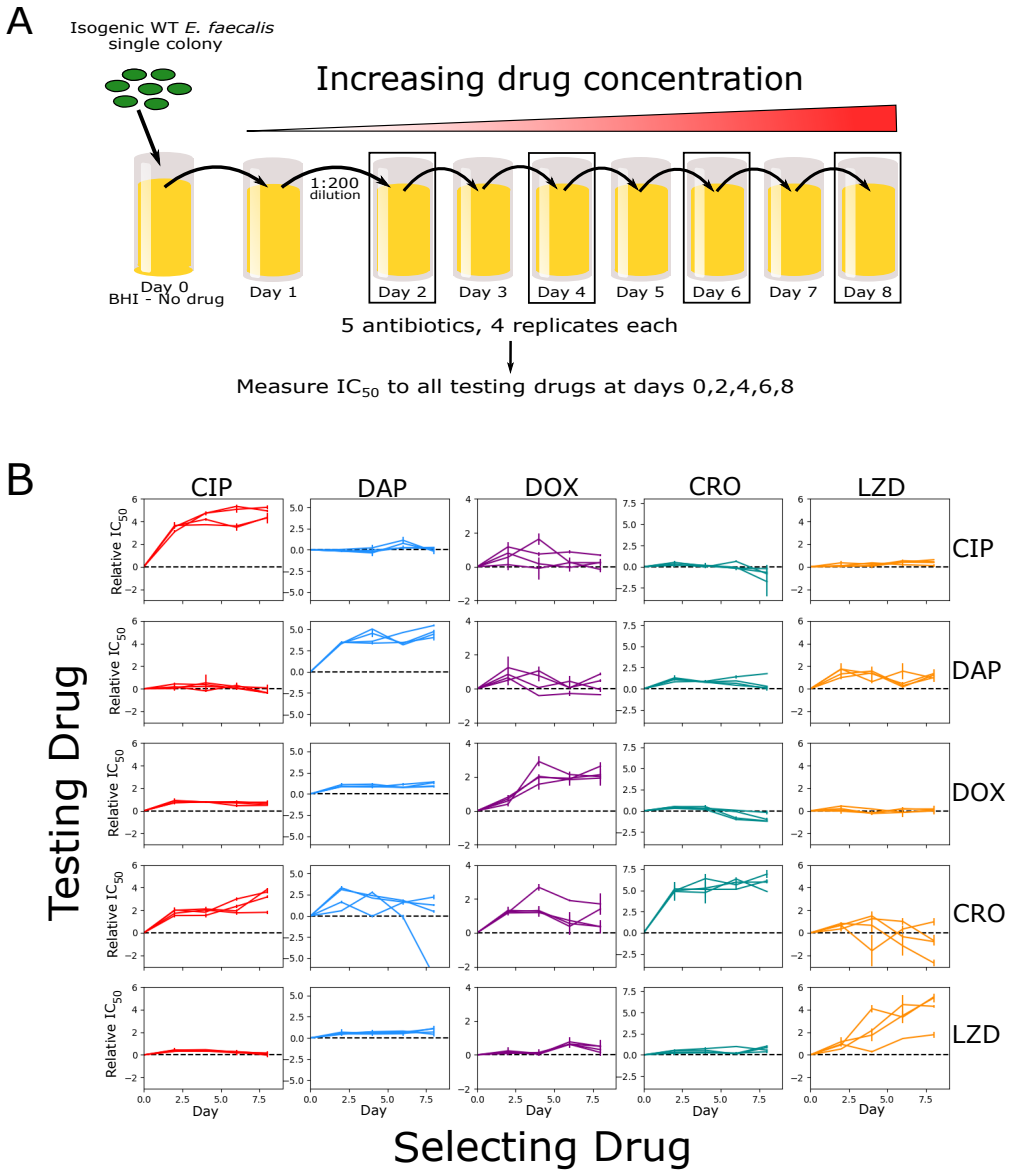

Figure 2.1: **Laboratory evolution of *E. faecalis* reveals diverse, temporally dynamic collateral sensitivity profiles.** **(A)** *E. faecalis* strain V583 was exposed to single antibiotics in escalating concentrations over the course of an 8-day serial-passage evolution experiment (roughly 60 total generations). Four independent populations were evolved in the presence of one of five selected antibiotics. The half-maximal inhibitory concentration (IC_{50}) was estimated for a single isolate from each population at days 2, 4, 6 and 8. **(B)** Resistance/sensitivity measurements taken every two days for each of the 20 mutants to each of the 5 antibiotics quantified by the $\log_2$-transformed relative increase in the IC_{50} of the testing drug relative to that of WT V583 cells (black dashed line at $y = 0$). Rows represent the drug used to select the mutant (selecting drugs: Ciprofloxacin (CIP) = red, Daptomyacin (DAP) = blue, Doxycycline (DOX) = purple, Ceftrixone (CRO) = teal, Linezolid (LZD) = orange), whereas columns represent the drug used in the testing assay. Error bars represent the standard error of the mean (SEM) for each individual experiment. Note that the y-scales are different for each column but the same within a column to allow for comparison of collateral effects (off-diagonal) with direct effects (diagonal).

respectively).

To further quantify these trends, we combined the data from all drugs and all time points and calculated the mean instantaneous collateral effects as a function of resistance to the selecting drug (Fig 2C, left panel). At this global level, the mean collateral effects (both instantaneous and cumulative) trend downward–toward sensitivity and away from resistance–as resistance to the selecting drug increases. Notably, the *instantaneous* collateral resistance at early stages (when resistance to the selecting drug is small) is sufficiently large that the mean *cumulative* collateral effects remain positive even at later stages that is, the trend toward collateral sensitivity is not strong enough to overcome the initial collateral resistance acquired at low levels of resistance to the selecting drug. Similarly, the probability (frequency) of collateral sensitivity increases (Fig 2C, right panel) Fig 2.5; $p_{\text{value}} < 0.05$ from logistic regression, see Methods and SI Supplemental Tables) and the probability of collateral resistance decreases (Fig 2.6,$p_{\text{value}} < 0.05$) as resistance to the selecting drug is increased. These qualitative trends do not depend sensitively on the specific thresholds used to define CS/CR (Fig 2.7).

One simple explanation of this phenomenon may be an abundance of easily accessible, low-level resistance mutations, perhaps related to efflux pumps[114, 115, 116] or a general stress response[117, 118], that broadly confer low-level multidrug resistance at early stages of adaptation. As the antibiotic concentration is increased the population is required to evolve more antibiotic-specific mutations that may be associated with collateral trade-offs.

2.2.3 Temporally dynamic collateral effects are difficult to predict at the level of individual drugs.

While global trends emerge when the data from all drugs is combined, it is not clear whether similar trends occur at the level of individual drugs. To investigate this question, we first calculated correlations between each of the 5 testing conditions to search for statistical similarities between different drugs. Depending on the metric used, we find that either 4 or 5 of the 10 pairwise combinations produce a statistically significant but relatively weak negative correlation. However, scatter plots indicate that these relationships are nonlinear with considerable scatter, even when statistically significant.

In addition, we found that collateral effects for specific drugs are difficult to predict from collateral profiles measured at earlier times in the same strain. For example, one DAP-adapted population exhibits a significant increase in resistance to CRO between days 2 and 4, however days 4 to 6 and 6 to 8 both come with a significant collateral sensitivity. Similarly, the LZD-selected strains confer resistance to DAP on days 2 and 8, but exhibit collateral sensitivity on days 4 and 6. To quantify this effect, we calculated how often an observation from the current time step correctly

predicted change in resistance measurement two days later. That is, if a particular isolate exhibited collateral sensitivity to a drug on day 2, how frequently did it also exhibit collateral sensitivity on day 4 Somewhat surprisingly, collateral profiles on day 2 correctly predict only 41% of day 4 collateral profiles. Similarly, day 4 only successfully predicted 37% of day 6 collateral profiles and day 6 accurately predicted 41% of day 8 profiles. These data indicate that, in contrast to resistance levels to the selecting drug, which tend to be non-decreasing over time, instantaneous collateral effects are largely uncorrelated after short periods (2 days; 10-20 generations) of adaptation. This lack of predictability might also arise if populations are largely heterogeneous over time, meaning that sampling single colonies from each population could result in the appearance of dynamic or stochastic evolution.

2.2.4 Collateral effects are dynamic within individual populations.

To investigate heterogeneity within the evolving populations, we focused on three selection-testing drug pairs (LZD-CRO, CRO-DOX, and CRO-CIP), which correspond to lineages adapted to one of three drugs (LZD, CRO, and CIP) and tested against a different drug (CRO, DOX, and CRO, respectively). In two examples (LZD-CRO and CRO-DOX), the original data suggested collateral resistance to the testing drug decreases over time, with resistance occurring at early stages and sensitivity at later stages. In the third example (CRO-CIP), the collateral effects are approximately constant (resistance) over time.

From each of the three populations, we isolated 48 colonies (12 colonies from each of 4 time points) and measured the response of each isolate to the testing drug using dose response curves (Fig 2.3). We found that the specific distributions of IC_{50} values vary in idiosyncratic ways–for example, the LZD-CRO population is characterized by a roughly unimodal distribution whose mean decreases over time, while the CRO-DOX population is characterized by coexistence of highly resistant and highly sensitive isolates at early times, while later time points contain primarily sensitive isolates. Indeed, the mean collateral resistance (i.e. fold change in IC_{50} relative to ancestor) is dynamic–specifically, it is not the same at every time point in the LZD-CRO (1-way Anova, $p_{\text{value}} = 0.0008$), CRO-DOX ($p_{\text{value}} = 0.001$), and CIP-CRO pairs ($p_{\text{value}} = 0.05$). See SI for pairwise comparisons at all time points.

In addition, we calculated the frequency of CR and CS across isolates. We found that the frequency of sensitive isolates increases over time in the LZD-CRO and CRO-DOX pairs (logistic regression, $p_{\text{value}} = 0.04$ and $p_{\text{value}} = 0.005$, respectively; see Methods) and the frequency of resistant isolates decreases in the LZD-CRO pair ($p_{\text{value}} = 0.007$; for CRO-DOX the trend is qualitatively similar but not significant, $p_{\text{value}} = 0.1$). In contrast to the first two populations, the third population (CRO-CIP) shows the opposite trend, with resistance increasing in frequency

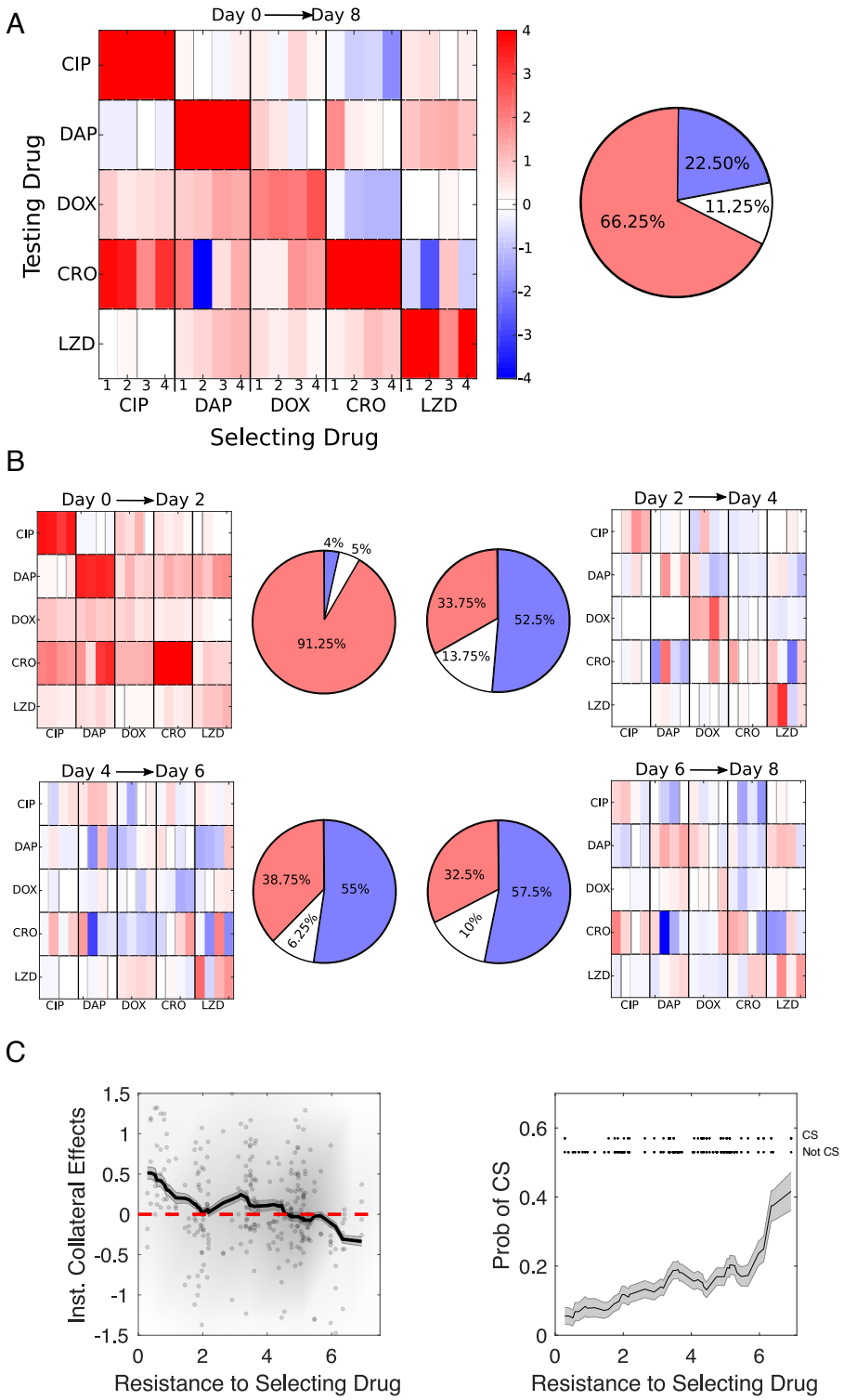

Figure 2.2: **Early evolution is dominated by collateral resistance followed by a diverse set of collateral responses as evolution continues.** (See next page)

Figure 2.2: **(A) Left:** Collateral profiles measured at the final time point (day 8), relative to the day 0 ancestor. Resistance (red) or sensitivity (blue) to each antibiotic is quantified via the $\log_2$-transformed fold change in IC_{50} relative to the ancestral strain (V583). A measurement is deemed to be collaterally resistant or sensitive if it falls above or below 3 times the standard error of the mean of the wild-type ($|c| > 3\sigma_{WT}$). For each selecting drug, there are 4 evolutionary replicates (thin rectangular columns). **Right:** Pie chart representing the fraction of collateral effects that confer resistance (red), sensitivity (blue) or no statistical change (white/gray). **(B)** Instantaneous collateral effects: collateral profiles measured for the same 20 mutants as A, but collateral sensitivity/resistance is defined relative to the previous time point (rather than the ancestor strain). Days 0-2, top left; days 2-4, top right; days 4-6, bottom left; days 6-8, bottom right. Over 90 percent of collateral effects conferred between days 0-2 resulted in collateral resistance. The subsequent 6 days of evolution (days 2-4, 4-6, and 6-8) only conferred collateral resistance 34%, 39% and 33% respectively. **(C)** Instantaneous collateral effects (i.e. collateral effects relative to previous timepoint) (left) and probability of collateral sensitivity (CS) (right) as a function of resistance to selecting drug. Left panel: dots are individual populations, shading indicates relative density of points, and curve is moving average (shading is $\pm$ standard error over each window). Right panel: curve is moving average (shading is $\pm$ standard error over each window). Upper inset shows individual data points (top row is CS, bottom row is not CS) used to calculate probability. Averages are performed over windows of size 2.

($p_{\text{value}} = 0.05$) and sensitivity decreasing in frequency over time ($p_{\text{value}} = 0.02$).

These results indicate that the adapting populations exhibit heterogeneity in collateral resistance profiles but nevertheless show clear temporal trends, even within single populations. In some cases (LZD-CRO, CRO-DOX), the trends are reminiscent of the global trends observed across drugs–that is, early stages of adaptation favor collateral resistance and later stages collateral sensitivity–but this is by no means universal (e.g. CRO-CIP exhibits opposite trends).

2.2.5 Success of switching to a second antibiotic is contingent on temporally dynamic collateral effects.

To investigate the effects of drug timing experimentally, we designed an evolution experiment (Fig 2.4A) meant to approximate a hypothetical drug-switching protocol involving two drugs (CRO and DOX) suggested by simulations to be particularly sensitive to the timing of drug switching [103]. Similar to our previous experiments, we performed serial passage evolution using escalating concentrations of the antibiotic CRO but now for a total period of 14 days. At the end of each day, we exposed a diluted sample of that population to varying concentrations of a second antibiotic, DOX, to probe how switching to a second drug may have increased or decreased the treatment efficacy. The entire process was repeated for 20 independent populations to quantify evolutionary variability (Fig 4B).

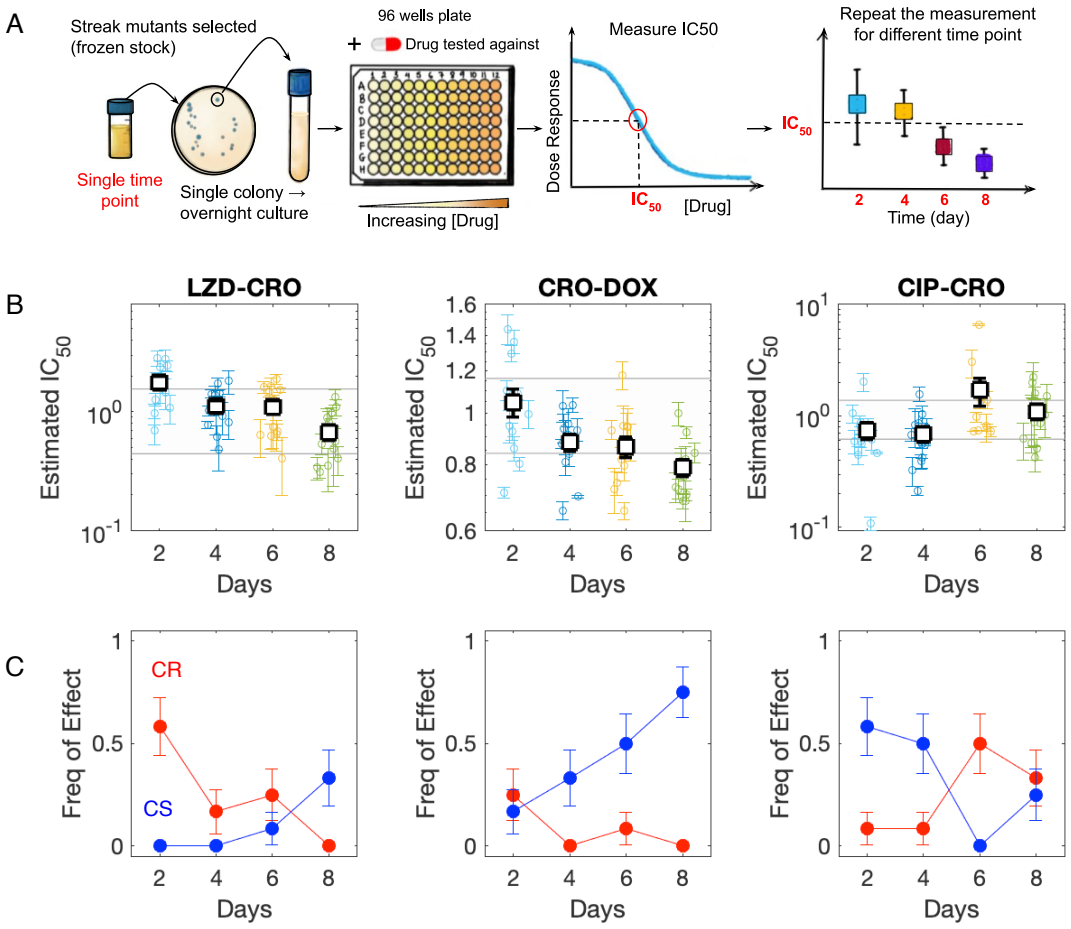

Figure 2.3: **Collateral effects are dynamic within individual populations. (A):** Samples from a single evolved population at days 2, 4, 6, and 8 are plated and 12 colonies from each time point are selected for phenotyping (IC_{50} characterization). **(B):** Measured IC_{50} values for 12 isolates at each of 4 different time points from populations adapted to LZD (left), CRO (middle), and CIP (right) and exposed to CRO (left), DOX (middle), and CRO (right). Shaded region indicates IC_{50} of ancestor strain ($\pm$ 3 standard error). Individual points represent the mean IC_{50} ($\pm$ standard error from 4 technical replicates) for a single colony. Open squares represent the population mean–that is, the mean across all colonies (error bars are $\pm$ standard deviation of the population). **(C):** Frequency of colonies exhibiting collateral sensitivity (blue) or collateral resistance (red) over time.

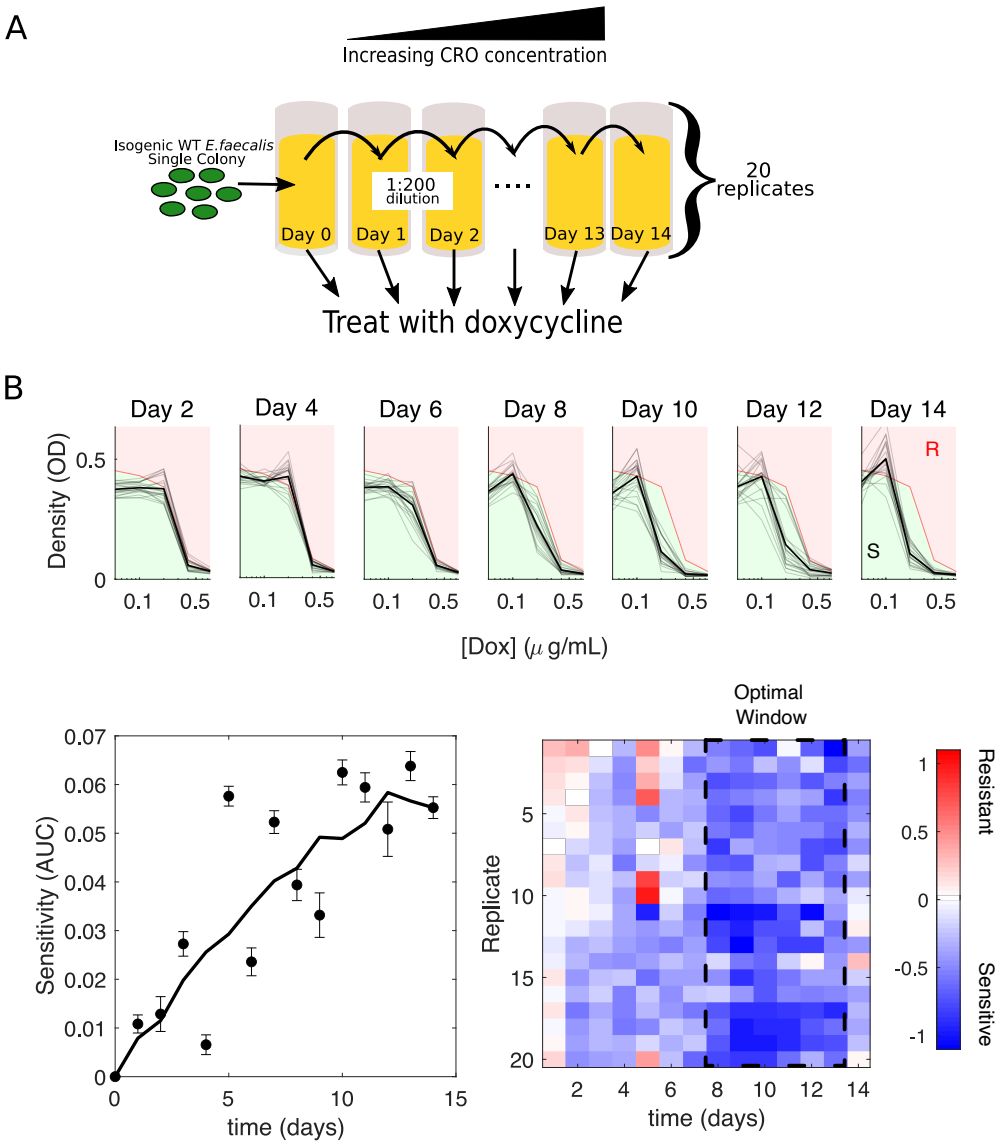

Figure 2.4: **Success of switching to a second antibiotic is contingent on temporally dynamic collateral effects. (A)** Twenty replicate populations of *E. faecalis* V583 were exposed to increasing concentrations of the antibiotic ceftrixone (CRO) over the course of 14 days via serial passage. At the end of each day a sample of the population was isolated and cultured in a range of doxycycline (DOX) concentrations for 24 hours. **(B) Top:** Density (OD) after 24 hours vs drug (DOX) concentration for all 20 populations (light gray), and the mean over the 20 populations (dark black) at different days of the evolution experiment. For comparison, the dose response curve in the ancestral strain (red curve) divides the space into regions of increased resistance (red) and increased sensitivity (green). **(B) Bottom left:** Average sensitivity over 20 populations (error bar standard error of the mean) at different time points. Sensitivity is defined as the difference in area under the curve between the ancestral dose response curve and the dose response curve of the population in question between the lowest ([Dox]=0.05 μg/mL) and highest ([Dox]=0.8 μg/mL) nonzero drug concentrations. Solid line is a moving average. **(B) Bottom right:** Collateral effects (quantified, as before, by $\log_2$-transformed fold change in the IC_{50}). Dashed region highlights a transient six-day window where collateral sensitivity is more pronounced.

To quantify sensitivity to DOX, we calculated both a global area-under-the-curve sensitivity score, where we take the difference between the area under the dose response curve of the ancestral strain and each evolved population (Fig 4B, bottom left), as well as the previously described collateral effect metric (i.e. the log-scaled fold change in half-maximal inhibitory concentration). Both metrics show that populations adapted to CRO become increasingly sensitized to DOX over time. The sensitivity is particularly notable between days 8 and 13, where the mean collateral sensitivity (across replicate populations) is maximized before starting to decline (Fig 4B, bottom right; post-hoc pairwise comparisons following 1-way Anova identify days 8-13 as a statistically distinct cluster; see SI Supplemental Tables). Switching to DOX at time points before or after that window produces different levels of average sensitivty and even leads to resistance in some populations. These results indicate that the effects of a new antibiotic can vary considerably depending on when, along the adaptation trajectory, the new drug is applied.

2.3 Discussion

Our work provides systematic evidence of temporal collateral drug effects in the pathogen *E. faecalis*. The time-dependent nature of collateral sensitivity and collateral resistance presents both additional challenges and new opportunities for designing multi-drug therapies to slow resistance. Full optimization of sequential drug therapies will likely involve not merely static, end-point measurements of collateral effects, but a full description of their temporal development.

The goal of this study was to broadly survey phenotypic resistance patterns over time in a systematic way. This approach comes with obvious drawbacks, and we are left with many unanswered questions. Most notably, our work does not provide any information about the molecular mechanisms underlying the collateral effects; such insight, while hard won even for a single pair of drugs, will be essential to fully exploit the phenotypic effects observed here. In addition, we focused on a single bacterial species, and all experiments were performed starting from the ancestral V583 *E. faecalis* strain. It is not clear how the results might change in a different strain or species, though data from several recent studies suggest the presence of dynamic features in collateral profiles in other species [42, 69, 67, 17]. Indeed, recent work underscores just how important genotype can be in antibiotic evolvability [119], and the search for more general patterns is ongoing [42, 69, 67]. It is also possible that at least some of the trends we observe are specific to the precise laboratory evolution protocol used here, where drug is systematically increased over time following serial dilution.

These results raise a number of questions for future work. Most notably, it is not clear why collateral resistance tends to emerge at early time points but sensitivity increases at later time points. From an evolutionary biology perspective, these results are qualitatively consistent with Fisher's

classic geometric model, which posits that mutations associated with large fitness effects are more likely to be detrimental. In the context of collateral sensitivity, this model suggests that low-level resistant mutants–those selected in the early stages of adaptation–harbor small fitness effects that are expected to be frequently beneficial in a wide range of environments. On the other hand, mutations that have a large fitness effect (high resistance to selecting drugs) may be less likely to be beneficial in different environments (increases sensitivity to other drugs). Previous works have indeed used similar approaches to study how mutations affect fitness changes across different drug environments [120, 121], and in this context, collateral effects can be formalized using the joint distribution of fitness effects [45]–distributions that may be informed by experiments like those reported here.

Future work will aim to sequence the genomes of multiple isolates over time in hopes of identifying classes of resistance genes (e.g. efflux pumps or target mutations) that preferentially occur at certain stages of adaptation (see next chapter for an example of this approach focused on a single drug, daptomycin). One might speculate that low-level mutations tend to offer drug-agnostic protection to the cells. One common example is multidrug efflux pumps, which are known to extrude a wide range of antibiotics out of the cell [122, 123, 124]. These pumps can contribute to cross-resistance to multiple antibiotics. However, in a later stage of adaptation, when the selecting drug concentrations are higher, cells with a higher level of resistance may require more drug-specific mutations–for example, modification of the binding site of the drug [125]. These high-level mutations may be increasingly specialized to a particular drug and could have unintended negative consequences (i.e. sensitivity) in the presence of other drugs. These trade-offs are reminiscent of the classic interplay between "specialists" and "generalists", and theoretical work suggests that switching between environments in judicious ways may be able to preferentially select for one or the other [126, 127, 38]. Applying these principles to drug cycling in the clinic, however, is an ongoing challenge [128, 69].

From a biological perspective, it would be interesting to identify how these patterns change in cells from different physiological states (e.g. biofilm [129]) or under different modes of selection pressure [130]. Perhaps more importantly, our work raises the question of whether similar global trends emerge in clinical scenarios, where the impact of collateral effects are less clear [69]. Answering this question will require not only retrospective studies that combine large large data sets from multiple patients (for example, [69]), but also studies focused on longitudinal sampling from individual patients. Fortunately, studies like this are already underway for different species of enterococcus (see, for example, [55]).

Finally, it is important to keep in mind the scope of our work. These evolution experiments are done in a highly controlled laboratory environment. Our protocols are not meant to guide clinicians, but instead focus on whether or not collateral profiles changed even in the simplest

of drug-evolution environments – free, for example, of the important but difficult-to-quantify interactions between host and pathogen. Translating these results into a clinically accurate model would require additional work to understand the mechanistic, clinical, and even theoretical principles governing drug sequence optimization. This work serves as a reminder of the complexities of evolution and the still long path we must walk to confidently prescribe effective dosing schedules in patients. At the same time, the results highlight the rich dynamical behavior of collateral sensitivity in even simplified laboratory populations, offering a largely unexplored frontier for evolution-based control strategies.

2.4 Materials and methods

2.4.1 Strains, antibiotics, and media

All resistance evolution lineages were derived from an *E faecalis* V583 ancestor, a fully sequenced clinical isolate with vancomycin resistance[131]. The 5 antibiotics used in this study and their mechanisms of action are listed in Table 2.1. Antibiotics were prepared from powder stock and stored at appropriate temperature. Evolution and IC_{50} measurements were conducted in BHI (brain heart infusion).

2.4.2 Laboratory evolution experiments

Evolution experiments were performed in replicates of four. Daily serial passage evolutions were conducted in 1 mL BHI medium in 96-well plates with a maximum volume of 2 mL. Each day populations were grown in three antibiotic concentrations spanning sub- and super-MIC doses. After approximately 16 hours of incubation at 37, the well with the highest drug concentration that contained visible growth was propagated into three new concentrations (typically one-half, 2x and 4x the highest concentration that had visible growth). A 1/200 dilution was used as an inoculum for the next day's evolution plate. This process was repeated for 8 days for the multi-drug study and 14 days for the CRO/DOX study. All strains were stocked in 30% glycerol and subsequently plated on pure BHI plates for further experimentation. A single colony was selected for IC_{50} determination. To help ensure no contamination occured, cells were regularly plated and visualized using DIC microscopy to ensure *E. faecalis* morphology.

2.4.3 Measuring drug resistance and sensitivity

IC_{50} determination experiments were performed in 96-well plates by exposing each strain to a drug gradient consisting of between 6-14 concentrations, typically in linear dilution series prepared in BHI medium with a total volume of $205\,\mu L$ ($200\,\mu L$ BHI, $5\,\mu L$ of 1.5 OD cells) in each well. After 20 hours, we measured the OD at 600 nm via an Enspire Multi-modal Plate Reader (Perkin Elmer) with an automated plate stacker. OD measurements for each drug were normalized by the OD600 in the absence of drug.

In order to quantify resistance to each drug, the OD600-generated dose-response curve was fit to a Hill-like function $f(x) = (1 + (\frac{x}{K})^h)^{-1}$ using a nonlinear least squares fitting. K is the IC_{50} and h is a Hill coefficient that represents the steepness of the dose-response curve. Strains were deemed "collaterally resistant" or "collaterally sensitive" if its IC_{50} had increased or decreased by more than 3 times the standard error of the wild-type mean IC_{50}. In previous work, we chose this

threshold because it minimized the number of false positives (e.g. all measurements of IC_{50} in the ancestor strains, across all drugs, fell within this $\pm 3\sigma_{WT}$ window) [56, 60]. All dose response curves were measured in technical replicates of 3 or 4.

2.4.4 Logistic regressions for estimating frequency trends

To characterize trends in the frequency of resistance (CR) or sensitivity (CS) we used standard logistic regression. Specifically, we assume the classic logit model where $\ln p/(1-p) = c_1 + c_2 X$, with p the probability of CR (or CS), c_1 and c_2 regression coefficients, and X the predictor variable of interest (either resistance to the selecting drug, as in Fig 2.2, or time, as in Fig 2.3. An increasing trend corresponds to $c_2 > 0$ and a decreasing trend to $c_2 < 0$. P-values (p_{value}) are given for each regression in the corresponding figure caption and in SI Supplemental Tables.

2.5 Supplemental Figures

Figures 2.5-2.8 are supplemental figures referenced in the main text.

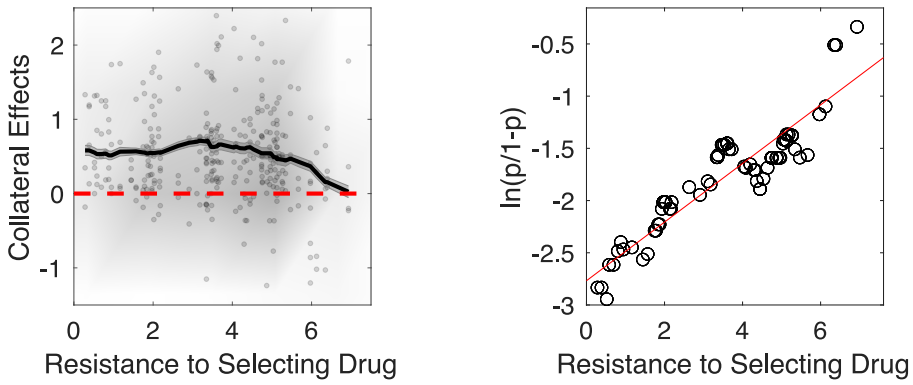

Figure 2.5: **Cumulative collateral effects exhibit early resistance but trend toward sensitivity with adaptation.** Left panel: cumulative collateral effects (relative to ancestor strain) as a function of resistance to selecting drug. Dots are individual populations, shading indicates relative density of points, and curve is moving average (shading is $\pm$ standard error over each window). Right panel: probability of instantaneous sensitivity (p) varies with cumulative resistance to selecting drug. Line is fit from logistic regression (i.e. fit of $\ln(p/(1-p)) = c_1 + c_2 R$, where R is resistance to selecting drug and c_1 and c_2 are intercept and slope parameters, respectively). Slope parameter: $c_2 = 0.3$ ($(0.08, 0.50)$, 95 percent confidence interval); $p_{\text{value}} = 0.006$. Averages and probabilities are calculated over sliding windows of size 2 (in units of resistance to selecting drug).

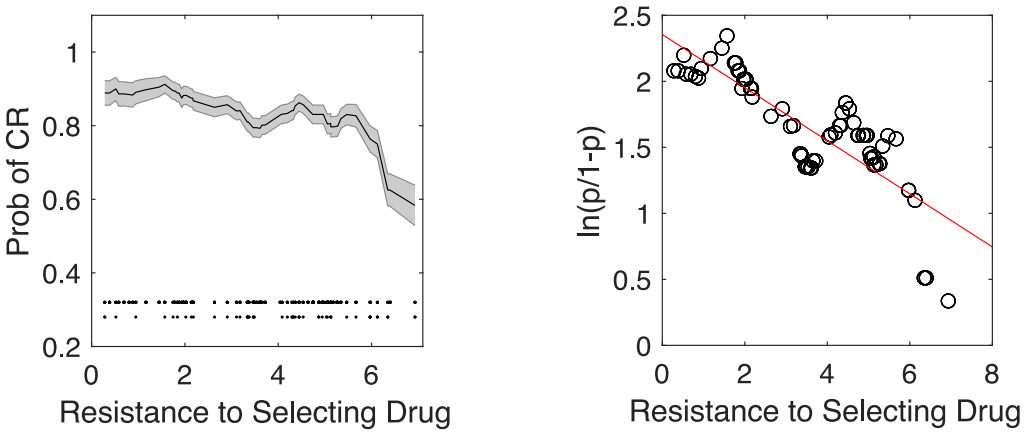

Figure 2.6: **Collateral resistance decreases as resistance to selecting drug increases.** Left panel: probability of (instantaneous) collateral resistance (CR) as a function of resistance to selecting drug. Curve is a moving average (shading is $\pm$ standard error over each window). Lower inset points show individual data points (top row is CR, bottom row is not CR) used to calculate probability. Right panel: probability of resistance (p) varies with resistance to selecting drug. Line is fit from logistic regression (i.e. fit of $\ln(p/(1-p)) = c_1 + c_2 R$, where R is resistance to selecting drug and c_1 and c_2 are intercept and slope parameters, respectively). Slope parameter: $c_2 = -0.2$ ($(-0.4, -0.01)$, 95 percent confidence interval); $p_{\text{value}} = 0.04$. Averages and probabilities are calculated over sliding windows of size 2 (in units of resistance to selecting drug).

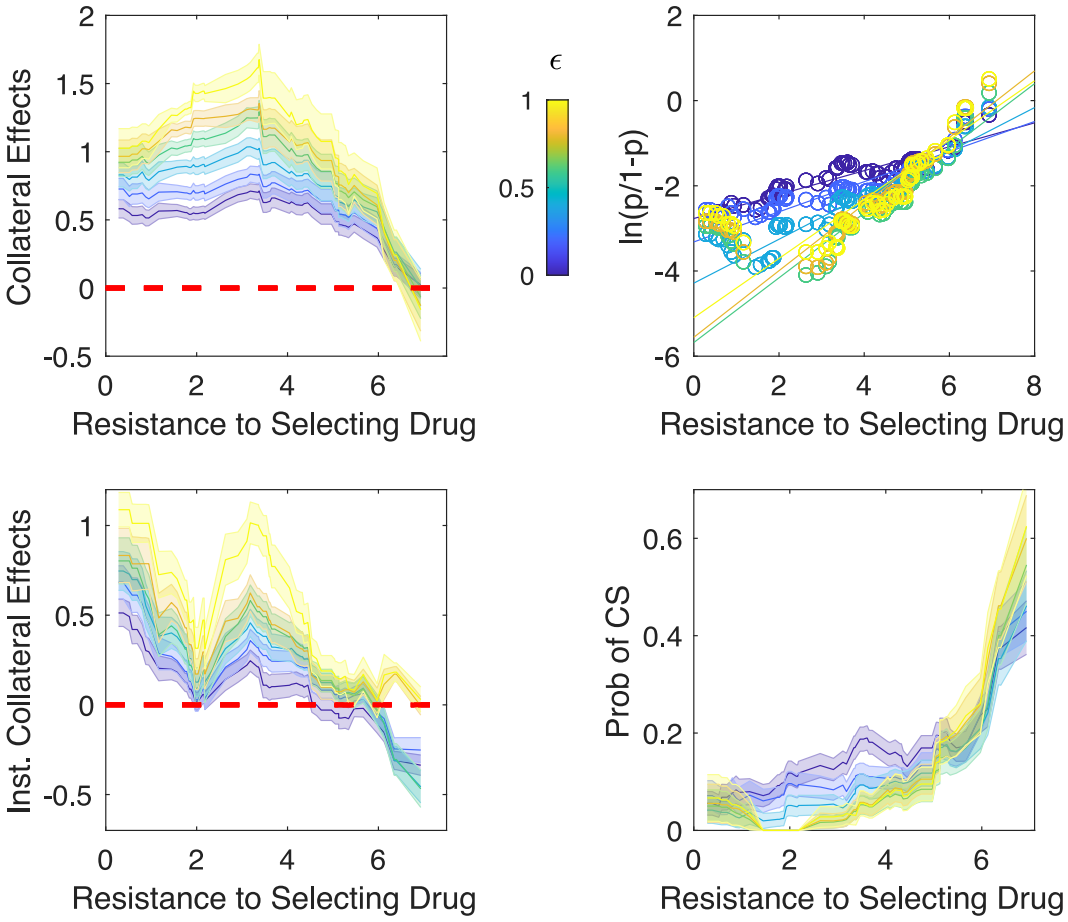

Figure 2.7: **Modulating threshold value does not change qualitative features of collateral effects** Collateral effects (top left), logit function (top right), instantaneous collateral effects (bottom left), and probability of collateral sensitivity (bottom right) as a function of resistance to selecting drug. All collateral effects (i.e. log of fold change in IC_{50}) with an absolute value less than ϵ are removed prior to analysis. Different colors represent the same analysis but with different values of ϵ. All moving averages are taken over a window size of 2. Compare to Figures 2.2, 2.5. For logistic regressions, $p_{\text{value}} < 0.05$ with a positive slope parameter (i.e. frequency of CS increases) for all values of ϵ.

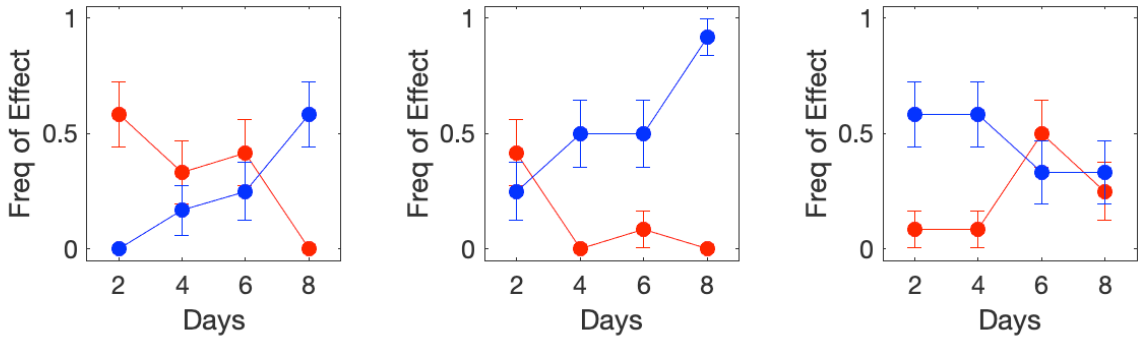

Figure 2.8: **Frequency trends within individual populations do not depend sensitively on threshold criteria for defining collateral effects changes.** Frequency of sensitivity (blue) or resistance (red) for different time points from populations adapted to LZD (left), CRO (middle), and CIP (right) and exposed to CRO (left), DOX (middle), and CRO (right). In this plot, collateral effects are considered significant if errorbars ($\pm$ 1 standard error) do not overlap. See also Figure 2.3 C.

CHAPTER 3

Heterogeneous Collateral Effects in Daptomycin-Adapted Populations of *E. faecalis*

This chapter was reproduced, in part, from the following manuscript, which will be uploaded to bioRxiv and will be submitted for publication after a brief period of feedback from the community: ***A. Huynh**, J. Maltas, and KB Wood, bioRxiv, 2023. doi: Pending.* The initial lab evolution experiments were performed by J. Maltas, as described in the previous chapter. I (AH) performed all other experiments, including all experiments to characterize phenotype and genotype of DAP-isolates and DAP-adapted populations (which make up all figures in this chapter). All authors contributed to experimental design, data analysis, figure design, and manuscript drafts/revisions.

3.1 Introduction

Antibiotic resistance is a growing threat to global health. The development of new antimicrobial drugs is a slow and difficult process, leading to substantial recent interest in evolution-centered strategies with the potential to slow resistance based on judicious–and perhaps unorthodox–deployment of currently available treatments. These treatment strategies exploit interactions between cells and their environment and rely on features such as spatial heterogeneity [18, 19, 20, 21], intercellular cooperation [22, 23, 24, 25], competition between subpopulations [26, 27, 28], and judicious use of drug combinations simultaneously [29, 30, 31, 32, 33, 34, 35, 36] or in temporal cycles [14, 15, 16, 17]. On potentially promising approach is based on the concept of collateral sensitivity–an extension of so-called antagonistic pleiotropy–which, in the case of antibiotics, occurs when a population selected by one drug exhibits increased sensitivity to a different drug. Collateral effects have been a topic of substantial recent interest, with multiple studies pointing to the benfits and potential limitations of this approach [37, 38, 39, 40, 41, 42, 43, 44, 45, 46].

In this work, we offer a case-study of daptomycin resistance–and the corresponding collateral effects–in laboratory-evolved populations of *E. faecalis*, a gram-positive opportunistic pathogen

that underlies a number of human infections[48]. Daptomycin (DAP) is a cyclic lipopeptide antibiotic that targets the cell membrane, where it causes rapid depolarization leading to cell death [93, 94, 95, 96]. Daptomycin is an important therapeutic option for treating multi-drug-resistant infections [97, 98, 99, 100, 101], including vancomycin-resistant enterococci (VRE). However, daptomycin resistance in enterococcus has been increasingly reported in the last decade in both the laboratory and the clinic [113, 132, 133, 134, 135, 136, 137].

Daptomycin resistance in enterococcus has been linked with dozens of genes [138, 52, 134, 139], many associated with multi-component signaling systems such as LiaFSR, which modules the response of the cell membrane to stress [140, 95, 141, 142, 143, 144]. In lab evolution experiments, mutations in the liaFSR system–or putative downstream targets–dominate the early stages of DAP-adaptation, followed by major increases in DAP resistance linked to other genes–for example, those encoding cardiolipin synthase [53, 52]. In strains lacking *liaR*, increasing doses of sub-MIC daptomycin selected for high-cost mutations in an alternative two-component signaling system (YxdJK) [104], which itself has been linked to bacitracin resistance, as well as mutations in a putative dihydroxyacetone kinase (DAK) family enzyme.

Collateral effects arising from daptomycin selection–and selection by a wide range of other antibiotics and environmental stressors [102, 60, 103]–have also been characterized phenotypically and, to a limited degree, genetically. As we saw in the previous chapter, at a global level–when collateral effects from all selecting drugs are considered–collateral profiles appear dynamic, with collateral resistance arising more frequently in early stages of adaptation and collateral sensitivity arising more frequently after longer periods of selection [103]. At the level of individual selecting drugs, however, the patterns are idiosyncratic [103], with some collateral effects matching the global trend (e.g. populations selected by linezolid show increased collateral sensitivity to ceftriaxone (CRO) over time) while other populations show opposing trends (e.g. populations selected by ciprofloxacin show decreasing collateral sensitivity to CRO over time).

In this work, we investigate how collateral effects arise in *E. faecalis* populations selected by daptomycin in laboratory evolution experiments spanning approximately 60 generations. Previous work has shown that isolates selected in daptomycin are characterized by heterogeneous collateral profiles [102, 103]. Most notably, the collateral response to ceftriaxone (CRO), an inhibitor of cell wall synthesis, ranges from resistant to highly sensitive in different isolates. The latter is reminiscent of the so-called "seesaw" effect, an inverse relationship between MICs to glycopeptides or lipopeptides and beta-lactams commonly observed in other Gram-positive species [145, 146, 147, 148, 149]. A similar "seesaw" effect has also been observed in *E. faecalis* [150, 151, 102], and recent work has linked CRO hypersensitivity to DAP-driven mutations in the LiaSFR system [152, 153]. To examine how these collateral effects arise during daptomycin adaptation, we phenotypically and genetically characterized dozens of individual isolates

selected from each of the four daptomycin-selected populations described in Chapter 2. In all populations, we identified isolates with mutations in one or more genes previously associated with DAP resistance, and these isolates are characterized by divergent phenotypic properties–including different levels of DAP resistance and different growth rates (i.e. fitness costs) in drug-free media. Interestingly, we also observed strongly divergent collateral responses to different antibiotics, particularly CRO, with collateral resistance arising in mutants harboring DAP-resistance mutations in cardiolipin synthetase (*cls*) or in genes linked to the two-componenent signaligng sytem YxdJK (*becR* or *ycvR*) [104]. By contrast, mutations in *liaX* arose in two of the four populations, with point mutations associated with CRO-sensitivity and a larger structural mutation associated with extreme CRO-sensitivity and a dramatically reduced growth rate. Our results reveal that multiple daptomycin-resistant lineages can emerge even in simple lab evolution protocols, reveal considerable phenotypic differences in mutations targeting the LiaSFR system, and highlight trade-offs between resistance to daptomycin, collateral profiles (most notably to CRO), and drug-free growth rates (fitness costs) in evolving lineages.

3.2 Results

3.2.1 Heterogeneous daptomycin resistance in DAP-selected populations

To investigate daptomycin resistance in the lab, we focused on four daptomycin-adapted populations described in Chapter 2. Briefly, we exposed four independent populations (each from a single colony of the ancestral V583 strain) to increasing concentrations of daptomycin over 8 days with 1:200 daily dilutions (Figure 3.1). Each day, 3 vials–each at a different DAP concentration, with concentrations spanning sub- and super-MIC levels–were seeded with dilutions from the previous day's population. At the end of the day, the sample that survived in the highest concentration was propagated on to the next day, where 3 new concentrations were chosen (typically one-half, 2x and 4x the highest concentration with growth from the previous day; see Methods in Chapter 2). Despite using a similar protocol to increase DAP concentration in each adaptation experiment, the variable responses of the 4 populations led to distinct differences in the DAP survival concentration (defined here as the highest concentration of DAP for which a given lineage survived each day) over time (Figure 3.1). In previous work, single isolates from these populations, along with those adapted to other drugs, were used to characterize collateral effects to a large library of antibiotics and other stressors [102, 60, 103]. Among a collection of collateral profiles, the single isolates selected from these four DAP-selected populations stood out as being particularly heterogeneous and dynamic over time.

To characterize these adapting lineages, we isolated 12 single colonies from each of the four

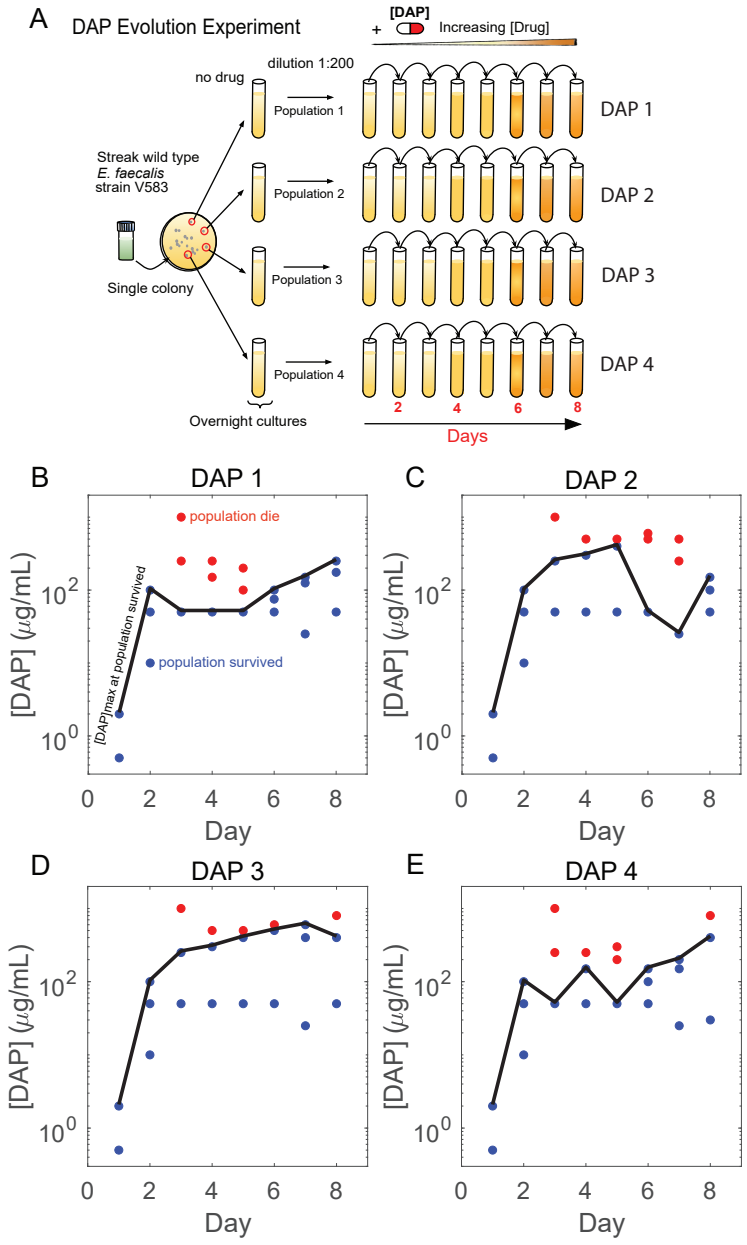

Figure 3.1: **Evolution of daptomycin resistance in the lab.** A) Schematic of laboratory evolution experiment with *E. faecalis* strain V583 treated with Daptomycin (DAP). The overnight cultures were exposed to (typically) increasing concentrations over an 8-day serial-passage with daily dilutions of 1:200. B) Panels B to E show trajectories of the 4 DAP populations ; black curves represent the survival concentration (defined here as the highest concentration of DAP for which a given lineage survived each day); blue (red) circles represent viable (non-viable) populations, as inferred from turbidity (see Methods, Chapter 2).

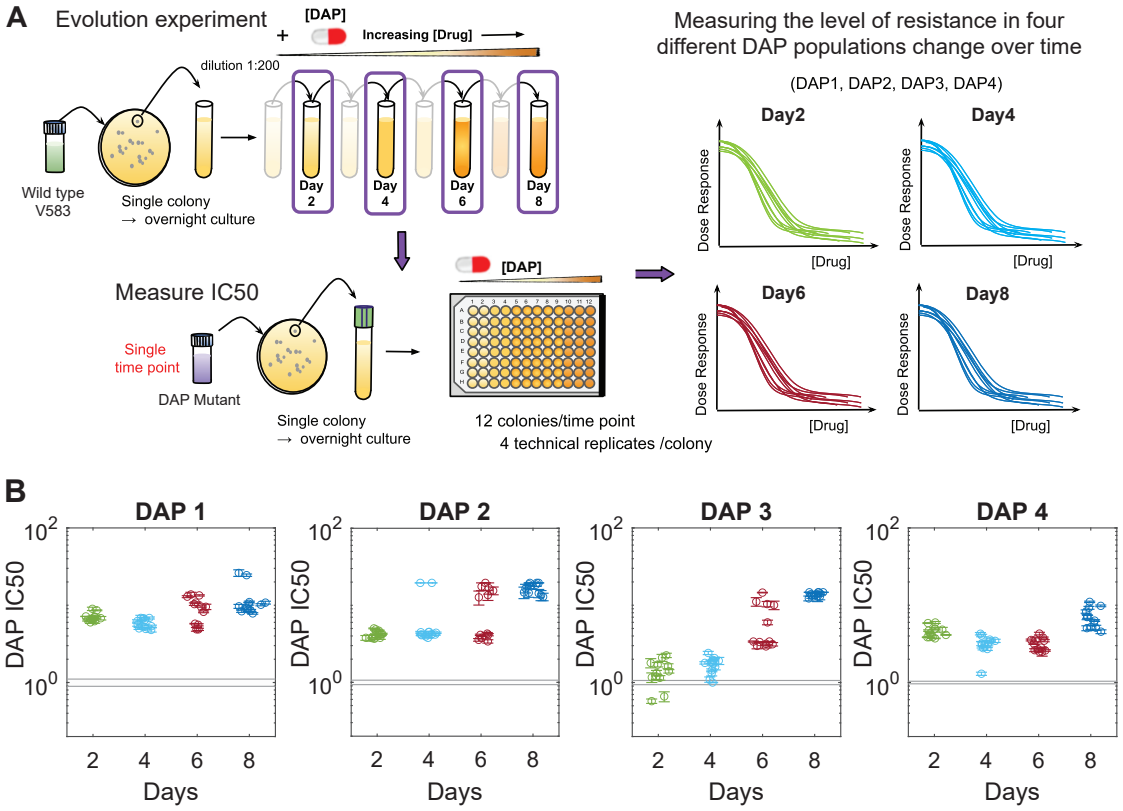

Figure 3.2: **Daptomycin resistance is heterogeneous and dynamic within individual populations** A) Dose-response curves (in technical replicates of 4) for twelve isolates from each DAP-evolved population (DAP-1 to DAP-4) at four different time points (days 2, 4, 6, and 8) were used to estimate IC50 to daptomycin. B) Daptomycin IC50 for each isolate, normalized by the IC50 of a collection of ancestral populations measured on the same day, over time for each of the four populations. Shaded region shows precision (± 3 standard error) of IC50 estimates in the ancestral control isolates. Isolates above the shaded region are considered DAP-resistant, while those below the shaded region exhibit increased DAP-sensitivity. Individual points represent the mean IC50 (± standard error from 4 technical replicates) for a single colony.

DAP populations at 4 different time points (days 2, 4, 6, and 8) and estimated the IC50 to DAP for each isolate from dose response curves (measured in technical replicates of 4). Despite similar evolution protocols, we found that resistance to DAP varied across the four populations 3.2. In three of the populations (DAP1, DAP2, DAP3), we observed substantial DAP resistance by day 2, while isolates from DAP3 did not achieve comparable levels of resistance until day 6. In addition, the distribution of IC50's varies across time, within individual populations, as well as across populations. Interestingly, these distributions appear bimodal at several time points, suggesting that multiple resistant lineages may be present–at substantial fractions– simultaneously.

3.2.2 Collateral effects to CRO vary dramatically across and within populations

Given the range of DAP-resistance in isolates, we next asked how the collateral effects to CRO change within and across populations. To estimate the distribution of collateral effects, we measured dose response curves to CRO for each of the previously selected isolates along with 36 additional isolates from each of the four time points for population DAP-1. Indeed, we found substantial variability in CRO sensitivity across isolates (Figure 3.3). In two of the four populations (DAP3 and DAP4), we observed low-levels of CRO resistance by day 2, with the distribution shifting slightly towards increased CRO resistance over time. By contrast, a substantial fraction of isolates in populations DAP1 and DAP2 were collaterally sensitive to CRO on day 2. In DAP-1, the distribution drifts to higher CRO resistance levels over time, though a subpopulation of highly CRO sensitive isolates–with decreases in IC50 of nearly 100 fold relative to the ancestral strain–emerges and is particularly noticeable by day 8. Surprisingly, the DAP2 population is dominated by the hyper-sensitive isolates even on day 2, and collateral sensitivity remains high throughout. These results suggest that the evolution of collateral effects in response to DAP exposure exhibits rich dynamics, even on relatively short timescales.

3.2.3 Idiosyncratic covariation of DAP and CRO resistance across populations

We also visualized the covariation of DAP and CRO resistance in a subset of individual isolates from the four DAP-selected populations (Figure 3.4). We found a range of different dynamics in the 2-d space of IC50s. Populations DAP1 and DAP4 are characterized by IC50 distributions whose mean drifts towards increased resistance to both drugs over time, though DAP1 includes a highly CRO-sensitive subpopulation by day 8. DAP2 isolates move toward increasing DAP resistance and decreasing CRO resistance, while DAP3 isolates show increasing DAP resistance but relatively little change in CRO resistance (which is low-level collateral resistance) over time.

3.2.4 Population and single-isolate genome sequencing reveals varied combinations of mutations in genes associated with DAP resistance.

To investigate the genetic underpinnings of the varied daptomycin-resistance dynamics, we performed population sequencing on each of the four populations over time and also sequenced the full genomes of 40 individual isolates. Despite the simplicity of the laboratory evolution, we observed a surprising diversity of DAP-R mutations across different populations (Figure 3.5). We identified a number of mutations in genes previously linked to DAP resistance (Table 3.1), and we

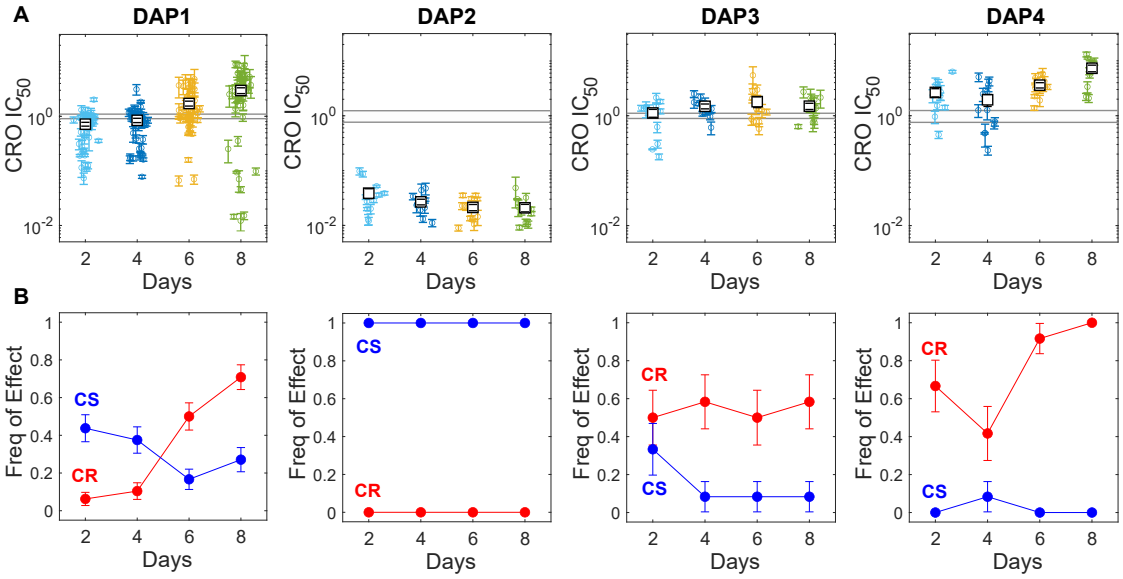

Figure 3.3: **Collateral CRO profiles differ markedly across and within DAP-selected populations.** Dose-response curves (in technical replicates of 4) for 48 isolates at four different time points (days 2, 4, 6, and 8) from population DAP1 along with 12 isolates at four time points for populations DAP2-DAP4 were used to estimate IC50 to ceftriaxone (CRO). A) CRO IC50 for each isolate, normalized by the CRO IC50 of a collection of ancestral populations measured on the same day, over time for each of the four populations. Shaded region shows precision (± 3 standard error) of IC50 estimates in the ancestral control isolates. Isolates above the shaded region are considered CRO-resistant, while those below the shaded region exhibit increased CRO-sensitivity. Individual points represent the mean IC50 (± standard error from 4 technical replicates) for a single colony. B) Frequency of collateral effects in individual isolates over time in four different DAP populations, with collateral sensitivity (CS) represented in blue and collateral resistance in red (CR).

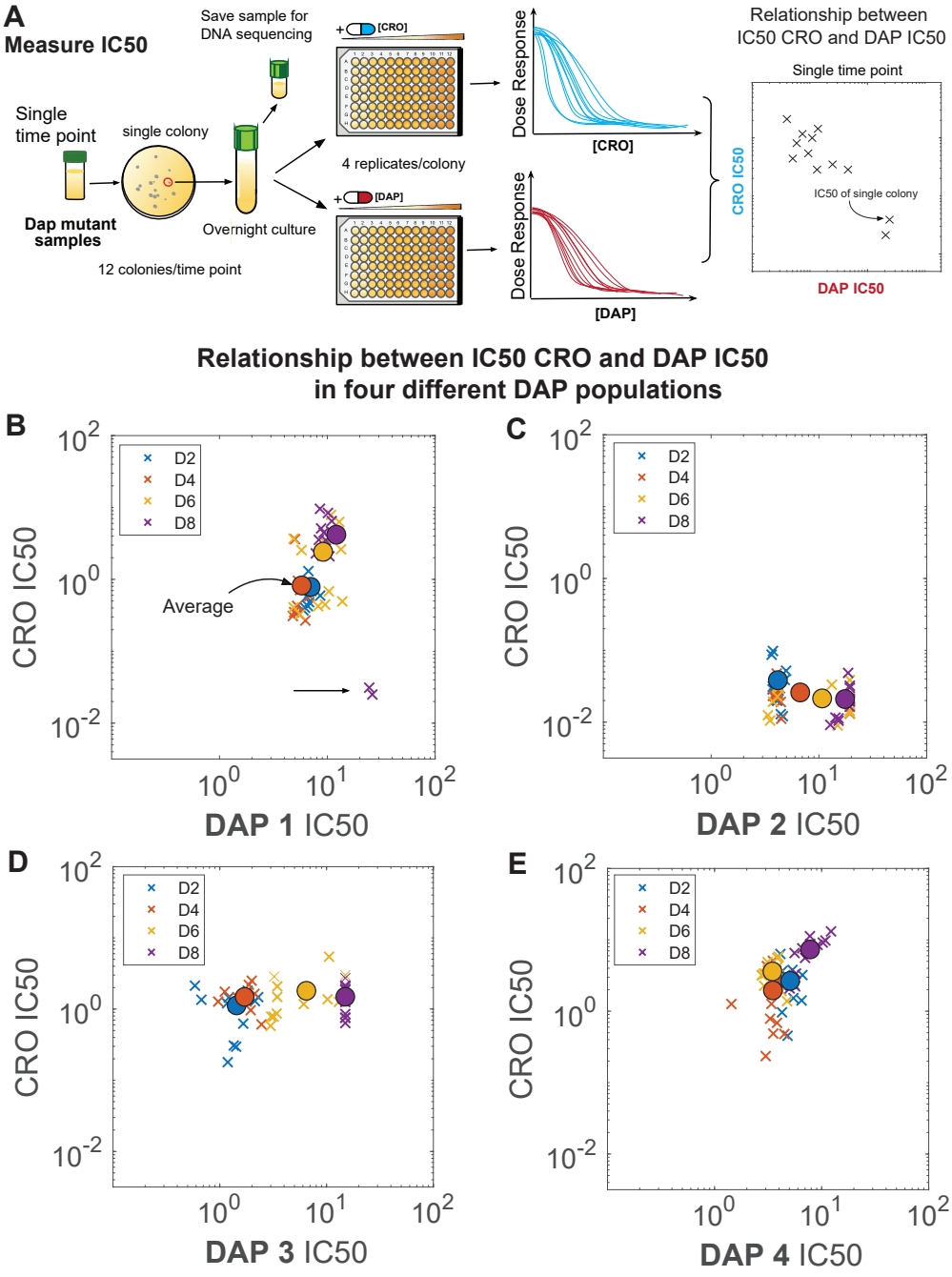

Figure 3.4: **Co-variation of DAP and CRO resistance across populations.** SA) Schematic of measuring covariation in CRO and DAP resistance in four different DAP-adapted populations. For each time point, dose-response curves for both CRO and DAP (each in technical replicates of 4) were measured for 12 isolates. B) IC50s for each drug are normalized by IC50 values in a collection of ancestral isolates measured on the same day. The IC50 of a single colony is represented by an x, while the population average of 12 colonies is represented by a circle. Isolates from day 2 are in blue, from day 4 are in orange, from day 6 are in yellow, and from day 8 are in purple.

found that different combinations of these mutations accumulated over time in different populations.

In three of the four populations (DAP1, DAP2, DAP3), mutations in the liaFSR occurred within the early stages of adaptation, consistent with previous findings [53, 52]. Point mutations in the gene *liaX* swept to fixation in population 1 but occurred only at low frequency in DAP3. We also identified larger IS256-mediated structural mutations in *liaX* in DAP1 and DAP2–and in the latter case, this structural mutant (which we refer to as *liaXs*) swept to fixation over time, while it remained a low-frequency variant in DAP1.

We also observed multiple DAP-R mutations not directly linked with liaFSR. In populations DAP1 and DAP3, lineages characterized by point mutations in *becR*, a gene associated with the two-component signaling system YxdJK previously linked with resistance to bacitracin and found in DAP-adapted strains lacking the liaFSR system [104], appeared to out-compete the initial *liaX* mutants. In DAP3, these *becR* lineages split into two competing lineages, one that acquired an additional mutation in *dgk*, a gene encoding a putative kinase involved in lipid metabolism, and a second with mutations in both *liaF* (from the liaFSR system) and *cls*. The mutation in *dgk* is reminiscent of similar adaptations previously seen in a dihydroxyacetone kinase (DAK) associated with lipid metabolism [104]. Mutations in cardiolypin synthetases, such as those in the *cls* gene, have also been commonly linked with DAP resistance [52]. Finally, in DAP4, a lineage dominated by a double mutant–with mutations in *ycvR* and EF1733 (a putative ABC transporter)– rose to high frequencies by day 6. This lineage later acquired mutations in *cdsA*, a C39 family peptidase linked with DAP resistance in other Streptococcus species [154], and subsequently in *dgk*. Finally, we observed mutations in *parB*, associated with chromosome or plasmid segregation but not, to our knowledge, with DAP resistance, at 4 different time points (days 2 and 6 of DAP2; days 2 and 4 of DAP4). While the pattern of their appearance, as well as the fact that these variants did not appear in any of the 40 individual isolates, suggests they may be spurious variant calls, we keep them here for completeness and because they appeared in multiple populations.

Table 3.1: **Mutations identified in selected populations.**

Locus Tags	Gene Names	Descriptions
EF1753	*liaX*	daptomycin-sensing surface protein *liaX*, part of LiaFSR 3-component signaling system
EF2913	*liaF*	cell wall-active antibiotics response protein *liaF*
EF0727	*dgk*	Diacylglycerol kinase catalytic domain protein
EFRS15620	*parB*	Family partition protein
EF0926	*becR*	DNA-biding response regulator/Two-component system HK-RR09
EF1608	*cls*	Cardiolipin synthetase
EF1733		ABC transporter
EF2752	*yvcR*	ABC transporter, ATP-binding protein
EFRS00550	*cdsA*	C39 family peptidase/hypothetical protein

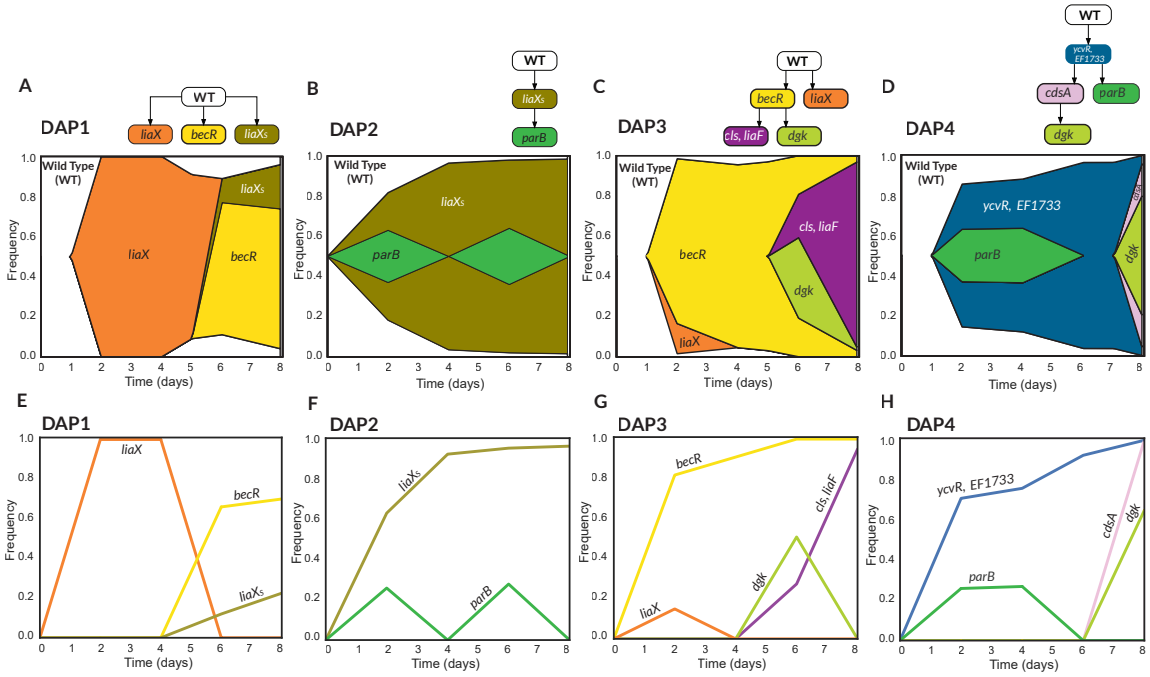

Figure 3.5: **Evolutionary dynamics of V583 evolving Daptomycin through independent evolution experiments.** Panels A–D correspond to the genotype tree and Muller plots for each DAP-adapted population over time. Panels E-H display individual genotype frequencies corresponding to each Muller plot. Muller plots were calculated from population sequencing data using the Lolipop pipeline, which is described in [1] and available on GitHub. See also Table 3.1 for a description of different mutations and Figure 3.8.

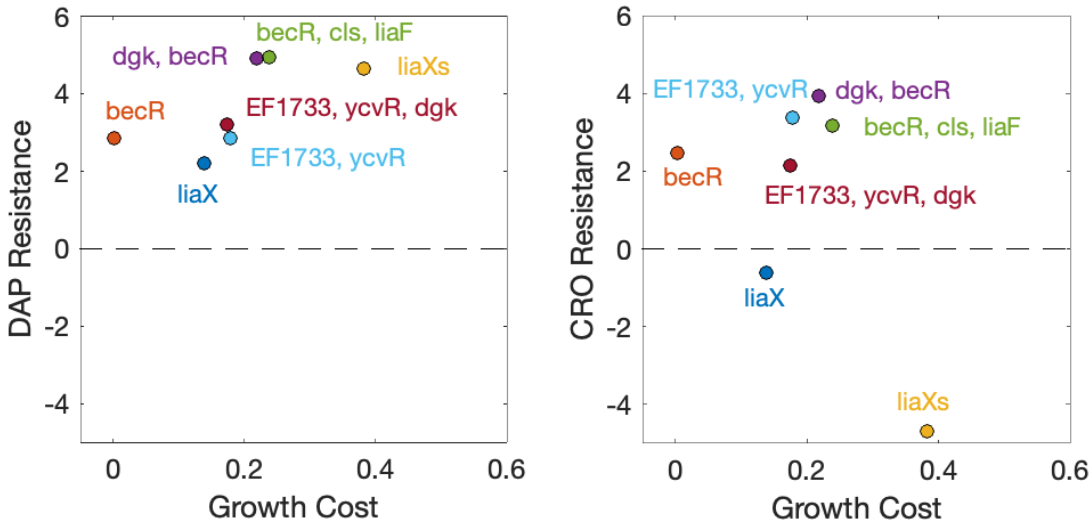

Figure 3.6: **Mutations and growth costs in isolates from different DAP-adapted populations** DAP resistance (left) and CRO resistance (right) vs growth cost for isolates representing each of the 7 observed mutants. Resistance is defined as the (log2-transformed) fold change in IC50 relative to the ancestral strain; positive values represent increased resistance, while negative values represent increased sensitivity. Growth cost is defined as the fractional decrease in maximum growth rate when strains are grown in drug-free media. The mutants include 3 single gene mutants (mutations in *becR* and two different mutations in *liaX*, a single nucleotide variant and an IS256-mediated insertion variant, the latter of which we designate by using an "s" suffix), 2 double mutants (mutations in *dgk* and *becR*; or in EF1733 and *ycvR*), and 2 triple mutants (mutations in *becR*, *cls*, and *liaF*; or in *becR*, *cls*, and *liaF*).

3.3 DAP-R mutant exhibit diverse range of resistance levels and fitness costs.

The genome sequencing reveals a surprisingly complex collection of evolutionary trajectories that include different combinations of individual mutations. However, it is not clear how a given combination of mutations are related to phenotypic properties of a given mutant. To investigate this question, we measured drug-free growth rate as well as DAP- and CRO-resistance (IC50) levels for isolates representing seven different mutant "classes" which were found among the 40 single-colony isolates. These mutants include 3 single gene mutants (mutations in *becR* and two different mutations in *liaX*, a single nucleotide variant and an IS256-mediated insertion variant, the latter of which we designate by using an "s" suffix), 2 double mutants (mutations in *dgk* and *becR*; or in EF1733 and *ycvR*), and 2 triple mutants (mutations in *becR*, *cls*, and *liaF*; or in *becR*, *cls*, and *liaF*).

We found that the different mutant classes exhibit considerable differences in drug-free growth rate (referred to here at "growth cost", see Methods), direct resistance levels to DAP, and collateral resistance levels to CRO (Figure 3.6; see also Figures 3.7). DAP resistance is weakly correlated with growth cost (Figure 3.6, left panel), with a double (*dgk, becR*) and a triple (*becR, cls, liaF*) mutant from DAP3 showing the highest levels of DAP resistance and elevated costs, while single mutants (*becR* and *liaX*) show lower levels of DAP-R but also decreased cost. Interestingly, the largest cost was associated with the structural (IS256-mediated insertion) mutation in the *liaX* gene; these mutation dramatically increased both resistance to DAP and the growth cost relative to the single nucleotide variant. In addition, all mutations outside of *liaX* showed small to moderate levels of collateral resistance to CRO. By contrast, mutations in *liaX* were associated with collateral sensitivity, with the IS256-mediated insertion mutant displaying extremely high levels of CRO sensitivity. These results are consistent with recent work linking CRO hypersensitivity to DAP-driven mutations in the LiaSFR system [152, 153] and, separately, to recent work indicating that phage or antibiotic stress can drive rapid genome-scale transposition in enterococci, including in *E. faecium* from human patients treated with daptomycin [155]. Our results complement these findings by showing how IS256-mediated genomic changes substantially increases collateral sensitivity and modulate the growth costs associated with *liaX* mutations in response to DAP pressure.

3.3.1 Disparate growth costs and resistance levels favor different mutants at low and high DAP concentrations.

In population DAP1 at days 6 and 8 we observed coexisting mutants (mutation in *becR* and IS256-mediated insertion in *liaX*, which we denote with subscript "s") with substantial differences in DAP IC50s and growth costs (Figure 3.5 and Figure 3.6). To further characterize these competing lineages, we measured growth rates of each at multiple concentrations of DAP as well as 3 additional antibiotics (DOX, CIP, LZD). Consistent with the previous end-point IC50 measurements (Figure 3.6), we found that the two mutants exhibit considerable differences in growth rate as function of DAP, with the becR mutant showing increased growth at low DAP concentrations–a result, in part, of its smaller fitness cost–while the *liaXs* mutant has a growth advantage at DAP concentrations greater than about 40 ug/mL (Figure 3.7).

On the other hand, the *becR* mutant tends to show increased growth (relative to the *liaXs* mutant) in the presence of other drugs, consistent with the opposing collateral effects we saw for CRO based on end-point measurements. While growth of becR mutants in the presence of CIP and LZD is similar to that of WT cells over most concentrations tested, the increased growth cost associated with *liaXs* leads to a substantial reduction in growth at low levels of CIP and LZD (Figure 3.7). In addition, both mutants are strongly sensitized to doxycycline, with growth rates nearing zero at concentrations largely sub-inhibitory in the wild type (ancestral) cells.

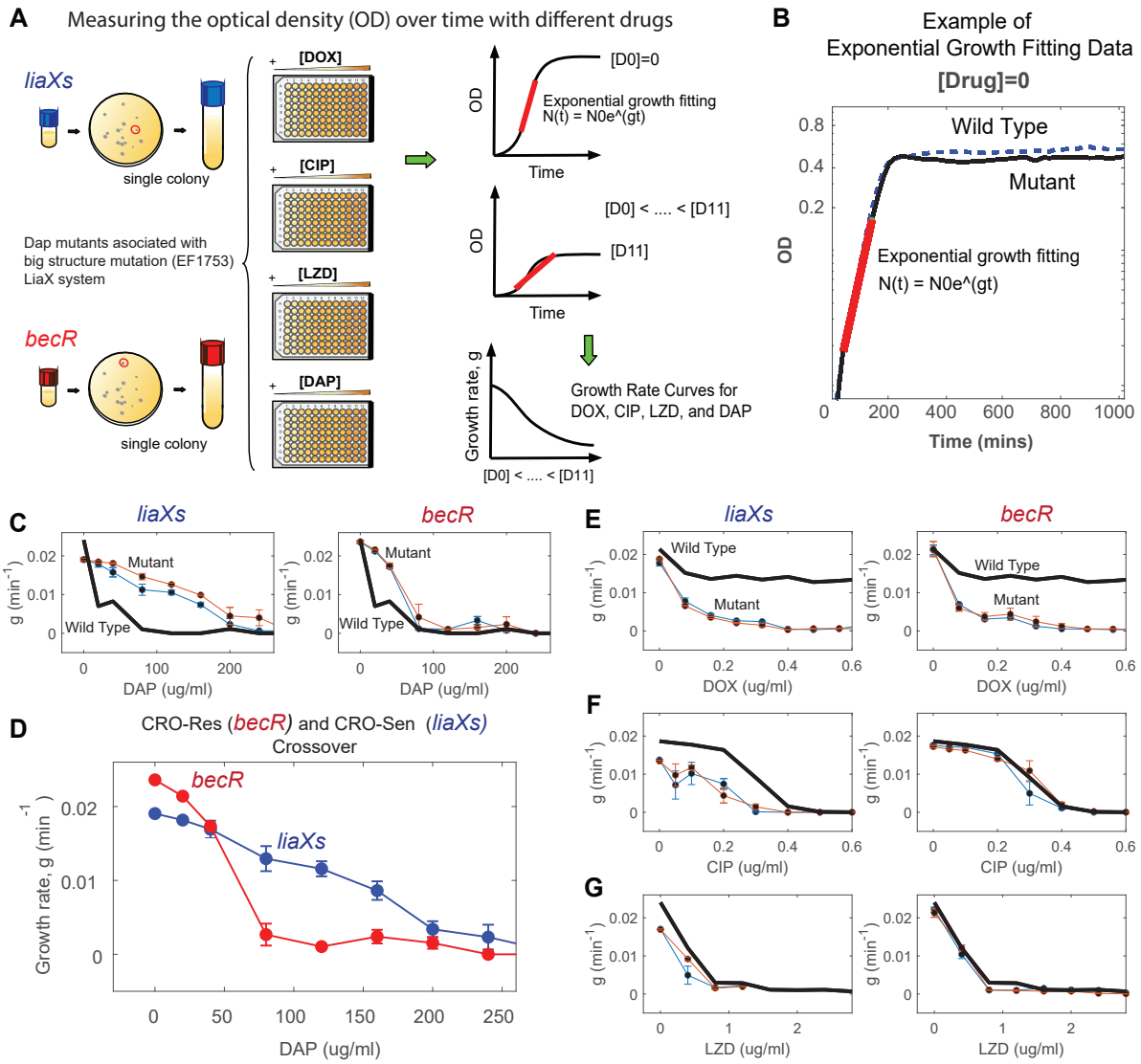

Figure 3.7: **Effects of different antibiotics on growth rates of *liaX*$_S$ and *becR* mutants.** A) Schematic of the measurement of per capita growth rate from optical density time series in two isolates isolated from DAP1 populations. The first isolate has a large structural mutation in EF1753 (denoted *liaX*$_S$); the second isolate has a point mutation in a repressor (*becR*) linked to the regulatory system YxdJK. B) Per capita growth rate was estimated from time series of optical density in exponential phase using nonlinear least squares fitting. Red line: example growth rate fits for two isolates with similar growth rates (blue and black curves). C) Per capita growth rate as a function of daptomycin (DAP) Black curves show growth of ancestral (WT) population. Individual points are the means over 4 technical replicates, with errorbars plus/minus 1 standard error. D) Growth rate dose-response curves are characterized by low-DAP regimes where *becR*-mutant grows faster and high-DAP regimes where *liaX*$_S$-mutant grows faster. The crossover point occurs at a DAP concentration of approximately 40 ug/ml. E-G) Same as C, per capita growth rate as a function of doxycycline (DOX, upper panel), ciprofloxacin (CIP, middle panels), and linezolid (LZD, lower panels) for *liaX*$_S$-mutant (left column) and *becR*-mutant (right column).

3.4 Discussion

Daptomycin is one of the last defenses against infections caused by multi-drug resistant bacteria, and the increasing prevalence of daptomycin resistance poses obstacles to the effective treatment of these infections. The results reported here add to our growing understanding of the molecular and genetic underpinnings of daptomycin resistance. Despite the relatively simple adaptation protocol–one performed under well-controlled laboratory conditions that are substantially simplifications of the natural environments faced in vivo–the evolution of daptomycin resistance is surprisingly complex and, in four independent populations, followed four largely distinct evolutionary pathways to resistance.

Our results complement, and are consistent with, a number of studies on daptomycin resistance that identified most of the mutational targets we observed [138, 52, 134, 139, 140, 95, 141, 142, 143, 144, 53]. Collateral effects have been explored in much less detail, though the collateral sensitivity we observe is consistent with the "seesaw" effect observed with glycopeptides or lipopeptides and beta-lactams in other Gram-positive species [145, 146, 147, 148, 149]. A similar "seesaw" effect was recently reported in *E. faecalis* [150, 151, 102]. Most notably, recent work (including a PhD thesis and seminar abstract) has linked CRO hypersensitivity to DAP-driven mutations in the LiaSFR system [152, 153], and we are hopeful that their continued efforts will lead to a deeper understanding of the molecular basis of this collateral sensitivity.

Collateral effects have also been reported in isolates of a related enterococcal species (*E. faecium*), which acquired sensitivity to other drugs when evolved in the lab in the presence of daptomycin [156]. They found daptomycin resistant mutations associated with the liaFSR, *yycFG*, and *cls* genes, all of which were associated with fitness costs. Additionally, they observed daptomycin resistant mutants with increased collateral sensitivity to the glycopeptide antibiotic vancomycin due to a large-scale insertion mediated by the IS1216E-transposon. Our results include a similar IS-mediated insertion–this time in *liaX*–and similar insertion events have been recently observed in *E. feacalis* populations under phage stress and in *E. faecium* from daptomycin-treated patients [155], suggesting that transposon-mediated dynamics play an important role in maintaining genome plasticity of enterococci.

Similar results–most notably, mutations involving the cls gene and those associated with the LiaSRF system [156, 138, 55], have also been observed in the clinic. In one example, researchers isolated strains of *E. faecalis* from a patient with fatal bacteremia before and after treatment with DAP. They found mutations associated with the liaF gene, cls, and GdpD (an enzyme also involved in phospholipid metabolism) [138]. Similarly, Woods and colleagues [55] found daptomycin resistance in *E. faecium* can evolve via multiple separate evolutionary pathways in patients, with most strains harboring mutations associated with the cardiolipin synthase (clsA) gene. Daptomycin re-

sistance was also shown to arise in off-target gut-associated populations during intravenous treatment [137].

Our results illustrate how DAP-R mutations can arise in different combinations, even under similar environmental pressures, and lead to different effects of fitness and collateral profiles. The work highlights several challenges, and potential opportunities, for applying collateral sensitivity in the clinic. In particular, it highlights that steering evolution down particular daptomycin-resistant pathways–in this case, pathways targeting the *liaX* gene–may lead to strong collateral sensitivities, opening the door to drug-switching strategies that target populations at their most vulnerable. On the other hand, we also showed that treatment with daptomycin under very similar conditions led to highly variable evolutionary trajectories across replicate populations. It is not clear the extent to which this variability is specific to daptomycin, which targets that cell membrane and may therefore be susceptible to a wide range of resistance mechanisms that module membrane composition and homeostasis. In addition, our adaptation experiments were performed in relatively small populations–potentially much smaller than those in the gut of human hosts. Previous work in chemostats [53, 104]–using larger populations–has indeed shown that daptomycin resistance occurs via a relatively predictable sequence, and it would be interesting to probe daptomycin adaptation at intermediate population sizes between these two extremes. In any event, harnessing these (apparently) stochastic trajectories may require application of advanced control-theoretic approaches, some of which have been recently applied to steering evolution [102, 66]. Future work may be able to exploit the fitness costs associated with certain genes to design more effective control strategies to steer evolution along clinically beneficial trajectories.

3.5 Methods and Materials

3.5.1 Strains, growth conditions, and drugs

Evolution experiments were conducted using the *E. faecalis* strain V583 and the resistance was derived from the same strain. Samples were stocked in 30% glycerol and stored at -80 C. Cultures for experiments were taken from single colonies grown on agar plates and then inoculated at 37^o C overnight before dilution in fresh media and the beginning of the experiment. All experiments and dose-response measurements were conducted in Brain-Heart Infusion or BHI (Remel). Drug stock solutions were prepared from powdered stock and stored at -20^o C in single-use aliquots. All experiments with daptomycin were supplemented with 20 μg/mL Ca^{2+}.

Table 3.2: **Antibiotics used in chapter 3.**

Drug Name (Abbreviation)	Supplier	Mechanism of Action
Ceftriaxone Sodium (CRO)	Sigma Aldrich	Cell wall synthesis inhibitor
Ciprofloxacin, 98% (CIP)	Acros Organics	DNA gyrase inhibitor
Daptomycin (DAP)	Acros Organics	Cell membrane insertion
Doxycycline Hydrochloride (DOX)	Reseach Products International	30S protein synthesis inhibitor
Linezolid, 98% (LZD)	Acros Organics	50S protein synthesis inhibitor

3.5.2 Measuring drug resistance

To measure IC_{50}, a sample acquired from the evolution experiment was streaked on a BHI Agar plate. From there, a single colony was selected and used for inoculation and incubated at 37° C overnight. Cells were then exposed to a drug concentration gradient, differing among each of the 12 wells on the plate, and the experiment was prepped in a BHI media with a total volume of 205 µL (200 µL of BHI, 5 µL of 1.5 OD cells) per well. Following 16 hours of growth at 37° C, OD at 600 nm (OD600) was measured with an Enspire Multimodal Plate Reader (Perkin Elmer). An IC_{50} measurement was taken for 12 colonies and each with 3 replicates.

In order to quantify the values for drug resistance, OD measurements for each drug concentration were normalized by OD measurements without the drug, and the dose-response curve was then fit to a Hill function ($g(d) = (1 + (d/k)^h)^{-1}$), with d the drug concentration, k the IC_{50}, and h the Hill coefficient.

3.5.3 Estimating growth costs

Growth costs were estimated by fitting time-series of optical density (for isolates grown in drug-free media) to a logistic growth function [157] given by $g(t) = g_0 +$

$K\left(1+\exp(4\mu(\lambda-t)/K+2)\right)^{-1}$, where μ is the maximum specific growth rate, λ is the lag time, and K is the carrying capacity. The fitness cost (c) is then defined as $c = 1 - \mu/\mu_{wt}$, where μ_{wt} is the maximum growth rate of the ancestral (WT) strain.

3.5.4 Whole-genome sequencing

To see if there are any genomic changes that influence the measurement of collateral phenotypes, we sequenced 40 individual colonies that evolved Dap mutants and 2 V583 ancestors for a control. Illumina Short Read sequencing (400 Mbp / 2.7 million reads) and DNA isolation were performed by the Microbial Genome Sequencing Center (MiGS) at the University of Pittsburgh. We also performed population level sequencing (2000Mbp/13.3 Million reads) on samples drawn from days 2, 4, 6, and 8 from each population (performed at SeqCoast Genomics).

The resulting genomic data was analyzed using the high-throughput computational pipeline breseq [158, 159], with default settings (and using polymorphism mode for population sequencing). Briefly, genomes were trimmed and subsequently aligned to *E. faecalis* strain V583 (Accession numbers: AE016830 - AE016833) via Bowtie 2. A sequence read was discarded if less than 90 percent of the length of the read did not match the reference genome or a predicted candidate junction. At each position a Bayesian posterior probability is calculated and the log10 ratio of that probability versus the probability of another base (A, T, C, G, gap) is calculated. Sufficiently high consensus scores are marked as read alignment evidence (in our case a consensus score of 10). Any mutation that occurred in either of the 2 control V583 strains was filtered from the results.

For population sequencing, we removed any variants that did not occur at a frequency of greater than 25 percent on at least one day. For simplicity, in the figures in the main text we also removed variants if they were either 1) not observed in any single isolates and 2) had not previously been linked with DAP resistance. Detailed Muller plots containing these additional mutations is shown in Figure 3.8. To make Muller plots, we used the Lolipop pipeline, which is briefly described in [1] and available on GitHub (https://github.com/cdeitrick/Lolipop).

3.5.5 Long-read sequencing to confirm structural mutations.

We confirmed the large-scale IS256 mediated structural mutations in liaX arising in population 2 using long-read Nanopore sequencing ([160]). Genome assemblies and sequencing were performed by MiGS according to the following: Quality control and adapter trimming was performed with bcl-convert and porechop for Illumina and ONT sequencing respectively; hybrid assembly with Illumina and ONT reads was performed with Unicycler; assembly statistics were recorded with QUAST and assembly annotation was performed with Prokka (Default Parameters + '–rfam').

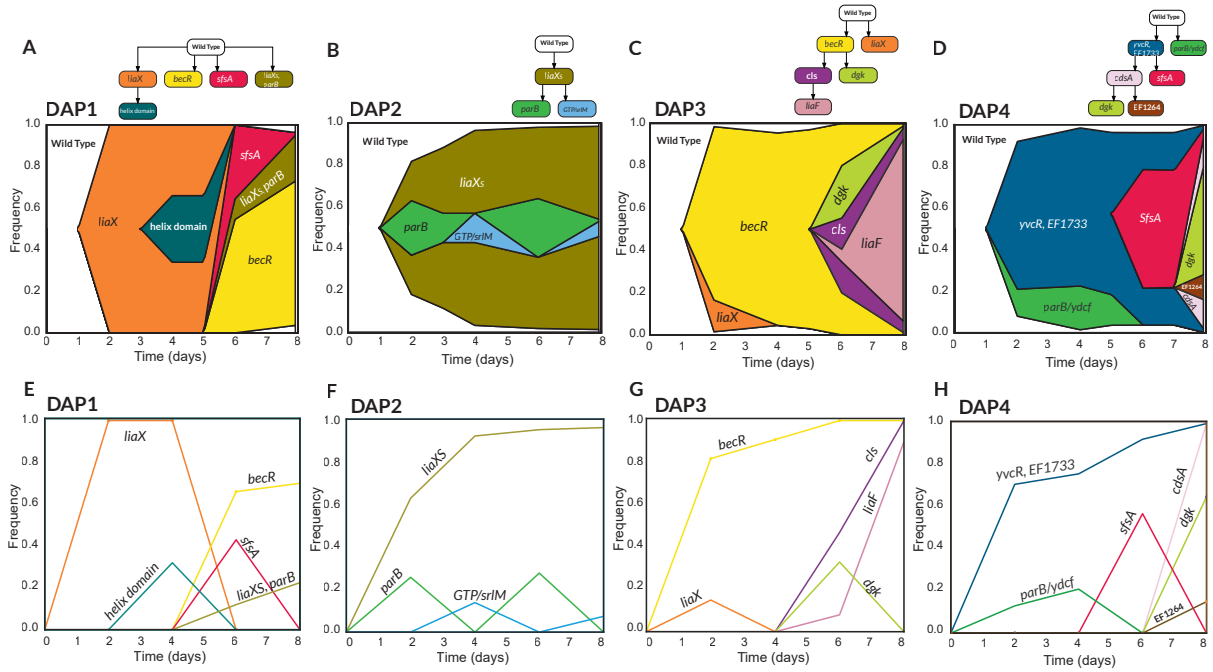

Figure 3.8: **Muller plot from all mutations**. Panels A–D correspond to the genotype tree and muller plots for each DAP population during evolution. Panel E-H plots individual genotype frequencies corresponding to each Muller plot.

3.6 Supplemental Figures

This section contains 4 supplemental figures referenced throughout the text

Table 3.3: **Additional mutations observed in population sequencing.**

Locus Tags	Gene Names	Descriptions
	Helix domain	Helix-turn-helix domain-containing protein
	sfsA	DNA/RNA nuclease SfsA
EFRS15670	GPT /*srlM*	Putative transcriptional activator
EFRS08000	*ydcf*	YdcF family protein
EF1264		Sulfatase domain protein / lipoteichoic acid synthase

The top boxes show simple mutations (like point mutations). The bottom box lists genes that could have large structural mutations in them. Yellow and green mean the genes are known to give DAP resistance.

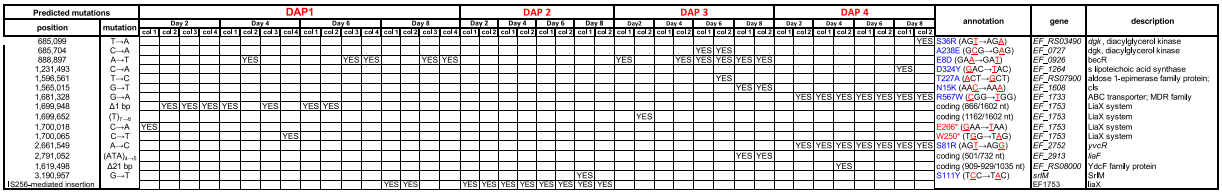

Figure 3.9: **DAP mutaions**. Mutations in 40 individual isolates from DAP1-DAP4 on different days.

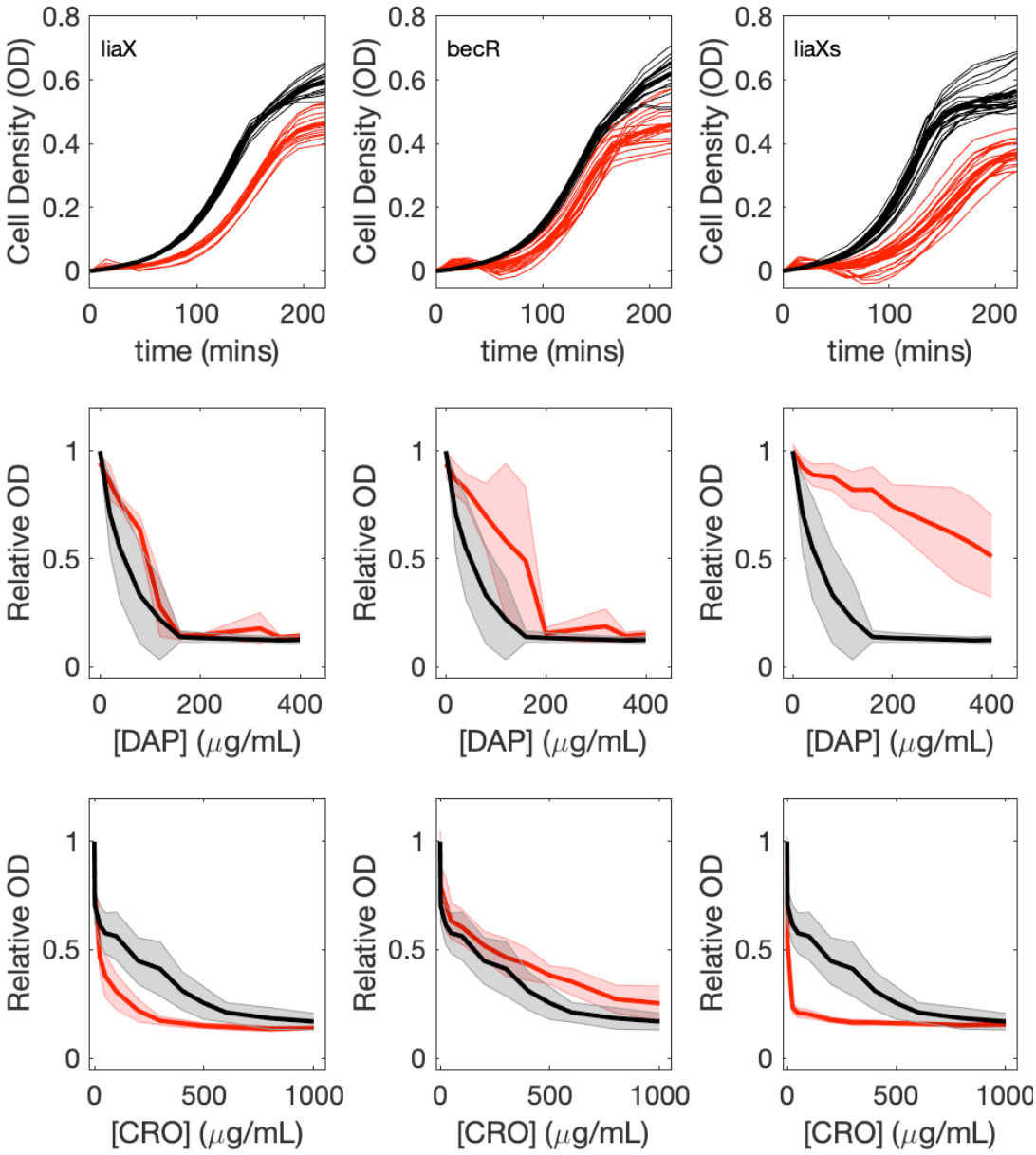

Figure 3.10: **Drug-free growth curves and dose-response curves for single DAP-resistant mutants.** The wild type (sensitive) is represented by black curves and the mutants are represented by red curves.

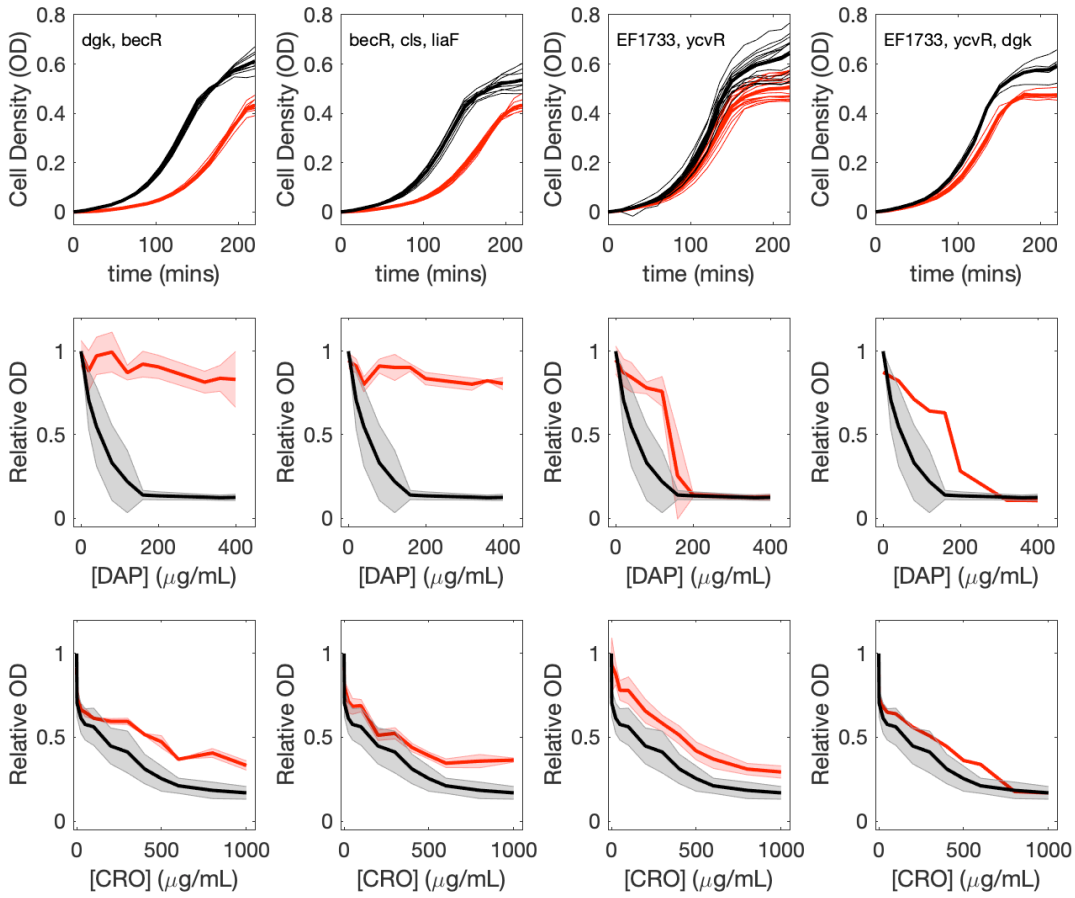

Figure 3.11: **Drug-free growth curves and dose-response curves for double and triple DAP-resistant mutants.** The wild type (sensitive) is represented by black curves and the mutants are represented by red curves.

Part II

Evolution and Competition in Multi-Strain Communities

CHAPTER 4

Interplay of Spatial Heterogeneity and Migration Modulate Evolution of Resistance in a Microbial Metacommunity

This chapter was reproduced, in part, from the following manuscript, which will be uploaded to bioRxiv and will be submitted for publication after a brief period of feedback from the community: ***A. Huynh****, A. Sharma, M. De Jong, and KB Wood, bioRxiv, 2023. doi: Pending.* A. Sharma and M. De Jong were important contributors to the initial design of this project, including the setup and initial calibration of the bioreactors used throughout. I (AH) performed all experiments shown in this chapter. All authors contributed to experimental design, data analysis, figure design, and manuscript drafts/revisions.

4.1 Introduction

The crisis of antibiotic resistance is continuing to increase at an alarming rate [7, 8, 9, 10]. While many remarkable discoveries at the molecular level have helped us understand the underlying molecular mechanisms that give rise to resistance [161, 162, 163, 164], it remains challenging to translate this understanding into therapies that combat resistance, in part because of the complexity of natural and clinical environments. For example, while the majority of studies focus on bacteria populations in well-mixed environments [165, 166, 167], in nature bacterial populations often are comprised of interacting "subpopulations" and live in heterogeneous environments. Natural communities evolve on spatially extended habitats that potentially yield complicated networks of interacting subpopulations [168], and understanding the role of this spatial structure in the evolution of resistance is an ongoing challenge.

A large body of theoretical work has investigated the impact of spatial heterogeneity on ecological and evolutionary dynamics in a wide range of contexts–from the spread of COVID [169] to conservation ecology [170]. Numerous elegant approaches exist for studying multi-habitat models on

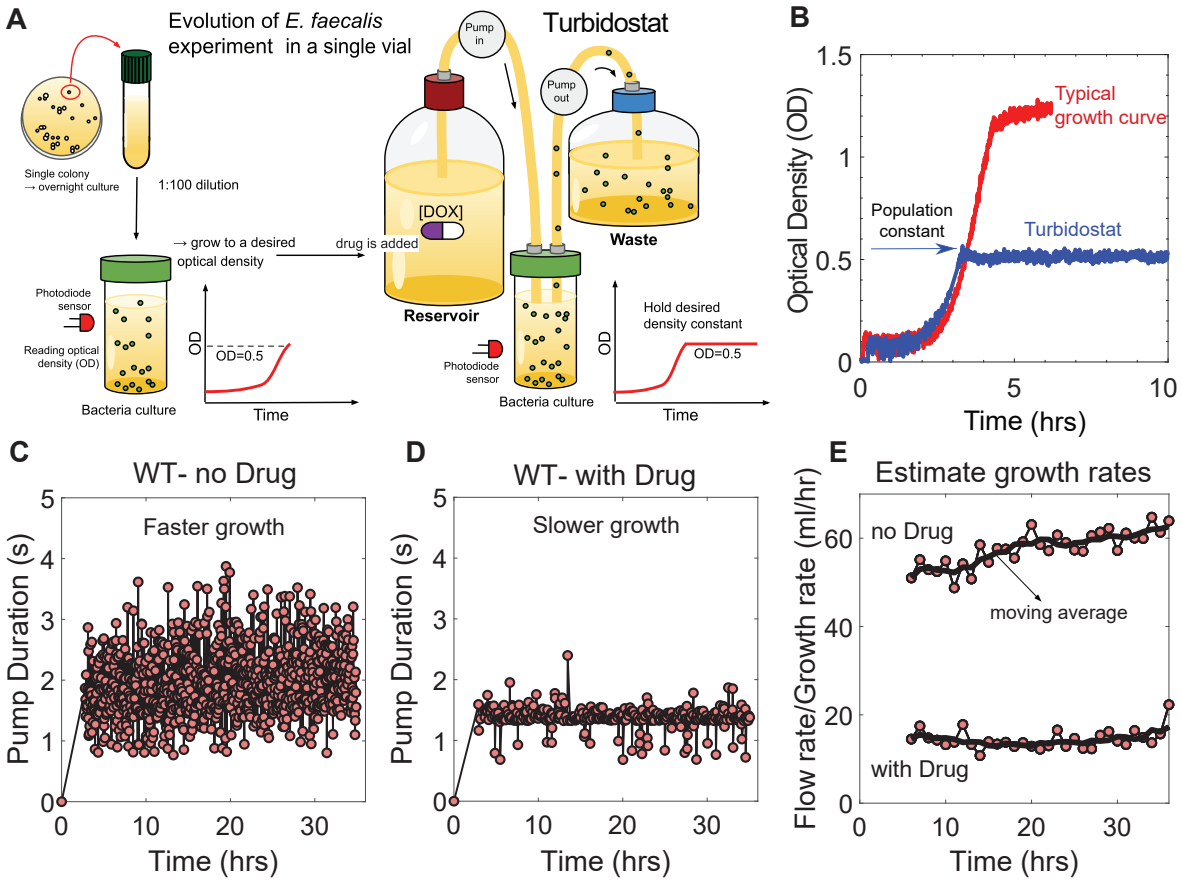

Figure 4.1: **Estimating real-time per capita growth rate using constant-density turbidostats.** A) Schematic illustration showing an experiment setup. An overnight culture from a single colony of *E. faecalis* was diluted into a fresh BHI medium (at a 1:100 ratio) in a glass vial (25mL), well-mixed, and grown to a desired density. Then, the turbidostat, a continuous well-mixed culture device was used. The population is kept constant by pumping in fresh BHI media from a reservoir at the same rate media and cells are pumped out to waste. Reservoirs can have different conditions such as with or without antibiotics (selection pressure). The pumps are controlled by a computer using feedback from an optical density (OD) measured with a photo-sensor. B) The blue curve shows a population kept constant at OD=0.5, and a typical growth curve is shown in red. C and D: Pump dynamics required to hold wild type (OG1RF) populations at constant density in the presence (D) and absence (C) of doxycycline. In practice, flow is not continuous; instead pumps alternate between "on" periods of a variable duration (pump duration) and "off" periods that are determined by a simple feedback algorithm. E). Time-averaged pump rates–proportional to population growth rate–in two example experiments over time.

graphs [171] or in particular limits (e.g. with a center manifold reduction) [172]. Theory suggests that how different subpopulations in a community are topologically "connected" can alter evolution. For example, if a subpopulation acts as a hub–that is, it serves as a central population with connections, such as migrational pathways, to and from multiple other subpopulations–mutations can be amplified and reach fixation faster [173]. Recent work in mammalian cells indicates that migration in a mixed population of wild type and resistant cells does not affect the average frequency of mutants but influences the distribution of mutants among subpopulations [174]), while recent experiments in microbial metapopulations migrating between spatially uniform can either slow or speed adaptation [175]. In the context of drug resistance, several recent theoretical and experimental studies have shown that spatial fluctuations in drug concentration significantly impact the evolution of resistance [82, 83, 79, 80, 81, 18, 78, 19]. These studies indicate that resistance emerges more quickly in the presence of spatial gradients in drug concentration [83, 79, 80, 18, 78, 19] or heterogeneous drug penetration [82, 81]. Despite these promising advances, experimental studies of evolution in spatially heterogeneous landscapes remain relatively rare.

In this work, using *E. faecalis* as a model, we investigate whether drug (doxycycline) concentrations in heterogeneous meta-communities can be tuned to modulate the emergence of drug resistance. Enterococci inhabit the gut of many mammals [176], and the gastrointestinal tract is a substantially heterogeneous spatially-extended system. Recent work on gut microbes has underscored the potential impact of spatial effects, such as cell-cell clustering, which can facilitate clearance microbial communities in the presence of antibiotics [84, 85] and even modulate the diversity of the human microbiota [86]. Spatially separated enterococcal populations in the gut may experience different levels of drug and nutrients, and it is not clear how this heterogeneity impacts evolution of resistance, particularly given that these subpopulations are likely connected by flow in the gut.

To investigate the interplay of spatial heterogeneity and inter-population exchange, we leverage a series of inter-connected, computer controlled bioreactors that allow us to simulate continuous "migration" between different well-mixed communities of fixed size held at potentially different drug concentrations. By measuring real-time growth rate in each individual community, we show that migration accelerates total population growth in mixed populations of drug-sensitive and drug-resistant cells–a result consistent with simple mathematical models and intuitively explained by the homogenizing effect of migration on the initial distribution of mutants. In addition, we investigate the emergence of resistance in initially sensitive populations on longer timescales in both single- and multi-habitat communities; on these timescales, the emergence of resistance appears as a sigmoidal-like increase in population growth rate, and we find that migration tends to delay this growth increase when the concentration of drug is not uniform across habitats. Genome sequencing of isolates from adapted populations suggest that resistance arises primarily due to

emergence of a single mutant type–single nucleotide mutations in the gene for ribosomal protein *rpsJ*, a target of doxycycline and a well known conduit of doxycycline resistance–and phenotypic characterization of isolates indicates that migration does not select for fundamentally new mutations but instead reshapes the distribution of sensitive and resistant populations across habitats. By contrast, we also observe cases where migration has little impact on growth adaptation, even when drug heterogeneity across habitats is substantial. These trends can be partially explained by changes in selection pressure across different habitats, which we show is correlated with the observed shift in adaptation times. Overall, these results show that migration and spatial structure can have substantial impacts on adaptation in microbial communities, even in simple scenarios where resistance is dominated by a selective sweeps of a single type of mutant.

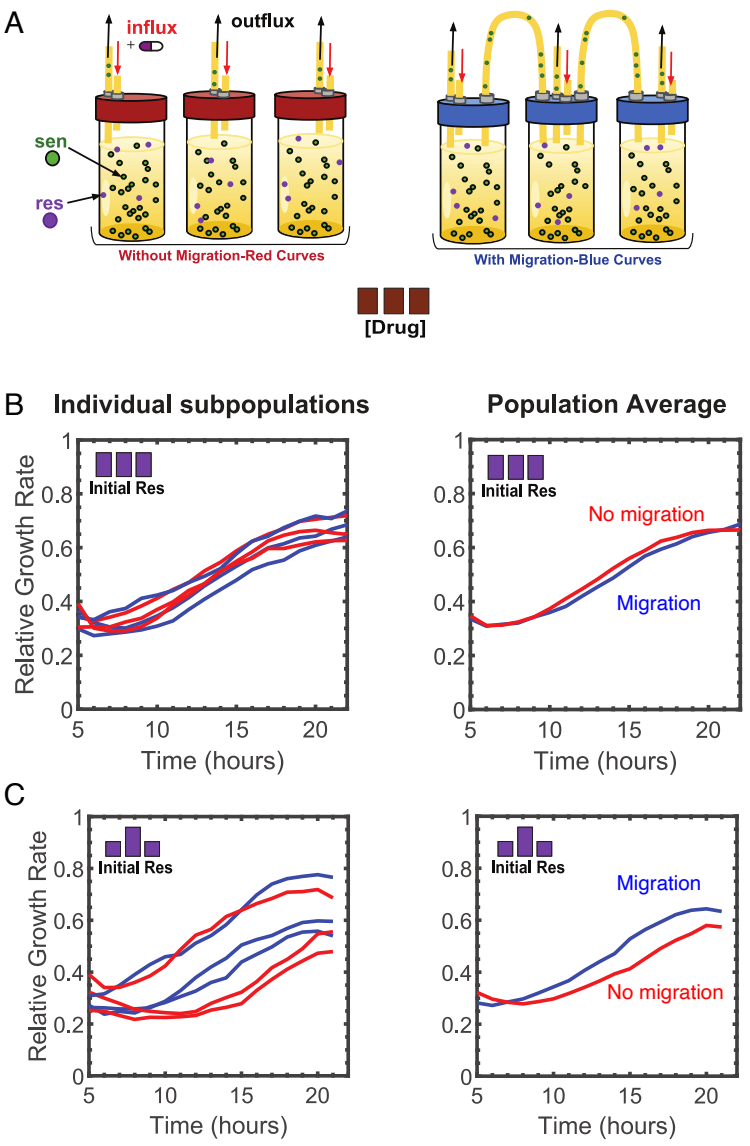

Figure 4.2: **Migration leads to accelerated population growth in meta-communities when mutants are initially distributed heterogeneously across habitats** A) Three-vial meta-populations are seeded with known fractions of sensitive and resistant cells. At time 0, a fixed concentration of drug is added to all three vials as well as the input reservoirs that provide fresh media to each vial. Each vial is operated as a turbidostat, and growth within each vial ("subpopulation") is estimated from the influx rate of fresh media required to keep optical density constant. In one meta-community (left), the three vials are not interconnected with one another. In the other meta-community (right), migration is simulated by connecting the 3 vials in a linear array (vial 1 - vial 2 - vial 3) and an independent set of pumps is used to exchange media between neighboring vials at a fixed rate. B and C: Per capita growth rates for individual populations (left) and the total population average (right) when the vials are seeded with homogeneous (B) or heterogeneous (C) mutant fractions under conditions of no migration (red) and migration (blue). Bar graph insets represent the initial mutant population in each vial. In all cases, the initial fraction of mutants in the entire population (i.e. across vials) is held fixed at 0.8 percent.

4.2 Results

To study population dynamics in spatially connected communities, we modified a recently developed bioreactor device (eVolver [87]) to allow for exchange of media between neighboring vials in a linear array of 3 individual growth chambers (Methods). In each chamber, we hold population size approximately constant (turbidostat mode) using a simple feedback algorithm to pump in fresh media and drug from a reservoir while simultaneously removing an equal volume of media plus cells 4.1. The per capita growth rate g in each vial can be estimated from the flow rate F required to maintain a constant optical density (OD) in that vial ($g = F/V$, where V is the total culture volume).

As in previous chapters, our model system is the gram positive bacterium *E. faecalis*, an opportunistic pathogen that underlies a number of human infections[48]. In this work, we focus on populations treated with doxycyline, a common bacteriostatic antibiotic that targets protein synthesis. We chose doxycycline because it is well characterized and, based on previous work from our group, has a relatively smooth dose response curve and does not exhibit strong density-dependent effects [88, 28], which could unnecessarily complicate the interpretation of our results.

To simulate migration, we connected neighboring vials in each 3-vial meta-community to allow for flow between habitats at fixed rates (Figure 4.2 A). We focus on perhaps the simplest possible connection topology–a linear array. In this arrangement, the two edge vials are not directly connected to one another but are indirectly coupled via connections to the central "hub" vial. While this setup also allows for intermixing of drug between vials, we choose migration rates sufficiently small that the effects of intermixing on drug concentration is typically small (less than 10 percent).

4.2.1 Dynamics of meta-populations of sensitive and resistant cells.

We began by investigating the dynamics of 3-vial communities containing mixtures of sensitive and resistant cells. In this case, the resistant strain is a fully sequenced, lab-evolved descendent of the sensitive strain (OG1RF); the resistant strain harbors a single point mutation in the gene for ribosomal protein *rpsJ*, a known target of doxycycline. At the beginning of each experiment, we seeded each vial in a connected ("with migration") meta-population with a known ratio of sensitive and resistant cells–with resistant cells initially present at a small fraction (typically ¡ 1 percent). In parallel, we ran an identical experiment with a second "no migration" metapopulation where the three vials are not connected and therefore act independently. In both cases, we estimated real-time per capita growth rate in each sub-population (each vial) and compared the total (averaged) population growth rates between the "migration" and "no migration" communities.

For simplicity, we start with a metapopulation where drug concentration is the same (216 mug/mL) in each vial (Figure 4.2). Over time, we see an increase in population growth rate in

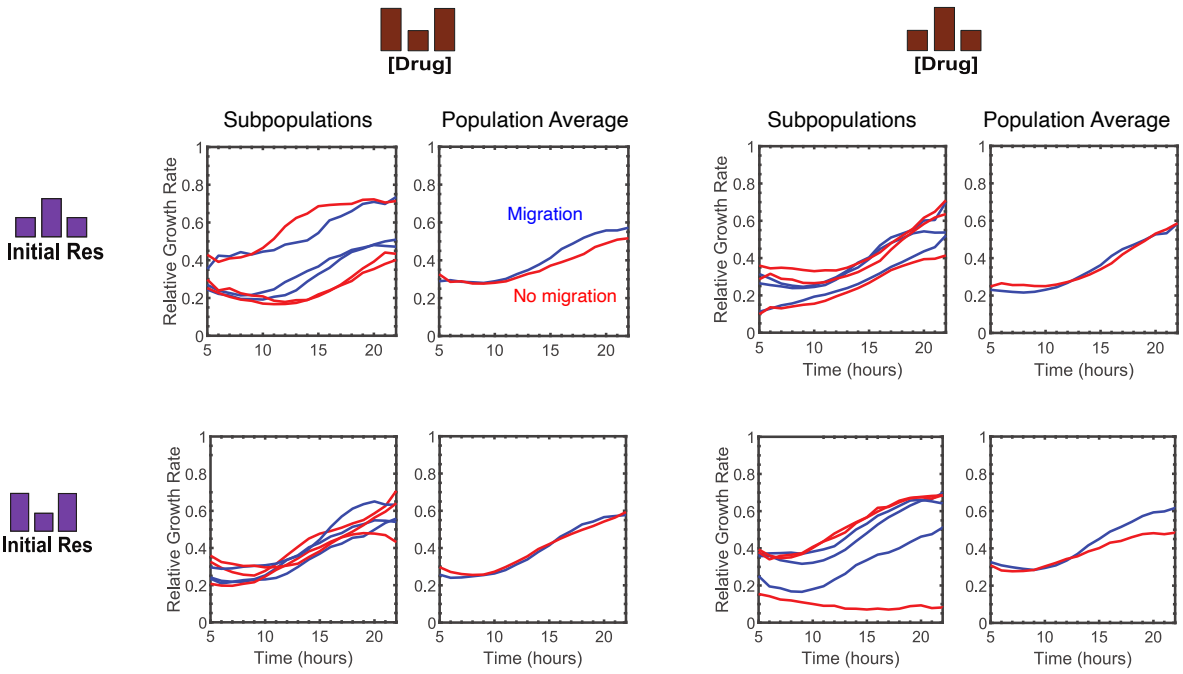

Figure 4.3: **Heterogeneity in drug concentration can accentuate or mitigate migration-induced acceleration of population growth.** Three-vial meta-populations are seeded with different size mutant populations (rows; see bar graphs at left) and drug concentration is heterogeneous but fixed across vials (columns; see bar graphs at top). Panels show per capita growth rates for individual subpopulations (left panel in each pair) and the total population average (right panel in each pair) under conditions of no migration (red) and migration (blue).

each vial, which is expected in the presence of drug because the resistant subpopulation–which grows faster in drug–should increase in frequency over time. When the resistant mutants are initially distributed uniformly across the community, we find that the growth rate increases similarly in each subpopulation, regardless of migration (Figure 4.2 B). Not surprisingly, then, we do not see significant impact of migration when conditions in the individual habitats are initially identical.

We next asked what would happen in the case where mutants are initially distributed heterogeneously across the different habitats. Because of the stochastic nature of evolution, one might expect such heterogeneity in mutation frequencies to arise naturally in spatially segregated communities, particularly when population sizes are small. In contrast to the homogeneous case, we now observe substantially accelerated growth in the presence of migration when mutants are initially more prevalent in the center vial (Figure 4.2). We observed a similar (though smaller) growth acceleration when other heterogeneous distributions of mutants–such as a stair-case–were used (Figure 4.11A-C).

In addition to heterogeneity in mutant composition, we investigated the effects of heterogeneity in drug concentration across the different vials. To do so, we repeated the experiments above

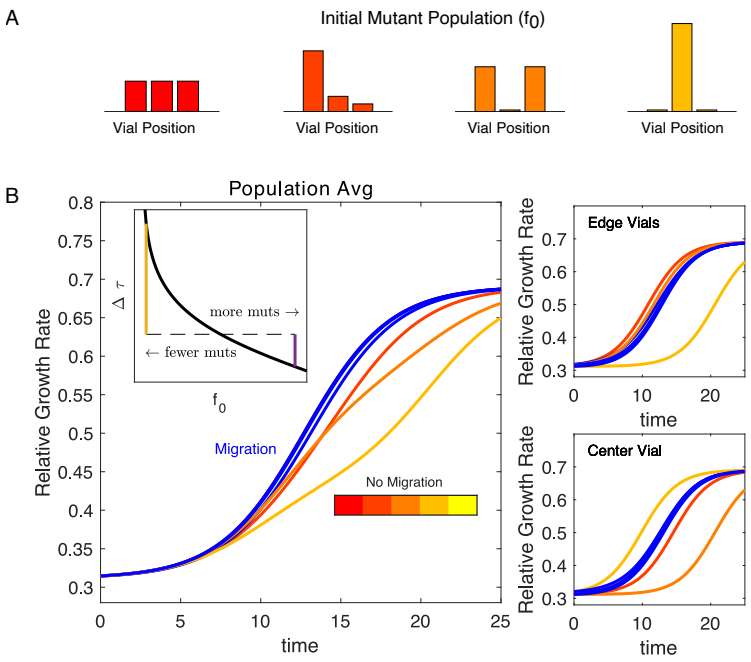

Figure 4.4: **A toy model provides intuition for migration-induced acceleration of growth.** A simple population dynamics model involves 3 exponentially growing, interconnected subpopulations that are seeded with different distributions mutants at time 0 (A). Panel B: per capita growth rate in the total population (left) and in the individual subpopulations (right panels; top is edge vials, bottom is center vial) for meta-populations with migration (blue curves) or without migrations (multi-colored curves, red to light orange, depending on the specific distribution of mutants). Inset: time to fixation (τ) in a single habitat model of two exponentially growing populations as a function of initial mutant fraction f_0. The fixation time depends nonlinearly on f_0, which means that the impact of reducing f_0 (represented by vertical yellow bar) is larger than that of increasing f_0 (vertical purple bar). In a meta-community with fixed (total) mutant population size, introducing heterogeneity would therefore be expected to slow fixation.

in meta-populations with heterogeneous drug profiles where either the middle vial or the edge vials contain higher drug concentrations. These profiles correspond to a central peak or a central valley in drug concentration and correspond to the simplest possible non-monotonic arrangement of drug concentrations. Importantly, we chose the drug concentrations so that the total population growth rate remained (approximately) constant at the beginning of each experiment–that is, each metapopulation begins with identical growth at the level of the entire population, despite the fact that the distribution of drug (and therefore growth rates) across vials may be variable.

As in the uniform drug populations, we found that migration can accelerate growth relative to paired, non-migrating populations (Figure 4.3). However, heterogeneity in drug concentration and initial migration distribution can also counter-balance one another, reducing the effect. For example, the previously observed acceleration of growth when mutants are initially enriched in

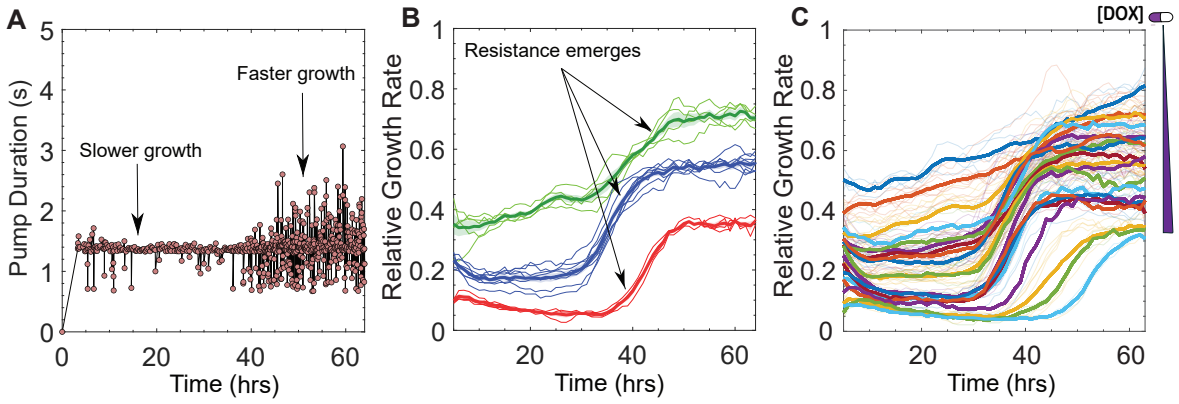

Figure 4.5: **Evolution of doxycycline resistance in well-mixed communities depends on drug concentration.** A) Bacterial growth is measured using the rate of the pumps. The pump duration is recorded, including when it was on and how long it stayed on (burgundy circles) to maintain the fixed volume (25mL). This plot is an example that shows that the population grows faster after 40 hours. B) Resistant mutants emerge under Doxycycline (DOX) at different concentrations: 177 ng/mL (green), 400 ng/mL (blue), and 800 ng/mL (red). Relative growth rate curves are normalized to the wild type without drugs. Individual trials are represented with thin curves and the average with thick curves. C) Evolution of E. faecalis as a function of the drug concentration increases from [DOX] min = 100 ng/mL to [Dox] max = 1200 ng/mL. In a small drug concentration regime (less than 177 ng/mL), the population growth rate curve behaves linearly and becomes an S-shape as the drug increases, allowing an estimation of the time when mutants emerge. The steepness of the slopes reflects how fast mutants takeover. Each vial started with an inoculation of 250 µL from a saturated culture of a single colony and population held constant at OD=0.5 (approximately 10^{10} cells when the drug is added).

the center habitat (Figure 4.3, upper left panels) can be minimized by increasing drug concentrations in the center environment and decreasing concentrations at the edges (Figure 4.3, upper right panels). A similar effect occurs when mutants are initially enriched in the edge environments: the migration-induced acceleration of growth is reduced when drug is increased at the edges and decreased in the center vial.

We observed similar dynamics under a range of different drug concentrations and initial mutant distributions (Figure 4.11). In every case, the effect of migration was to accelerate growth or leave the dynamics essentially unchanged; notably, we did not find situations where migration leads to a substantial slowing in the rate of growth increase. These results are consistent with predictions of perhaps the simplest possible population dynamics model: one where cells in each habitat grow exponentially and cells can "migrate" to neighboring habitats (see Methods; Figure 4.11). The model is parameterized by independently measured growth rates (see Figure 4.10 for example).

While the results may appear initially surprising, they have a simple intuitive interpretation. In a single habitat, exponentially growing population, the time (τ) required for growth rate to reach some threshold–say, fifty percent–of its final value is (up to an additive constant) proportional to $\tau \propto \ln((1 - f_0)/f_0)$ (see Methods). The convexity of this function means that the effect of adding additional mutants–which decreases τ–and the effect of removing mutants–which increases τ–are not symmetric (Figure 4.4B, upper left inset). In words, removing mutants at time zero slows fixation more so than adding mutants speeds fixation. In a disconnected meta-community with uniform drug concentrations, heterogeneity is therefore expected to increase fixation time (i.e. to slow the increase of population growth) relative to a homogeneous community. In connected communities, migration serves to homogenize the initial mutant distribution, which in turn leads to an decrease in fixation time (i.e. accelerates the increase in population growth).

Solutions to the simple model confirm this intuition: even when drug is uniform across habitats, migration leads to accelerated growth under various heterogeneous distributions of mutant seeding (step-like decrease, central valley, central peak, Figure 4.4B). In each case, removing migration–which effectively increases heterogeneity in the initial mutant distribution–has opposing effects on the middle and edge vials: speeding growth acceleration in one and slowing growth acceleration in the other Figure 4.4B, right panels). However, the slowing effects tend to dominate, leading to a slow down in the growth curves for the entire population (Figure 4.4B), left panel). These results offer intuition for the accelerating effects of migration, which serves to homogenize initial fluctuations in the mutant distribution.

4.2.2 Evolution in single habitats with fixed drug concentration.

To this point, our results have focused on population dynamics in mixed populations that are seeded, up front, with known fractions of sensitive and resistance cells. In this section, we investigate adaptation on longer timescales in populations that start from a single sensitive colony. In these populations, adaptation in growth are (as we will see) associated with emergence of resistant mutants that eventually dominate the population.

For simplicity, we being by growing sensitive populations of cells for multiple days in the presence of a fixed concentration of doxycyline (Figure 4.5). Under these conditions, a typical trajectory starts at a low growth rate (determined by the concentration of drug) before undergoing a rapid increase in growth, often after 30-40 hours of adaptation. Both the timing and the steepness of the growth increase depend on drug concentration, with higher concentrations typically leading to steeper increases that start at later times ((Figure 4.5 B-C)). These results are mostly consistent with classical models of population dynamics, where the fixation time of the resistant strain is inversely proportional to the selection pressure (in the simplest case, the difference in growth rates between sensitive and resistant strains). However, we do note that at high drug concentrations, growth initially decreases gradually for 20 or more hours (Figure 4.5), a trend that does not occur in the simplest population dynamics models but may reflect complex drug binding dynamics of ribosome-targeting drugs like doxycyline [177, 178]. As expected, strains isolated from the end of these adaptation experiment exhibit increased IC50 (the concentration of drug at which the effect is half-maximal), indicating they are resistant mutants–a result we confirm (below) with genome sequencing.

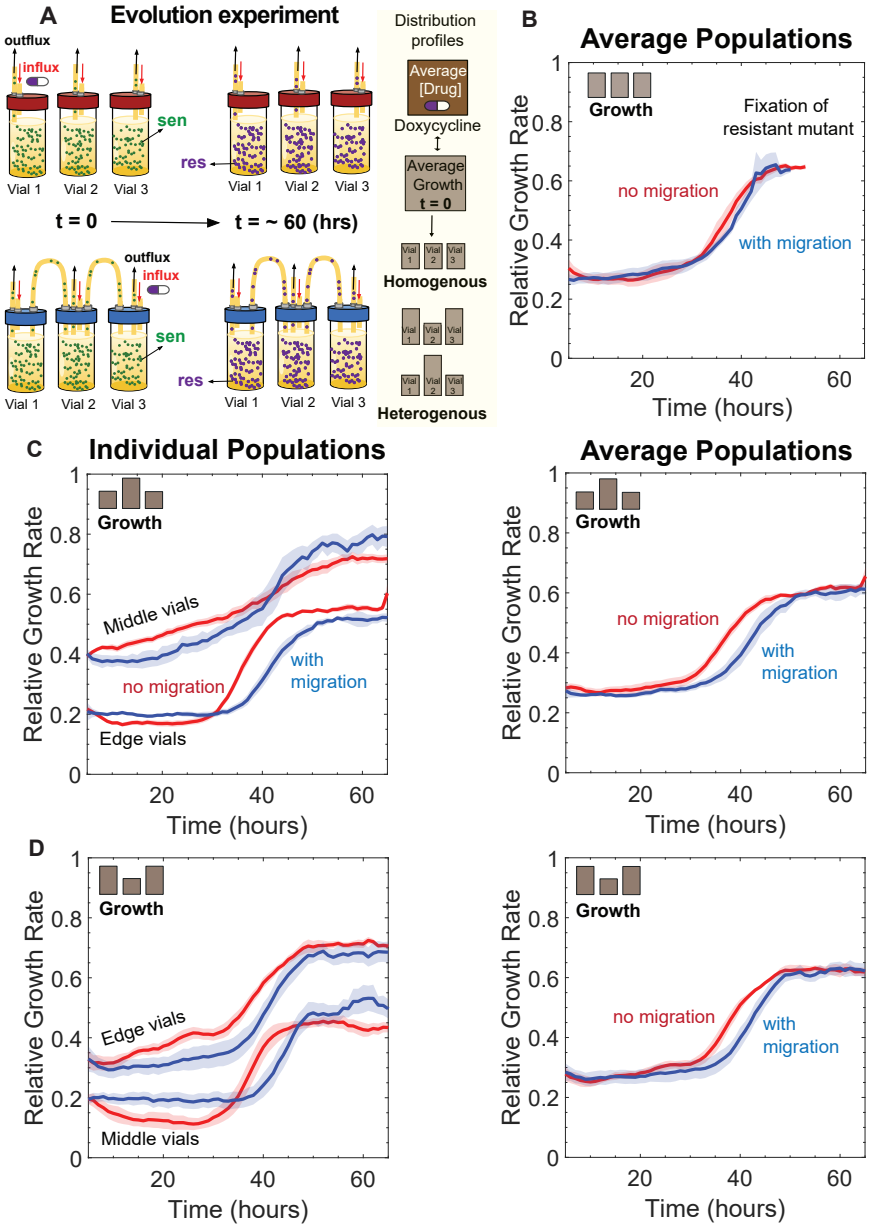

Figure 4.6: **Migration can slow adaptation when drug concentrations are non-uniform across habitats.** See next page.

Figure 4.6: (caption continued) A) The subpopulations in a metacommunity are each exposed to a fixed concentration of drug. Profiles of drug include uniform distribution across vials, a drug valley (where drug is largest in the center habitat), and a drug peak. The profiles can also be represented in terms of initial population growth; in that case, high drug corresponds to lower (initial) population growth. B) Growth rate trajectories for individual subpopulations with (blue) and without (red) migration in metacommunities with uniform drug distributions ([Dox] = 216 ng/mL). C-D) Growth rate trajectories for individual subpopulations (left panel) and the full metapopulation (right panel) both with (blue) and without (red) migration. Panel C corresponds to a metacommunity where drug concentration is maximum (initial growth minimum) in the edge vials ([Dox] = 400 ng/mL) and lower ([Dox] = 125 ng/mL) in the center vial. In panel D, drug concentration is lower ([Dox] = 177 ng/mL) in the edge vials and a higher drug concentration in the middle vial ([Dox] = 600 ng/mL).

4.2.3 Migration can slow adaptation when drug concentrations are non-uniform across habitats.

To investigate the impact of spatial heterogeneity on the emergence of resistance, we next performed lab evolution experiments in 3-vial metapopulations initially seeded with sensitive populations (Figure 4.6 A). Similar to the single vial case, we see adaptation occurring in each individual habitat of these metacommunities as a sharp increase in population growth that typically occurs after 20 or more hours of drug exposure. The results are highly repeatable across replicate populations, a result we attribute to the size of the populations. These populations are large–each 25 mL culture vial contains on the order of 10 billion cells–and the dynamics of these populations are likely dominated by selection on a pre-existing distribution of mutants that is statically similar in each vial when the experiment begins.

When the drug concentration is uniform across the different vials, migration has little impact on the time it takes for growth to increase to a plateau–a time we frequently refer to as the "fixation" time (Figure 4.6 B). On the other hand, when drug concentration is non-uniform across different vials, adaptation in the individual vials (Figure 4.6C and D, left panels) and in the total population growth rate (Figure 4.6 C and D, right panels) are substantially affected by migration. In contrast to results in pre-mixed populations (e.g. Figure 4.3), where migration tends to accelerate growth adaptation, we now find that migration leads to a delay in fixation time under multiple profiles of drug heterogeneity, including cases where drug is lowest (initial growth is highest) in the center habitat (Figure 4.6 C) and cases where drug is highest in the center habitat (Figure 4.6 D). We find that this shift in fixation is maintained across a range of migration rates achievable with our setup (Figure 4.14).

However, this delay does not occur in all cases where the distribution of drug is heterogeneous. For example, when metapopulations are exposed to similar drug profiles (peak or valley in drug

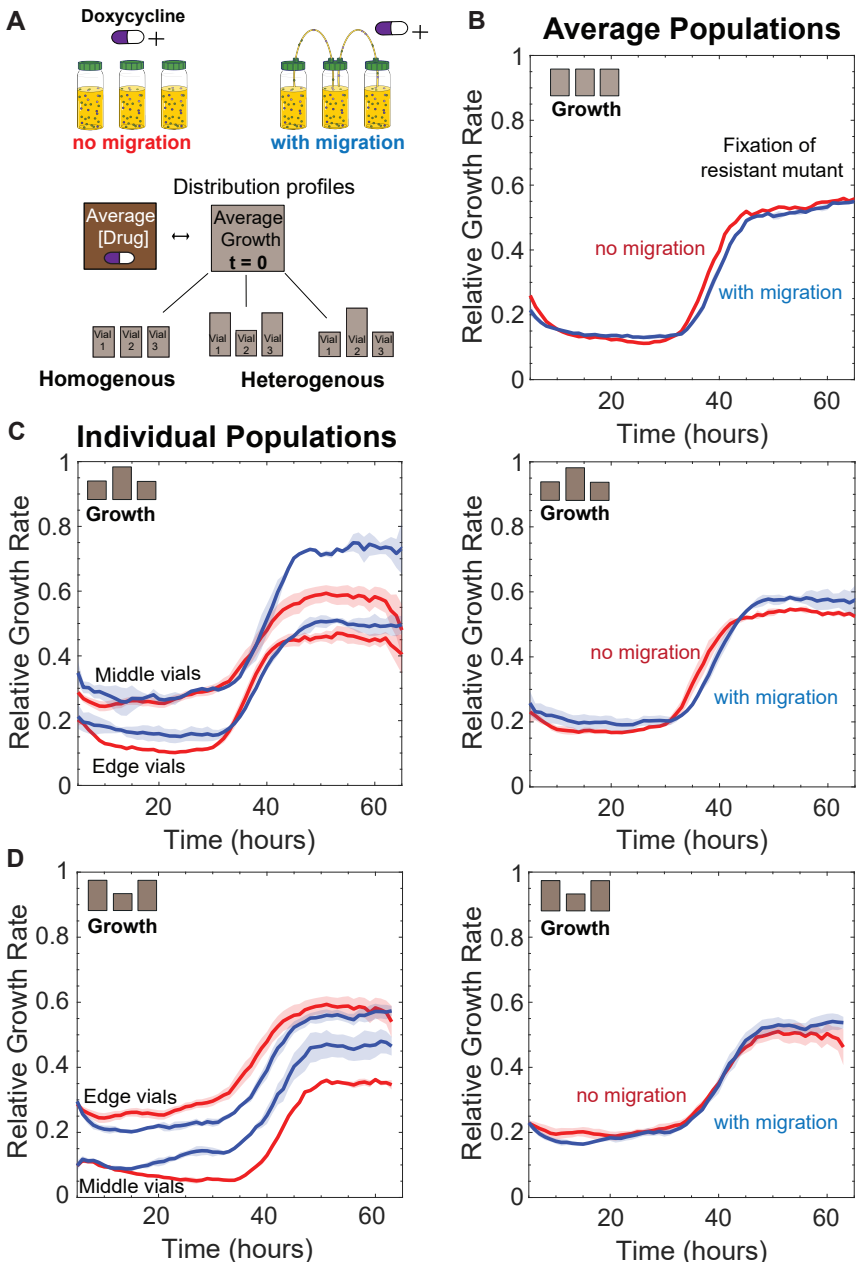

Figure 4.7: **Drug heterogeneity is not sufficient to drive migration-induced slowing of adaptation.** See next page.

concentration in center habitat) but at higher overall drug concentrations, adaptation at the level of the entire population occurs on similar timescales regardless of migration (Figure 4.7 B-D, right panels). In this case, however, adaptation in each individual vial is impacted–to varying degrees–by migration, but the effects in the different subpopulations largely cancel out at the level of the entire community. Therefore, while non-uniform profiles of drug concentration can lead to migration-driven slowing of adaptation in some cases, this non-uniformity alone is not sufficient to guarantee

Figure 4.7: A) The subpopulations in a metacommunity are each exposed to a fixed concentration of drug. Profiles of drug include uniform distribution across vials, a drug valley (where drug is largest in the center habitat), and a drug peak. The profiles can also be represented in terms of initial population growth; in that case, high drug corresponds to lower (initial) population growth. B) Growth rate trajectories for individual subpopulations with (blue) and without (red) migration in metacommunities with uniform drug distributions ([Dox] = 433.3 ng/mL). C-D) Growth rate trajectories for individual subpopulations (left panel) and the full metapopulation (right panel) both with (blue) and without (red) migration. Panel C corresponds to a metacommunity where drug concentration is maximum (initial growth minimum) in the edge vials ([Dox] = 525 ng/mL) and lower ([Dox] = 125 ng/mL) in the center vial. In panel D, drug concentration is lower ([Dox] = 250 ng/mL) in the edge vials and a higher drug concentration in the middle vial ([Dox] = 800 ng/mL).

the effect.

In addition to comparing adaptation with and without migration, we also compared adaptation trajectories between different meta-communities with different drug-profile distributions. As in the experiments with mixed populations (e.g. Figure 4.2), to facilitate comparisons between different drug concentration profiles, we chose the drug concentrations that lead to different distributions of drug but keep the overall population growth at time zero approximately constant. That is, the profiles will lead to different distributions of (initial) growth in the individual subpopulations but will lead to the same average population growth rate of the entire community. In the drug profiles with lower total drug concentration, we find that the homogeneous and heterogeneous metapopulations exhibit similar fixation times in the absence of migration, but migration leads to a delay in fixation in heterogeneous populations (Figure 4.15, top panels). By contrast, at higher concentrations, heterogeneous populations show slightly accelerated fixation in the absence of migration, while migration appears to eliminate the effect (Figure 4.15).

4.3 Migration does not select for new mutations but alters the spatial distribution of sensitive and resistant cells.

To investigate the genetic underpinnings of these evolutionary dynamics, we selected dozens of isolates from different subpopulations at the end of these lab evolution experiments. For each isolate, we measured a dose response curve to doxycyline and estimated the IC50. In addition, we sequenced the full genomes of a subset of isolates.

The IC50 measurements reveal that isolates fall roughly into 2 phenotypic classes: sensitive strains, with resistance similar to that of the WT ancestor, and dox-R strains, whose IC50 is increased by approximately 5-fold (Figure 4.16). This division into two classes is confirmed by

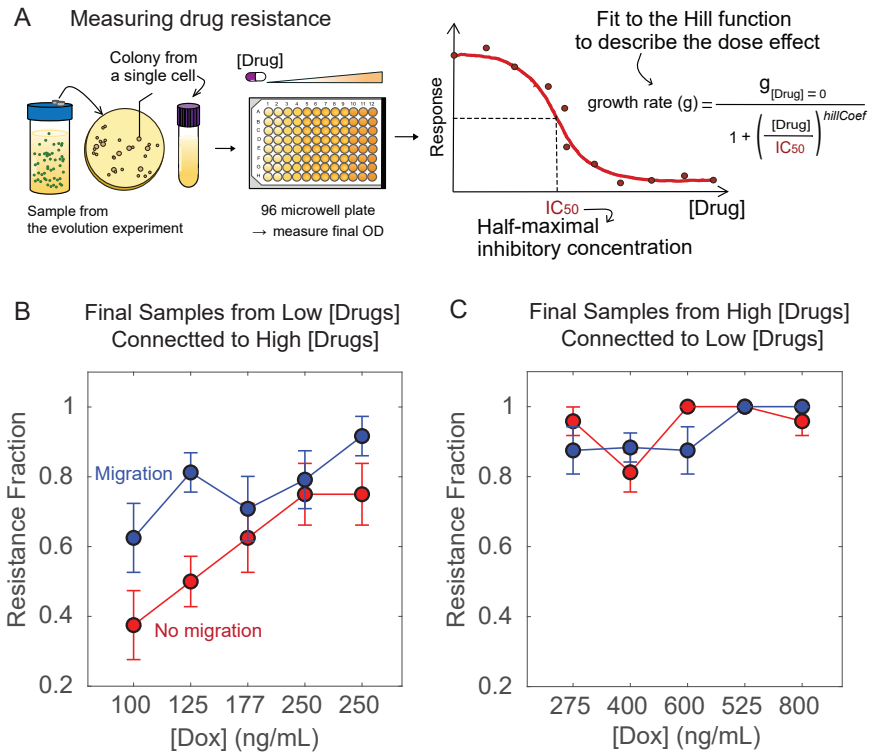

Figure 4.8: **Quantifying mutant resistance by measuring the dose response from the final sample of the evolution experiments.** A) Schematic of experiment: a sample was saved after the evolution experiment and streaked on a BHI agar plate, allowing it to form a colony from a single cell. The cells were inoculated in BHI media overnight at 37^{o}C and exposed to Dox with increasing concentrations (96 microwell plates). After 6 hours, OD (OD600) was measured by using a plate reader. A nonlinear response curve was fitted to the Hill function to describe the dose effect by estimating half maximal inhibitory concentration (IC_{50}).B)The resistance fraction of final samples from low drug concentration vials connected to higher drug concentrations. The red line indicates results without migration and the blue line indicates results with migration. C) Showing the resistance fraction of final samples from higher drug concentration vials connected to lower drug concentrations. The same legends apply as in panel B. The connections between the low drug concentrations in panel C and the higher drug concentrations in panel D (and vice versa) are followed: [Drug 100] (24 replicates for each with and without migration) connected to [Drug 275] (24 replicates for each with and without migration), [Drug 125] (48 replicates for each with and without migration) connected to [Drug 400] (60 replicates for with migration and 48 replicates without migration), [Drug 177] (24 replicates for each with and without migration) connected to [Drug 600] (24 replicates for each with and without migration), [Drug 250] (24 replicates for each with and without migration) connected to [Drug 525] (24 replicates for each with and without migration), and [Drug 250] connected to [Drug 800] (24 replicates for each with and without migration)

sequencing: the vast majority of resistant isolates harbored a single point mutation in the gene for ribosomal protein *rpsJ*, a target of doxycycline and a well known conduit of doxycycline re-

sistance. Somewhat surprisingly, we did not identify any isolates with mutations in other genes commonly associated with doxycycline resistance. Together, these results suggest that adaptation in these populations is dominated by emergence of a common variant, regardless of the level of drug heterogeneity or migration.

While migration does not select for new variants, we found that it does shift the distribution of sensitive and resistant cells in the different subpopulations. To investigate this issue, we used the phenotypic IC50 measurements to estimate the population fraction of resistant cells in different vials of the metacommunities (Figure 4.8). To do so, we split the vials into two groups: those representing subpopulations that are connected to subpopulations with higher drug concentrations, and suppopulations that are connected to vials with lower drug concentrations (Figure 4.8B-C). Not suprisingly, in the absence of migration, the fraction of mutants increases approximately monotonically with drug concentration. These results indicate that for low drug concentrations, resistant cells have not achieved fixation on the timescale of our experiment, while for high drug concentrations (greater than about 250), mutant represent more than 90 percent of the final population. In the presence of migration, these fractions are predictably shifted: the resistant fraction is typically increased in vials connected to habitats with higher drug concentrations ((Figure 4.8)B, left panel), while migration tends to slightly lower (or not impact) mutant frequencies at high drug concentrations. These results are consistent with similar findings in mammalian cells, where less fit alleles persist at a higher fraction that predicted by standard mutation-selection balance [174].

4.3.1 Mutation-induced shifts in fixation time are correlated with heterogeneity in selection pressure across subpopulations.

Our results indicate that in the presence of spatial heterogeneity, migration can sometimes, but not always, delay the evolution of resistance. While it is not clear what features lead to slowed adaptation, we hypothesized that shifts in fixation times would be related to heterogeneities in *selection pressure* between interconnected vials, not merely heterogeneity in drug concentrations. Because both the sensitive and resistant strains are inhibited by drug–though at very different concentrations–it is not clear, a priori, that increasing drug concentration will always lead to an increase in selection pressure. In the simplest case, where selection pressure can be approximated by a difference in growth rates between sensitive and resistant cells, the nonlinearity of the dose response curves means that selection pressure can depend non-monotonically on drug concentration.

To test this hypothesis, we estimated the selection pressure in a given habitat as the difference in growth rate between wild type (sensitive) and resistant (mutant) populations at that concentration. For each experiment, these growth rates can be estimated directly from non-migration experiments

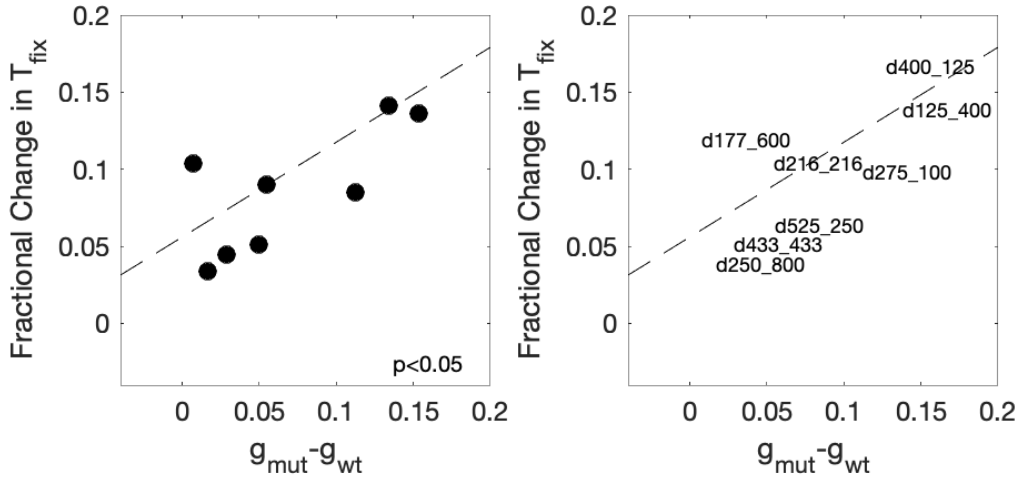

Figure 4.9: **Shift in fixation time depends on growth rate differences between ancestor and mutant strains in different habitats.** Fractional changes in fixation time–defined as the time it takes the growth rate of a population to reach half of its maximum (fully adapted) value–as a function of $\Delta(g_{\text{mut}} - g_{\text{wt}})$–which we treat as an estimate for the difference in selection pressure (growth rate difference) between the center and edge vials.

by averaging growth shortly after drug exposure (when the single vial population is dominated by sensitive cells) and at the end of the adaptation, when growth has reached steady state and the population is comprised of mostly resistant cells. For each metapopulation, we calculate the quantity $\Delta(g_{\text{mut}} - g_{\text{wt}})$–which compares the difference in S and R growth rates between neighboring vials. We treat $\Delta(g_{\text{mut}} - g_{\text{wt}})$ as an estimate for the difference in selection pressure (i.e. growth rate difference) between the center and edge vials (in the absence of migration). Large values of $\Delta(g_{\text{mut}} - g_{\text{wt}})$ indicate the population is highly heterogeneous, with edge vials favoring mutants significantly more or less than center vials. By combining data from all evolution experiments–spanning both homogeneous and heterogeneous metacommunities (see Figures 4.12 and 4.13 for full summary)–we found that $\Delta(g_{\text{mut}} - g_{\text{wt}})$ was significantly correlated with shifts in fixation time (Figure 4.9). These results underscore the notion that migration-induced shifts in fixation are associated with non-uniformity in selection pressure, which sometimes-but not always-corresponds to non-uniformity in drug concentrations.

4.4 Discussion

Overall, these findings illustrate that that migration and spatial structure can have substantial impacts on adaptation in microbial communities, even in simple scenarios where resistance is dominated by the emergence of a single resistant phenotype. In mixed populations where resistant cells comprise a sizable fraction of the population, these dynamics are well described by simple multi-deme population models, which capture the observed migration-induced acceleration of growth. On the other hand, these models to not reliably predict the substantial delay in fixation we often observe in longer timescale evolution experiments, where resistance emerges spontaneously from an initially sensitive population. However, these findings are reminiscent of predictions from evolutionary graph theory, which indicate that (even in the absence of heterogeneity across vials (i.e. drug concentration)), metacommunities with a central hub can slow fixation under some conditions [171, 175]. Recent work also suggests that small asymmetries in migration [174] can modulate fixation. At this stage, it is not clear whether similar mechanisms could be driving fixation shifts in our system.

The simple models described here neglect a number of features that may partially explain these dynamics. For example, we have not included effects of competition and clonal interference, both of which could be relevant factors for large populations like these and can be incorporated with classical modeling approaches [28]. In addition, the models used so far are entirely deterministic and fail to capture stochastic effects related to mutation and demographic noise–some of which can persist even for large systems. Our ongoing work aims to develop more realistic models to investigate these dynamics in more detail. It is also possible that cooperation between resistant and sensitive cells–something previously observed with other antibiotics in this species [179]–could explain some of our results.

It is also possible that evolutionary dynamics involve more than just a single resistant strain. While our endpoint measurements suggest that later stages of adaptation involve only one resistant strain, it is possible that other mutants emerge and then disappear during adaptation–and future work could investigate this phenomena with time-resolved sampling and sequencing. Furthermore, it is not clear whether the largely repeatable evolutionary dynamics we observe are specific to doxycycline. It might be interesting to repeat these experiments with (for example) daptomycin, one of the final resources to treat multidrug resistance due to its unique mechanism targeting the cell membrane [180]. In previous chapters, we saw that daptomycin resistance involves multiple mutations that are acquired in complex combinations in homogeneous (but small) populations. It would be interesting to evolve DAP resistance under these spatially-extended conditions with larger populations, which may lead to more predictable dynamics. One challenge of this approach is that the turbidostats measure growth based on optical density, but DAP targets the cell membrane

and leads to lysis [181], which complicates the interpretation of OD measures.

It would also be interesting to explore spatial heterogeneities involving more than one drug. For example, we could conduct an experiment to measure the collateral effects of DOX-resistance against rifamycin (RIF), an RNA polymerase inhibitor. Previous findings [56] showed variable collateral effects when DOX-resistant strains are tested against RIF. It could be interesting to further explore this how these collateral effects impact evolution in populations exposed to heterogeneous environments that alternate between the two drugs. Finally, future work will also aim to understand how these dynamics change for different connection topologies in the metapopulation. Recent experimental work indicates that different topologies can impact fixation in homogeneous populations [175], and it would be interesting to investigate how those effects interplay with heterogeneity in drug concentrations.

Overall, our findings underscore the important role that spatial heterogeneity and migration can play in modulating resistance. It also highlights how initially counter-intuitive dynamics can–at least sometimes–be understood with simple mathematical models. We hope these results motivate continue explorations of resistance evolution, theoretical, experimental, and clinical.

4.5 Methods and Materials

4.5.1 Strains, growth conditions, and drugs

Evolution experiments were conducted using the *E. faecalis* strain OG1RF and a resistant isolate that was evolved from the same strain. Samples were stocked in 30% glycerol and stored at -80 C. Cultures for experiments were taken from single colonies grown on agar plates and then inoculated at 37^o C overnight before dilution in fresh media and the beginning of the experiment. All experiments and dose-response measurements were conducted in Brain-Heart Infusion or BHI (Remel). Doxycycline Hydrochloride (Fisher) antibiotic was used for this study, which is prepared from powdered stock and stored at -20^o C.

4.5.2 Experiment using a turbidostat

Experiments were performed in modified versions of the eVOLVER platform, which is an automated continuous culture device developed by the Khalil lab [87]. Bacterial cultures were inoculated in 5 mL of media (from a single colony) at 37^oC overnight, then 250 µL of the culture was added into a 25 mL vial with fresh media and allowed to grow to a desired optical density (typically around OD = 0.5, which is far below carrying capacity). The specific drug concentrations were distributed across 3 vials for the homogeneous and heterogeneous cases. The same drug concentration was also added to interconnected media reservoirs, which provide influx of media to maintain population size in each individual vial (i.e. individual vials are "turbidostats"). In addition, the three vials that comprise each meta-community are interconnected by silicone tubes, allowing us to simulate migration between habitats by exchanging fluid at a prescribed rate. Unless stated otherwise, intermixing ("migration") was performed at a rate of 2 mL per hour, which corresponds to an effective migration rate of $\beta = 0.08$ hr^{-1}, which is the same order of magnitude (but a bit slower) than typical per capita growth rate of bacterial populations under these conditions. While this setup does allow for intermixing of drug between vials, simulations show that this intermixing has a small effect (typically less than 10 percent) on drug concentrations in each vial.

4.5.3 Whole-genome sequencing

Illumina Short Read sequencing (400 Mbp / 2.7 million reads) and DNA isolation were performed by the Microbial Genome Sequencing Center (MiGS) at the University of Pittsburgh. The resulting genomic data was analyzed using the high-throughput computational pipeline breseq [158, 159], with default settings. Briefly, genomes were trimmed and subsequently aligned to *E. faecalis* strain OG1RF (Accession numbers: AE016830 - AE016833) via Bowtie 2. Any mutation that occurred

Table 4.1: **Parameters used in math models.**

Panels	[Dox] ng/mL distributions			Relative growth rates				Resistance fractions (f_{mt})		
	Edge 1	Middle	Edge 2	Wild type (g_{wt})		Mutant (g_{mt})		Edge 1	Middle	Edge 2
				Edge vials	Middle vials	Edge vials	Middle vials			
B1	216.6	216.6	216.6	0.29 (D216.6)	0.29 (D216.6)	0.63 (D216.6)	0.63 (D216.6)	0.008	0.008	0.008
B2								0.0004	0.0232	0.0004
B3								0.016	0.004	0.002
C1	400	125	400	0.19 (D400)	0.43 (D125)	0.60 (D400)	0.71 (D125)	0.008	0.008	0.008
C2								0.0004	0.0232	0.0004
C3								0.0118	0.0004	0.0118
D1	177	600	177	0.33 (D177)	0.16 (D600)	0.71 (D177)	0.42 (D600)	0.008	0.008	0.008
D2								0.0004	0.0232	0.0004
D3								0.0118	0.0004	0.0118

in either of the 2 control OG1RF strains was filtered from the results.

4.5.4 Measuring drug resistance

To measure IC_{50}, a sample acquired from the evolution experiment was streaked on a BHI Agar plate. From there, a single colony was selected and used for inoculation and incubated at 37° C overnight. Cells were then exposed to a drug concentration gradient, differing among each of the 12 wells on the plate, and the experiment was prepped in a BHI media with a total volume of 205 µL (200 µL of BHI, 5 µL of 1.5 OD cells) per well. Following 6 hours of growth at 37° C, OD at 600 nm (OD600) was measured with an Enspire Multimodal Plate Reader (Perkin Elmer). An IC_{50} measurement was taken for 12 colonies and each with 3 replicates. This was then repeated for every mutant that samples were acquired from, both for vials with migration and without migration, organized according to the following drug concentrations: 100ng/ml, 125 ng/ml, 177ng/ml, 216.6 ng/ml, 250ng/ml, 275 ng/ml, 400ng/ml, 433.3 ng/ml, 525ng/ml, 600ng/ml, and 800 ng/ml as well as the wild type.

In order to quantify the values for drug resistance, OD measurements for each drug concentration were normalized by OD measurements without the drug, and the dose-response curve was then fit to a Hill function ($g(d) = (1 + (d/k)^h)^{-1}$), with d the drug concentration, k the IC_{50}, and h the Hill coefficient.

4.5.5 Mathematical Model

We use a simple deterministic model that involves a single resistant mutant without competition to investigate the relationship between spatial heterogeneity, migration, and selection pressure af-

fecting the outcome of evolution experiments in metapopulations. Equations for the fraction of resistant cells in each subpopulation, denoted by Fr_1, Fr_2, and Fr_3, are given by:

$$\frac{dFr_1}{dt} = Fr_1(t) \cdot (1 - Fr_1(t)) \cdot (gr_1 - gs_1) - \mu \cdot Fr_1(t) + \mu \cdot Fr_2(t) \tag{4.1}$$

$$\frac{dFr_2}{dt} = Fr_2(t) \cdot (1 - Fr_2(t)) \cdot (gr_2 - gs_2) - 2 \cdot \mu \cdot Fr_2(t) + \mu \cdot (Fr_1(t) + Fr_3(t)) \tag{4.2}$$

$$\frac{dFr_3}{dt} = Fr_3(t) \cdot (1 - Fr_3(t)) \cdot (gr_3 - gs_3) - \mu \cdot Fr_3(t) + \mu \cdot Fr_2(t) \tag{4.3}$$

The growth rate in each sub population, denoted by G_1, G_2, and G_3, can be calculated from:

$$G_1(t) = gr_1 \cdot Fr_1(t) + gs_1 \cdot (1 - Fr_1(t)) \tag{4.4}$$

$$G_2(t) = gr_2 \cdot Fr_2(t) + gs_2 \cdot (1 - Fr_2(t)) \tag{4.5}$$

$$G_3(t) = gr_3 \cdot Fr_3(t) + gs_3 \cdot (1 - Fr_3(t)) \tag{4.6}$$

We denote the known seeding initial fraction resistant cells in vial 1, vial 2, and vial 3 as Fr_{01}, Fr_{02}, and Fr_{03}, and they serve as initial conditions for Equations 4.1 to 4.3. The parameters gr and gs represent the per capita growth rates of resistant and sensitive cells, respectively; these parameters were measured, and values vary based on drug concentration (Table 4.1). μ represents the constant migration rate of 1 ml/s per 30 minutes. We can also estimate the subpopulation's growth rates over time . They are denoted as G_1, G_2, and G_3. (Equations 4.4 to 4.6)

When migration is 0, the three habitats are independent, and each evolve according to

$$F_r = \frac{F_0 e^{dgt}}{1 - F_0 + F_0 e^{dgt}} \tag{4.7}$$

where $dg = g_r - g_s$ and F_0 is the initial mutant fraction. The time τ required to reach a threshold fraction f_{th} is therefore

$$\tau = \frac{\ln\left[\frac{(1-f_0)f_{th}}{(1-f_{th})f_0}\right]}{dg} \tag{4.8}$$

4.6 Supplemental Material

This section includes a number of supplemental figures referenced in the main text.

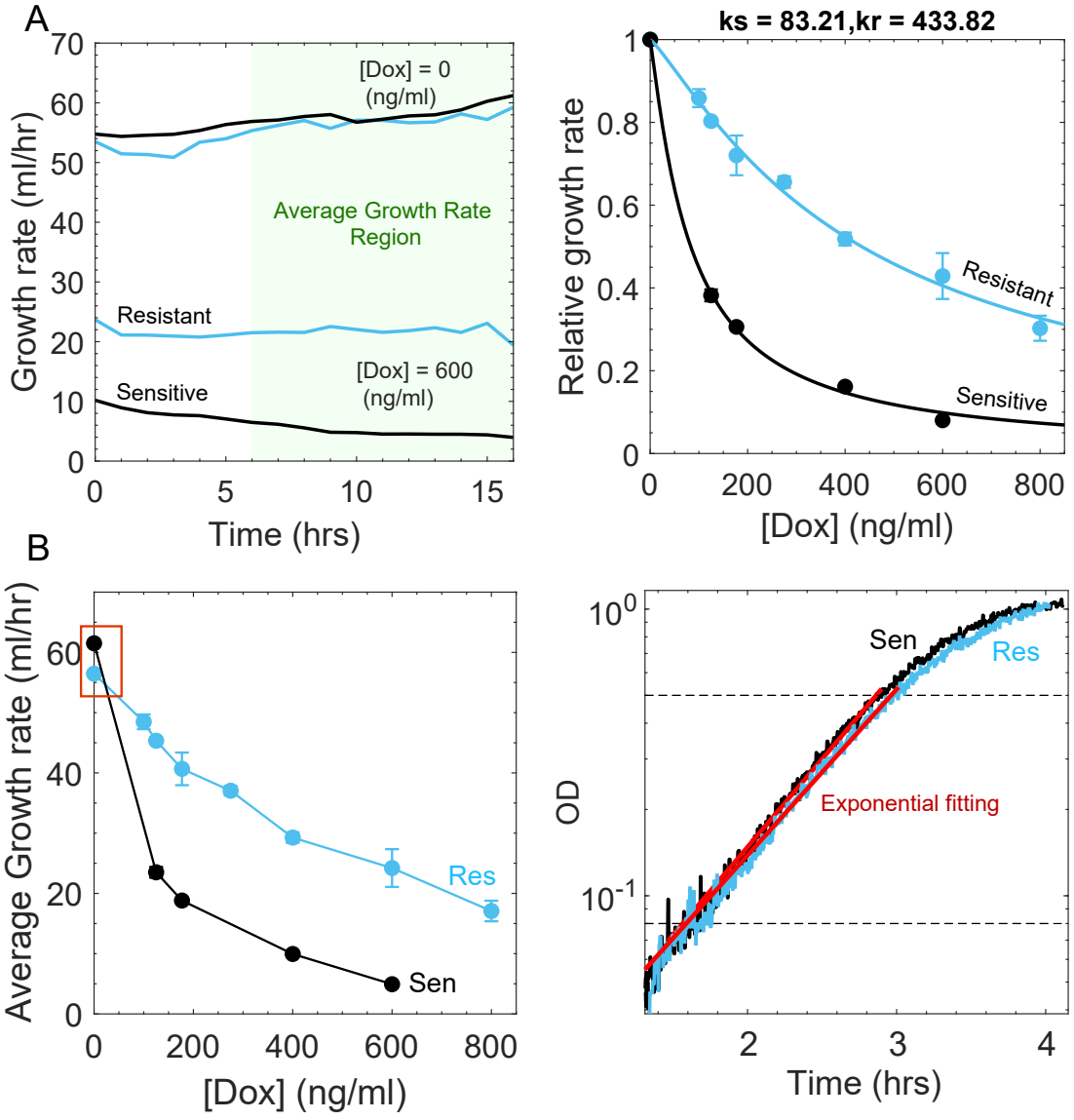

Figure 4.10: **Measuring growth rates in bioreactors.** A) Left panel: an example of measuring the growth rate of resistance (blue curves) and wild type (black curves) over time in the present of drug ([Dox] = 600 ng/ml) and without drug, then finding the average growth rate at each specific drug concentration in 10 hours (in the green region). Right panel shows fitting the data to the Hill function to estimate the IC50 of wild type (ks = 83.21 ng/ml) and the Hill coefficient (hs = 1.12), and the IC50 of the resistant type (kr = 433.82 ng/ml) and its Hill coefficient (hr = 1.18). B) This panel shows the growth rate of resistance is smaller compared to wild type, as measured by growth rate over time in the absence of drug (in the red rectangle) in the left panel, and by fitting the optical density over time data to exponential functions (in red), which shows wild type has a steeper slope compared to resistant in the right panel.

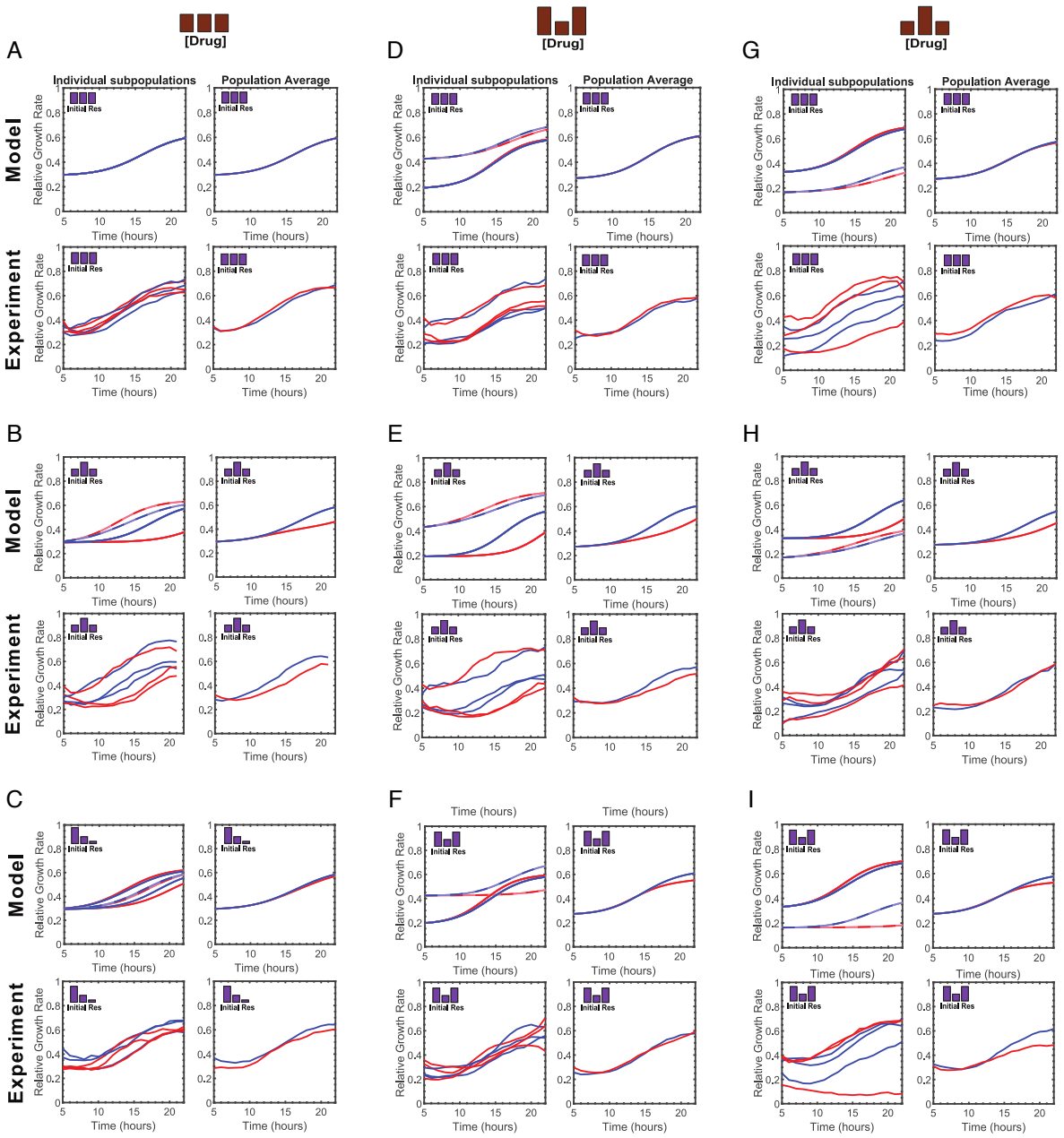

Figure 4.11: **Fixation dynamics are well captured by a simple model.** Growth rates of individual populations (left panels) and the population average growth rate (right panels) for meta-populations with potentially spatial heterogeneity in both drug concentrations (see schematic drug bar graphs at top of panels) and initial mutant fractions (indicated by bar graphs within each panel). Drug concentrations are homogeneous across habitats (A-C), higher in the edge habitats (D-F), or higher in the central habitat (G-I). Top panels are from a simple mathematical model. Bottom panels are experiment. Red curves indicate experiments without migration between habitats; blue curves are experiments with migration. All parameters and variables in this figure are listed in Table 4.1

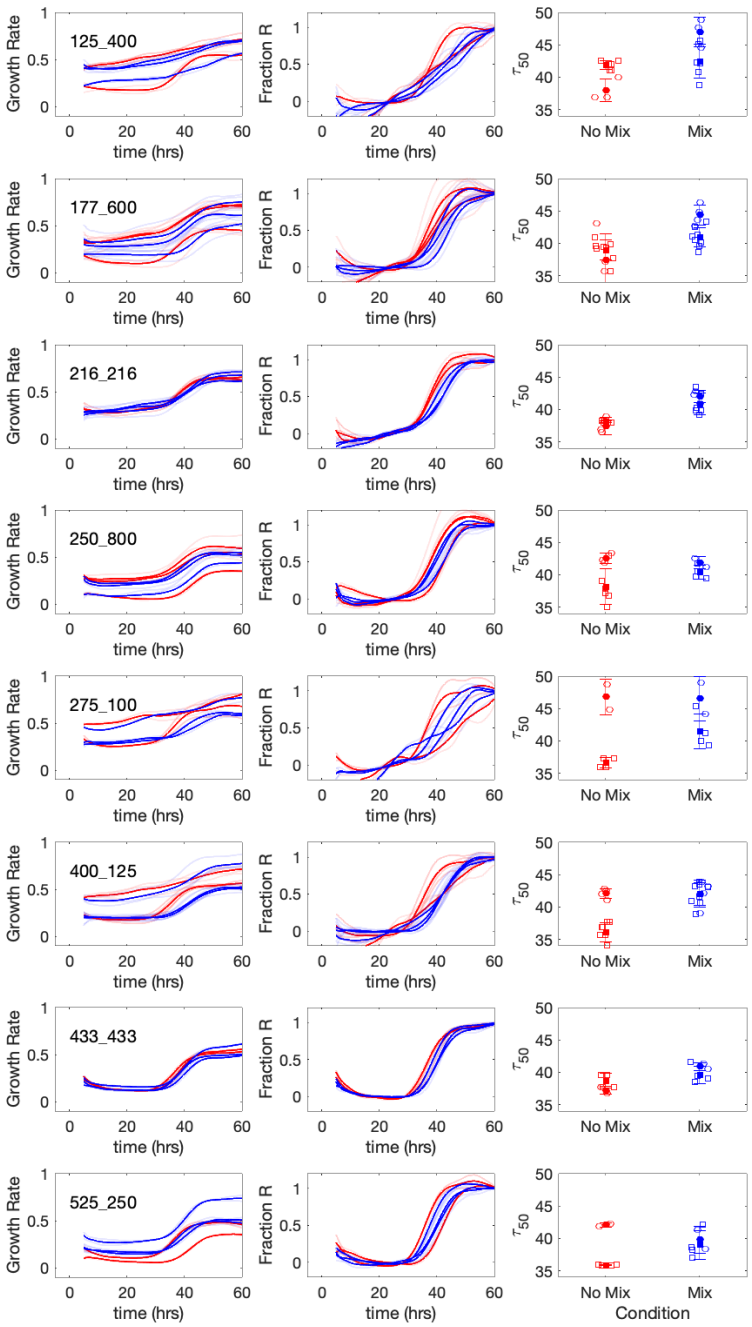

Figure 4.12: **Adaptation trajectories for individual subpopulations**. Growth rate trajectories for individual subpopulations in metacommunities with (blue) and without (red) migration. Left panels: growth rate trajectories; Center panels: growth rate trajectories normalized so that growth rate varies between 0 and 1, which serves as a coarse estimate of mutation fraction; Right panels: estimated fixation times (τ_{50}) at which growth rate is halfway between 0 (minimum) and 1 (maximum) value. Text insets (left panels) indicate drug concentration in edge and center vials.

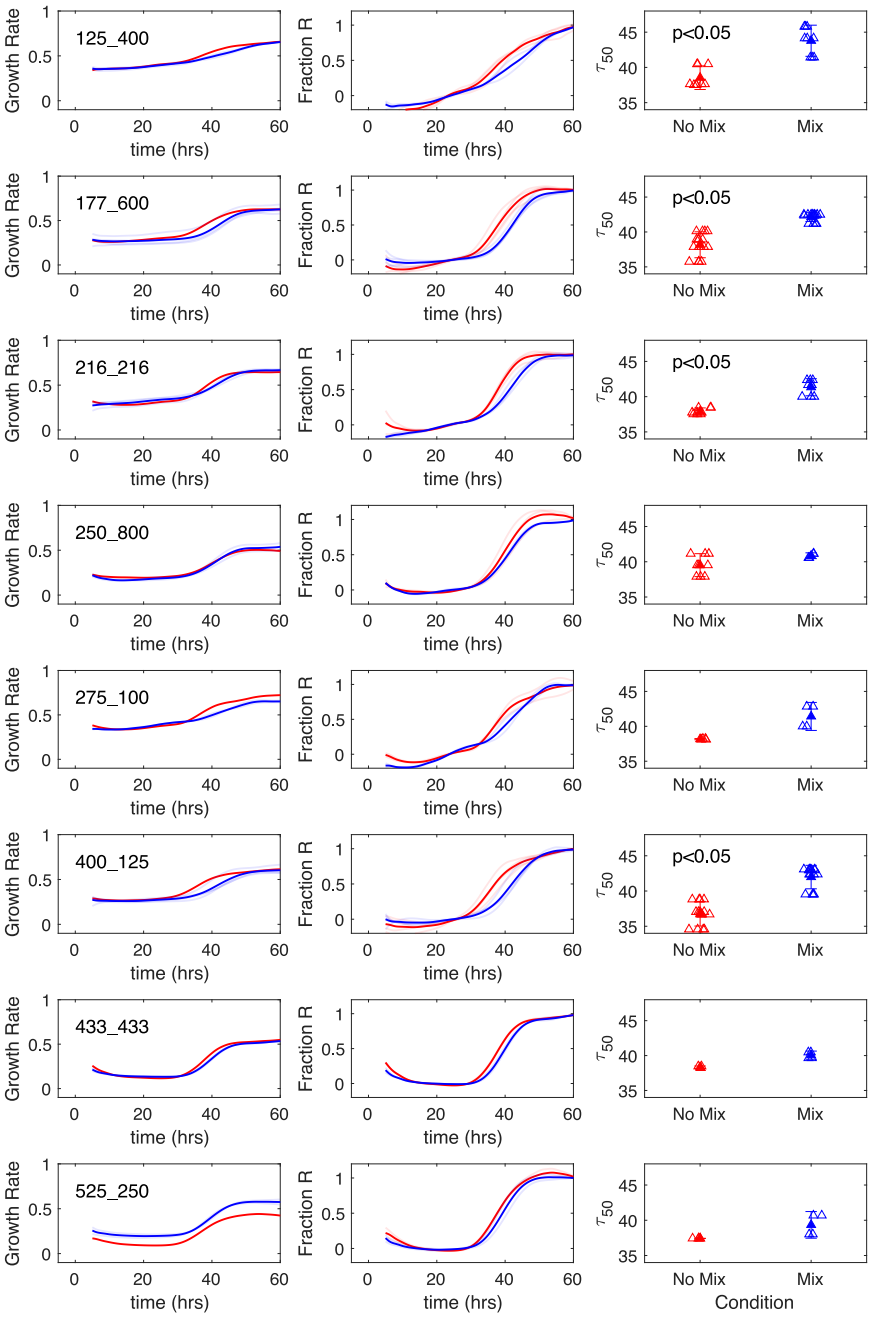

Figure 4.13: **Adaptation trajectories for total metapopulations**. Growth rate trajectories for the total metacommunity populations with (blue) and without (red) migration. Left panels: growth rate trajectories; Center panels: growth rate trajectories normalized so that growth rate varies between 0 and 1, which serves as a coarse estimate of mutation fraction; Right panels: estimated fixation times (τ_{50}) at which growth rate is halfway between 0 (minimum) and 1 (maximum) value. Inset text indicates when difference in τ_{50} is significant at $p < 0.05$. Text insets (left panels) indicate drug concentration in edge and center vials

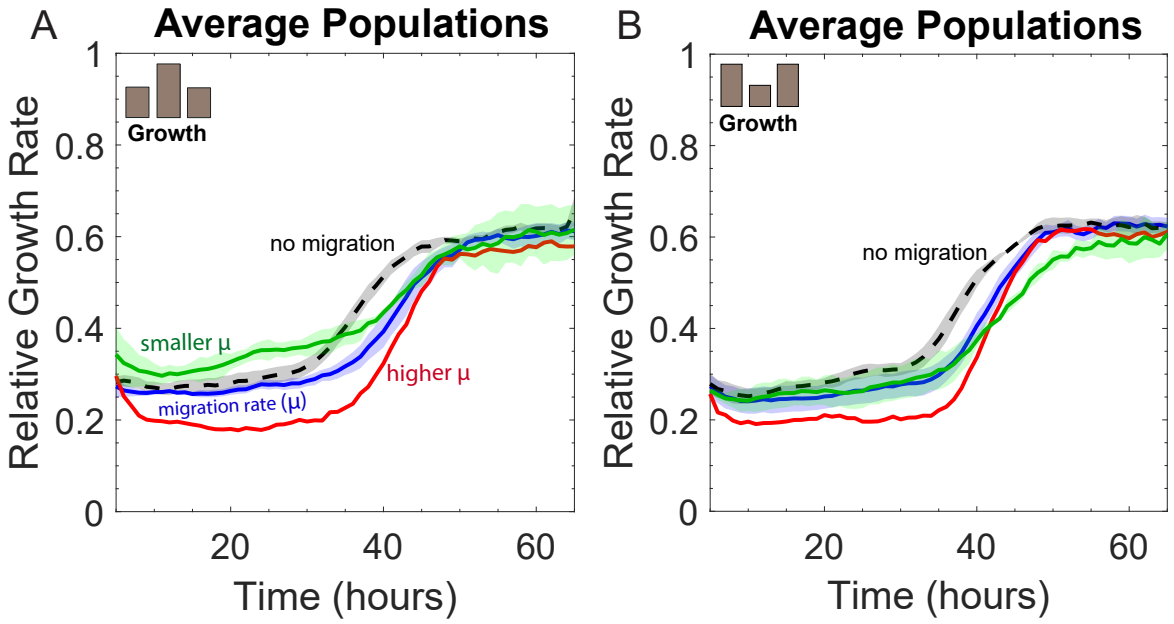

Figure 4.14: **Comparison of average growth rate of metapopulation with different migration rate μ in heterogeneous drug profiles.** A) The heterogeneous growth profile represents in the gray bars, indicating lower growth on the edge vials ([D] = 400 ng/ml) and lower growth in the middle vial ([D] = 125 ng/ml). The average growth of populations without migration represents in black dash curve. The average growth of metapopulation represent in colors, blue curve represents with migration rate of μ (1ml/s migrate every 30 mins), green curve represents with a smaller μ (1ml/s migrate every 45 mins), and higher red curve represents with a higher μ (2ml/s every 30 mins) B) Similarly, but with a heterogeneous growth profile of higher growth on the edge vials ([D] = 177 ng/ml) and lower in the middle vial ([D] = 600 ng/ml).

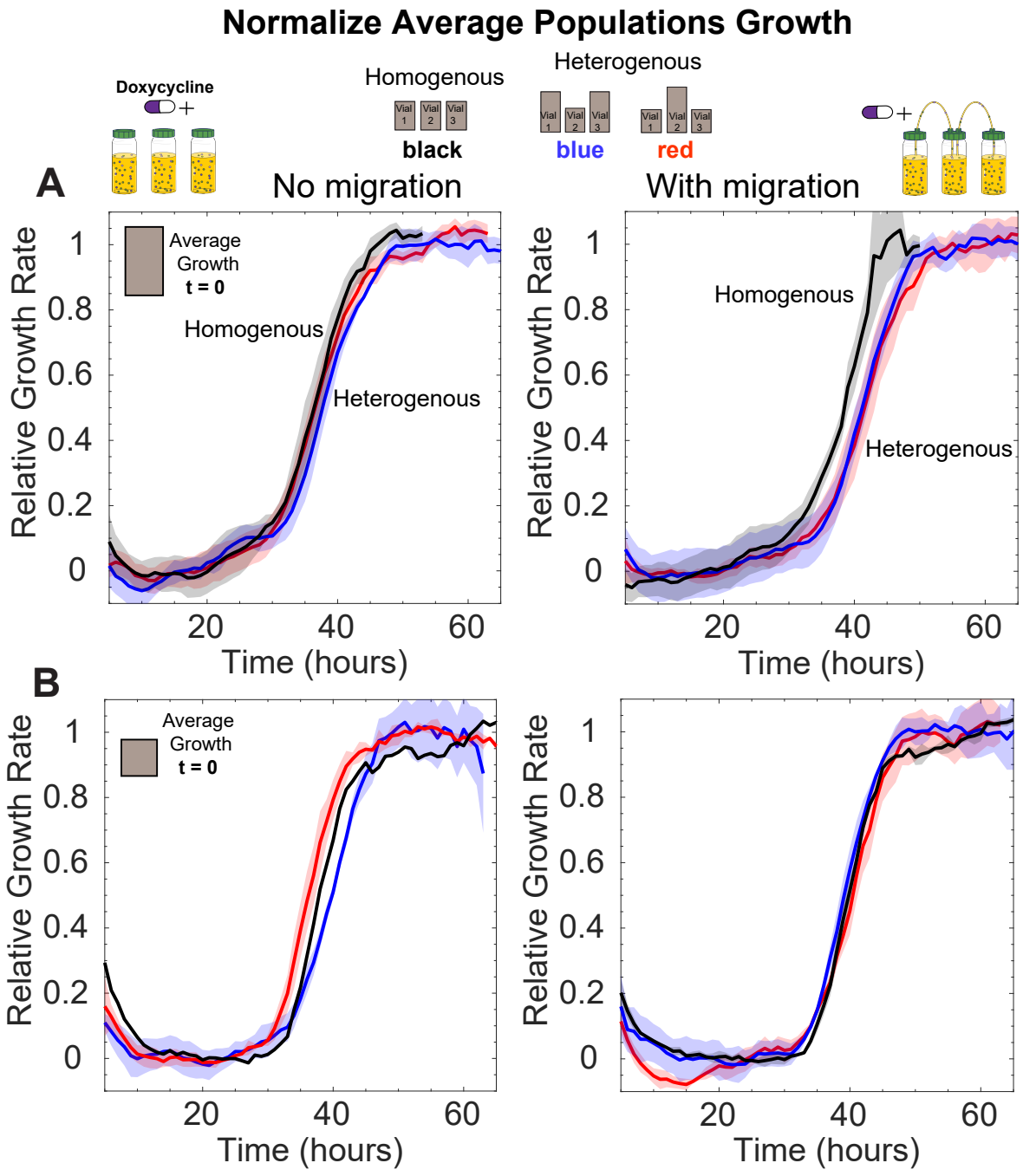

Figure 4.15: **Normalize average populations with and without migration in homogeneous and heterogeneous drug profiles** A) The nomalize average growth rates of populations without migration (left panel) and the average growth rate of population with migration (right panel). The growth curve of homogeneous drug or growth profiles are represented in black curve, the heterogeneous profiles are shown in colors, which are represented by gray bars (growth). B) Similarly to A, but the experiment is set up with a higher average drug concentration or the average of the ancestor at t = 0 has a slower growth compared to A.

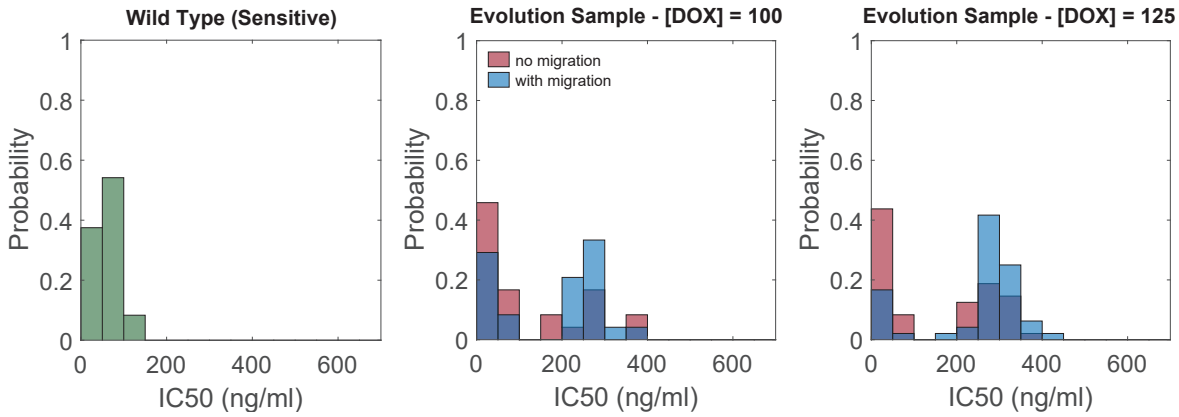

Figure 4.16: **Distribution of IC50s suggest two classes of isolates** IC50 histograms from samples that were isolated at the end of the evolution experiment. The measurements were used to compare the phenotyping of 24 colonies of the wild type (green bar, first panel). The middle panel shows the IC50 of 24 colonies isolated from each sample from migration (blue bars) and no migration (red bars) at D = 100 ng/ml. The third panel shows measurements from 48 colonies from each sample from migration and no migration at D = 125 ng/ml.

CHAPTER 5

Population Density Modulates Fixation of Drug-Resistance Mutants

5.1 Introduction

As the threat of antibiotic resistance increases, one goal of treatment may be to delay treatment failure for as long as possible. Aggressive treatment involves using high drug concentrations that can eliminate the susceptible cells, but this creates a selection pressure for resistance, which eventually causes treatment failure [182, 183]. Recent studies propose that we could utilize the interactions between bacteria as an advantage, leveraging competition to slow down the spread of resistance [89, 90, 28]. For example, using *E. coli* as a model system, recent work showed that a mixed population containing a large number of sensitive cells can be contained below a threshold density longer than matched populations without the sensitive cells [28]. The experimental setup involves treating the mixed population with a low drug concentration, allowing the sensitive cells to compete with resistant strains for resources. The results show that the mixed population can contain the treatment for a longer time compared to the resistance population alone, but only when populations can be maintained at a sufficiently high density [90, 28].

Inspired by this study, this chapter describes preliminary work investigating how competition affects the evolution of doxycycline resistance in *E. faecalis* at different population sizes, as well as in mixed populations that contain a large number of sensitive cells. To test this, we conduct experiments using two different approaches. First, we grew populations at fixed densities using a turbidostat, where feedback algorithms pump in fresh media (and expel old media) to maintain a constant cell density. In these experiments, drug concentration is constant and the population growth rate increases over time as adaptation takes place. Our second approach is similar, but not identical, to that in [28]. In that case, the population size is not fixed, but we attempt to maintain the population below a threshold size using an adaptive treatment algorithm that adds drug when growth is sufficiently high.

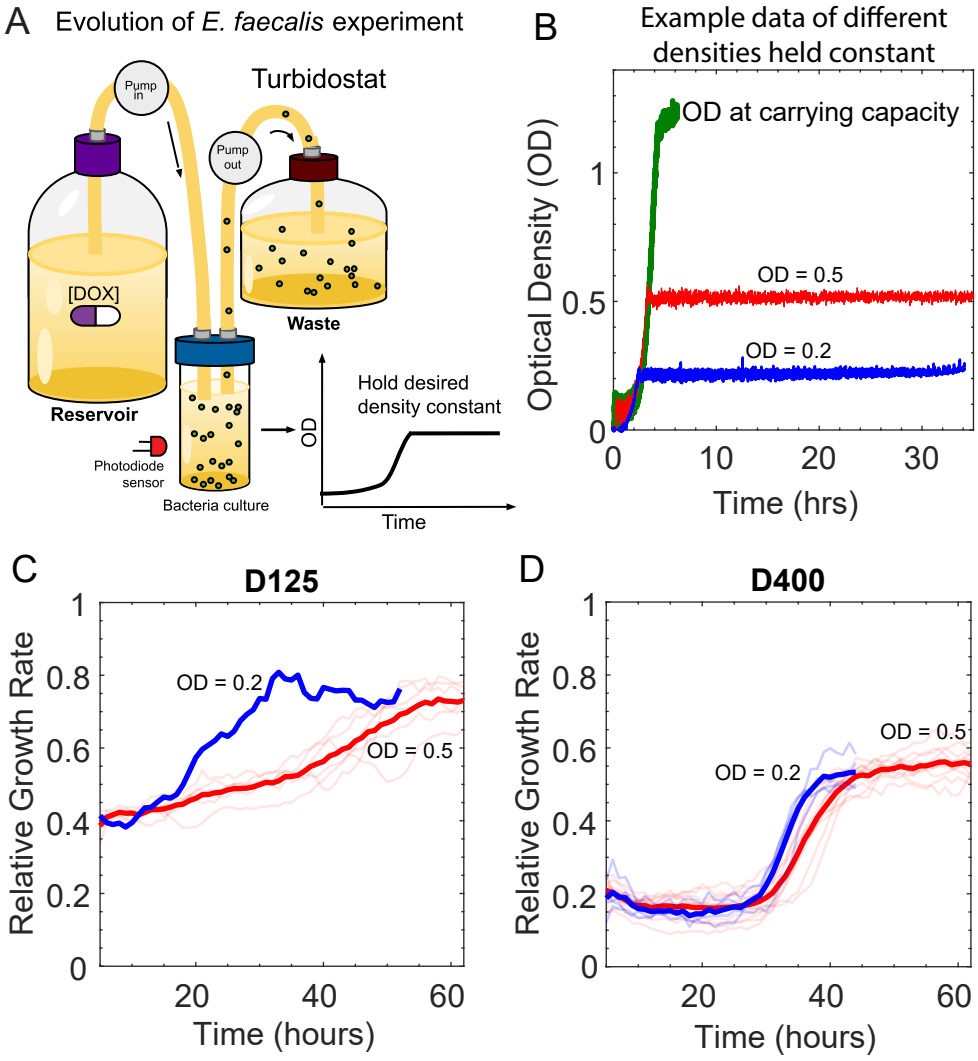

Figure 5.1: **The evolution of doxycycline resistance in well-mixed cultures evolves faster at lower density.** A) Schematic illustration showing an experiment setup. An overnight culture from a single colony of *E. faecalis* was diluted into a fresh BHI medium (at a 1:100 ratio) in a glass vial (25mL), well-mixed, and grown to a desired density. The population is held at a constant desired density using the turbidostat mode, where the pumps are controlled by a computer that receives feedback from an optical density (OD) measurement with photodiode sensor. Fresh BHI media is pumped in from a reservoir at the same rate that media and cells are pumped out to waste. B) This is an example data of populations of different sizes, where the population density was held constant at OD = 0.5 (red) and OD = 0.2 (blue), which are lower than the carrying capacity (green). C) Doxycycline resistance evolved at [Dox] = 125 ng/ml, with a comparison between the higher population size at OD = 0.5 (red curve) and the lower population size at OD = 0.2 (blue curve). D) Similarly to B, Doxycycline resistance evolved at [Dox] = 400 ng/ml.

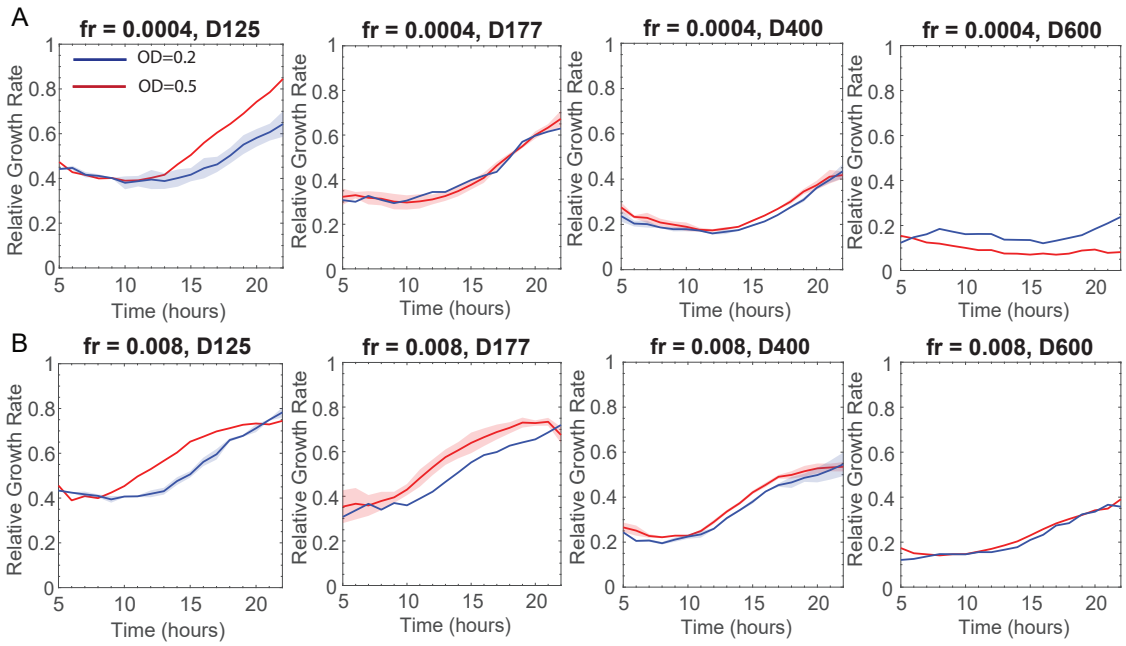

Figure 5.2: **Growth is accelerated at high densities in mixed population of sensitive and resistant cells**. A) The blue curves, which represent a mixed population of a fraction of resistant cells (fr) of 0.0004, were added to the sensitive population at a lower density (OD=0.2), while the red curves were at a higher population density (OD=0.5). The drug concentrations increase from left to right: [Dox] = 125 ng/ml, [Dox] = 177 ng/ml, [Dox] = 400 ng/ml, and [Dox] = 600 ng/ml. B) Similarly, a fraction of resistant cells (fr) of 0.008 was added to the sensitive population.

5.2 Results

5.2.1 Population size modulates adaptation in fixed density populations.

Our preliminary results include both expected and surprising findings. First, we found that evolution of resistance (from an initially sensitive population) is accelerated when the evolution takes place at higher population densities (Figure 5.1). Specifically, we exposed *E. faecalis* OG1RF populations to a constant drug concentration using the turbidostat, which is a continuous culture device that maintains a constant population (Figure 5.1A). This allowed us to measure the real-time growth rate of two populations held at different densities, with optical densities of 0.5 and 0.2 (both of which are far below carrying capacity (OD = 1.2), Figure 5.1B). Both populations were exposed to doxycycline, an inhibitor of protein synthesis. Our results indicate that the higher population (OD = 0.5) takes longer to evolve (Figure 5.1 C and 5.1 D). These findings are consistent with previous results showing competition can slow fixation in mixed communities–though the current results extend those ideas to longer timescales and de novo evolution regimes–and they can be qualitatively explained by simple competition models.

Surprisingly, however, we see clearly different results in other regimes: at sufficiently low drug concentrations we find an apparent acceleration of adaptation in mixed communities seeded with a small resistant fraction (Figure 5.2). Specifically, we seeded sensitive populations of varying sizes (OD =0.2 and OD = 0.5) with a small fraction of resistant mutants (0.4 percent, top panels, or 0.8 percent, bottom panels) at time 0 and exposed the populations to different drug concentrations. At high concentrations (e.g. D = 600 ng/ml), the smaller populations appeared to grow slightly faster at the small resistant fraction (Figure 5.2 A), consistent with inhibitory effects of competition. By contrast, at low drug concentrations we observed a surprising result: larger populations exhibit accelerated growth. This effect cannot be explained by simple models of competition and may point to drug- and strain-specific cooperative effects where, for example, sensitive cells act as sinks for the drug and high density. Investigations along these lines are currently underway.

5.2.2 Adaptive dosing strategies reveal rich dynamics of containment and escape.

In this section, we investigate adaptive dosing strategies that are similar, but not identical, to the approaches studied in [28]. In these experiments, the population size is not fixed, but we attempt to maintain the population below a threshold size using an adaptive treatment algorithm that adds drug when growth (or optical density) is sufficiently high (Figure 5.3 A). We seeded populations of different initial densities with a fixed ratio of sensitive and resistant strains. Then, using feedback control algorithms with 2 different delay time parameters (note: delay time is a parameter that determines how frequently the concentration can be updated based on past OD measurements), we attempted to maintain populations for as long as possible at their initial density by adding drug. Consistent with results from [28], we found cases where higher density populations could be contained for longer times than their low-density counterparts (Figure 5.3 B and C, left panels), while in other cases the escape times were similar ((Figure 5.3) B and C, right panels).

While density appears to module the initial escape time, the dynamics after escape are more complex. We explored these dynamics for a range of drug concentrations and initial densities (Figure 5.5; see also Figure 5.5 for a summary). For example, we observed scenarios where the higher density population reaches its steady state density faster than the lower density populations, even when escape times are comparable (Figure 5.5A). These results motivate continued investigation of not just escape time dynamics, but the dynamics of post-escape growth in adaptive therapies.

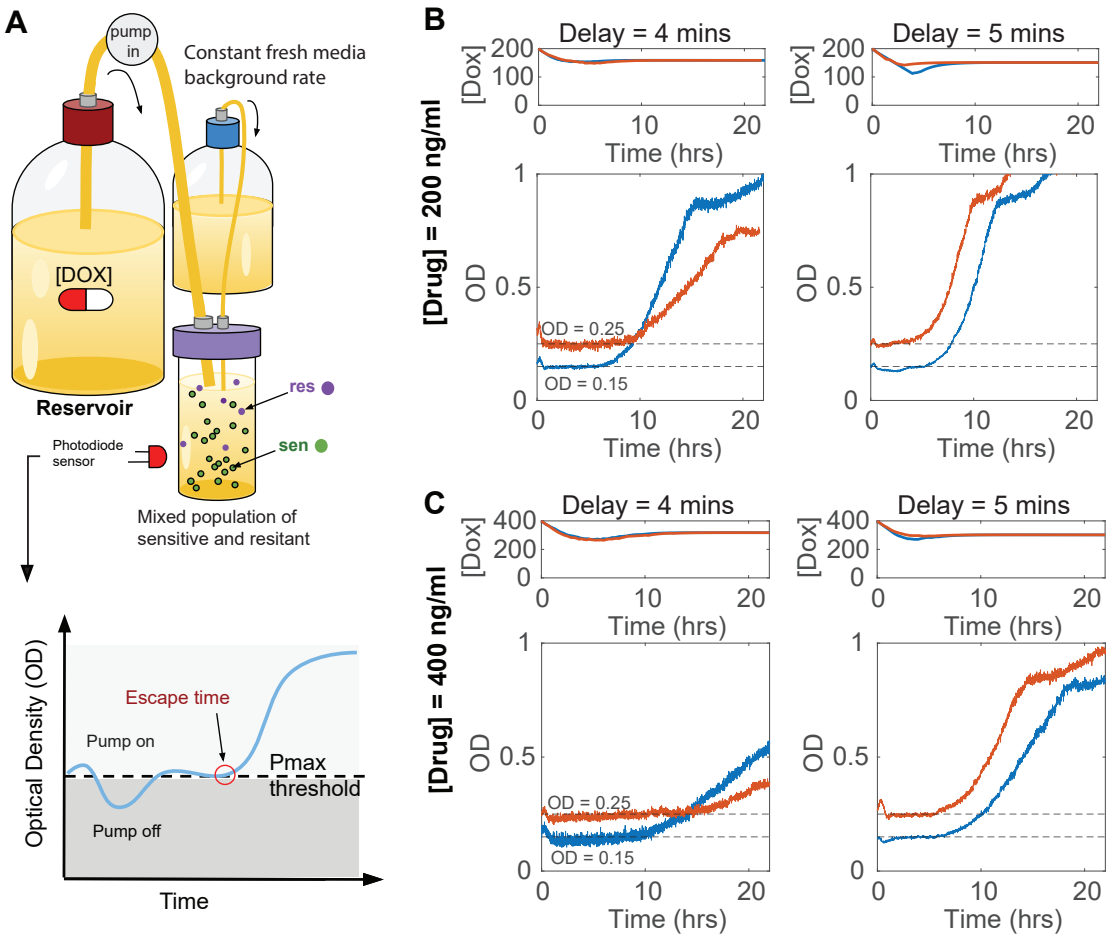

Figure 5.3: **Population size and drug delay time modulate the growth of mixed populations.**A) Schematic show the experiment was set up by using a chemostat to measure the optical density (OD) of mixed populations containing 90-10 ratio of sensitive to resistant cells in real-time. The OD provided feedback for drug dosing. The drug dosing is adjusted based on the threshold population size, Pmax, which determines the point where treatment fails. The delay time is the interval of time between "checking" the OD and deciding whether or not to add more drugs. Additionally, refresh media is added at a constant rate FN = 0.067 mL min. B) The blue curves represent a mixed population with a lower density of 0.15, while the red curves represent a population with a higher density of 0.25. The population threshold of each population is represented by the dashed lines. The top panels show the drug concentration in the vial over time, starting at [Dox] = 200 ng/ml. The delay time is 4 minutes on the left and 5 minutes on the right. C) Similarly, this panel shows the result from [Dox] = 400 ng/ml.

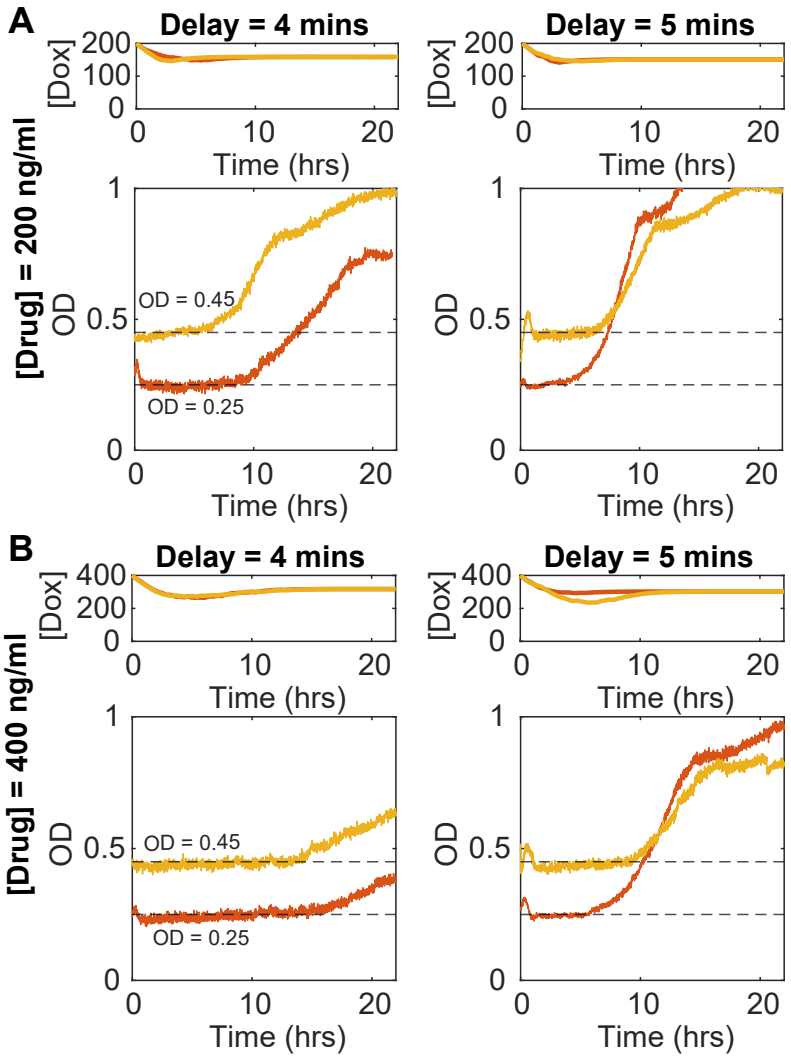

Figure 5.4: **Population size and drug delay time modulate the growth of mixed populations.** A) Similar to figure 3, this figure shows the result of comparing a higher population density of 0.45 (in yellow) to a lower population density of 0.25 (in red). The population threshold of each population is represented by the dashed lines. The top panels show the drug concentration in the vial over time, starting at [Dox] = 200 ng/ml. The delay time is 4 minutes on the left and 5 minutes on the right. B) Similarly, this panel shows the result from [Dox] = 400 ng/ml.

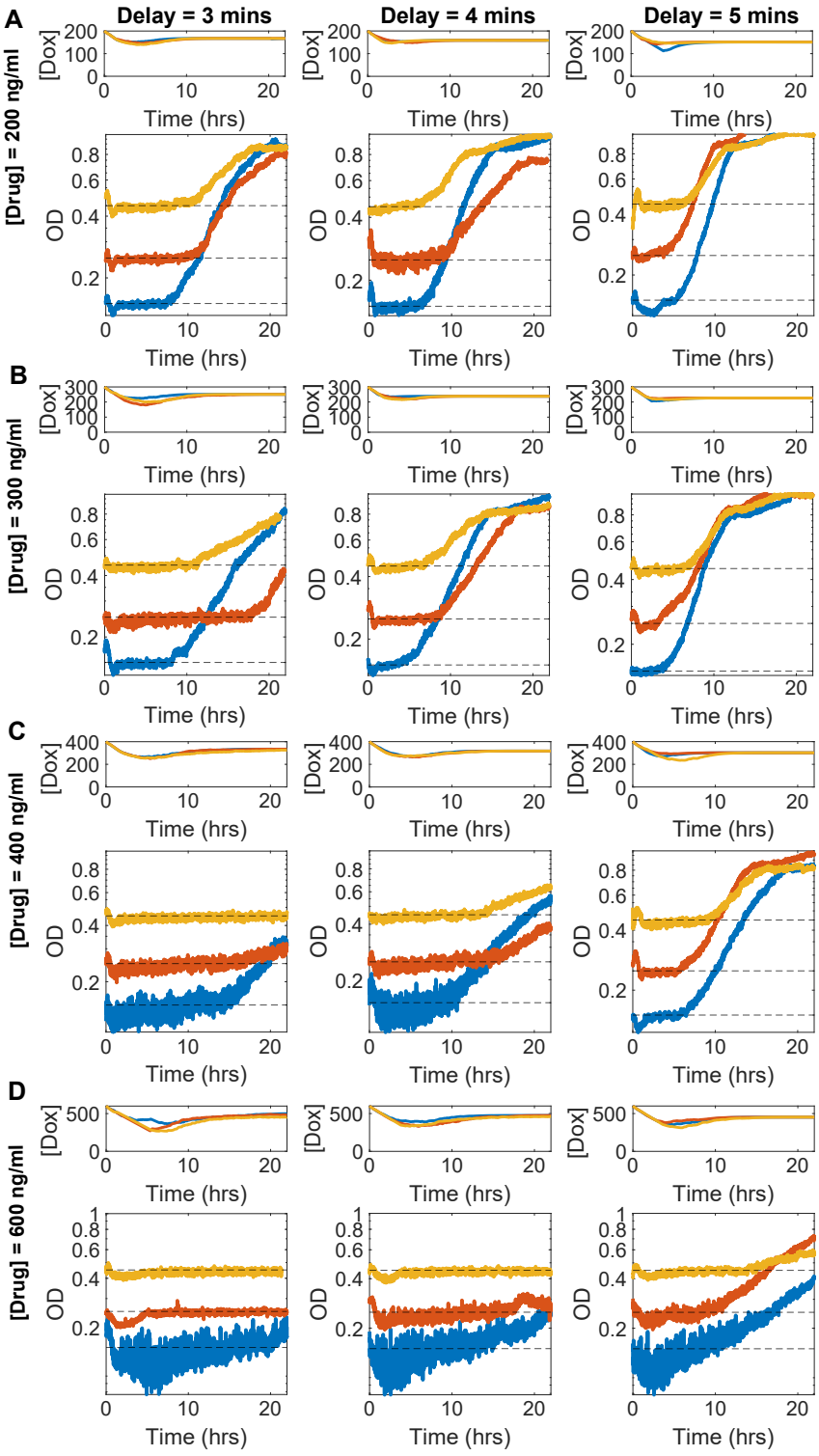

Figure 5.5: **Summary of adaptive dosing experiments at different delay times and drug concentrations.** See next page.

Figure 5.5: This figure shows the data from various mixed population sizes of: Pmax = 0.15 (in blue), with the initial OD of resistant cells is 0.015 and initial sensitive cells density of 0.135. Pmax = 0.25 (in orange), with the initial OD of resistant cells is 0.025 and initial sensitive cells density of 0.225. Pmax = 0.45 (in yellow) with the initial OD of resistant cells is 0.045 and initial sensitive cells density of 0.405. The experiment involved exposing the mixed populations to varying concentrations of doxycycline and different delay times. The dashed lines in the figure represent the thresholds for each mixed population. In all panels, the top graphs show the drug concentration in each mixed population, while The bottom graphs compare the different population sizes (ODs) using a log scale. A) The experiment results when exposed to a drug concentration of [Dox] = 200 ng/ml, with delay times increasing from left to right (3 mins, 4 mins, and 5 mins). B) The experiment results when exposed to a drug concentration of [Dox] = 300 ng/ml. C)The experiment results when exposed to a drug concentration of [Dox] = 400 ng/ml. D) The experiment results when exposed to a drug concentration of [Dox] = 600 ng/ml.

5.3 Discussion

While incomplete, these results reveal several unexpected findings that are the basis for multiple ongoing projects. One of the important factors affecting the interaction between resistant and sensitive strain is mutation rates. Previous work showed mutation rates can be influenced by the concentration of drug [184] and population size. One possible future experiment we could do is to measure the mutation rate using the Luria and Delbrück method, which is known as a fluctuation assay, and is used to estimate the mutation rate [185]. Future work also will aim to investigate potential molecular and phenotypic properties of cooperation between doxycycline resistant and doxycycline sensitive cells. We will also build on previous competition-based models to investigate whether drug sequestration may explain the apparent cooperative effects observed in experiments.

5.4 Methods and Materials

5.4.1 Strains, growth conditions, and drugs

Evolution experiments were conducted using the *E. faecalis* strain OG1RF and the resistance was derived from the same strain. Samples were stocked in 30% glycerol and stored at -80 C. Cultures for experiments were taken from single colonies grown on agar plates and then inoculated at 37^o C overnight before dilution in fresh media and the beginning of the experiment. All experiments and dose-response measurements were conducted in Brain-Heart Infusion or BHI (Remel). Doxycycline Hydrochloride (Fisher) antibiotic was used for this study, which is prepared from powdered stock and stored at -20^o C.

5.4.2 Evolution experiment using a turbidostat

We used a chemostat (eVOLVER), which is a continuous culture device developed by the Khalil lab in this study [87]. Sensitive strain and resistant strain were inoculated in 5 mL of BHI media (from a single colony) at 37^oC overnight, then 250 µl of the culture was added into a 25 mL vial with fresh media and allowed to grow to a desired optical density (higher density OD = 0.5 and lower density OD = 0.2). The same desired drug concentration was added to the vials, which are interconnected media reservoirs. The flow between the reservoirs, the culture vials, and the waste were computer-controlled to maintain specific bacterial populations.

5.4.3 Experiment with a mixed population with a single resistant mutant and wild type

The sensitive strain and resistant strain were inoculated in 5 mL of BHI media from a single colony and incubated at 37^oC overnight. Then, 250 µL of the culture was transferred to a 25 mL vial containing fresh media and allowed to grow to a desired optical density. The setup is similar to the previously described setup. Please note that the wild type and mutant cultures have a similar OD when the mixing begins, depending on the desired mutant ratio, while the total volume is kept constant.

5.4.4 Experiment setup to investigate the effects of different mixed population sizes, drug concentrations, and waiting times (delay times) on the escape time.

The sensitive strain and resistant strain were inoculated in 5 mL of BHI media from a single colony and incubated at 37^oC overnight. Then, 250 µl of the culture was transferred to a 25 mL vial containing fresh media and allowed to grow to a desired optical density. Next, the populations were mixed with 90% sensitive cells and 10% resistance cells, and the desired drug concentration was added to the interconnected media reservoirs. In this experiment, we exposed mixed populations to different drug concentrations of 200 (ng/ml), 300 (ng/ml), 400 (ng/ml), and 600 (ng/ml). The drug dosing was adjusted based on the threshold population size, Pmax (OD = 0.15, OD = 0.25, and OD = 0.45). The delay time was also varied (3 minutes, 4 minutes, and 5 minutes), which refers to the interval of time between "checking" the OD and deciding whether or not to add more drugs (pump on or pump off). Additionally, refresh media was added at a constant rate of FN = 0.067 ml/min.

5.4.5 Measuring drug resistance

To measure IC_{50}, a sample of resistant and wild type strains was streaked on a BHI agar plate. From there, a single colony from each strain was selected for inoculation and incubated at 37° C overnight. 250 µl volumes of each cell type were diluted into fresh 25 ml vials and incubated until they reached the desired optical density (OD), then exposed to a variation of drug concentrations. Following about 15 hours of growth at 37° C in a turbidostat at a constant OD. Pump duration was recorded to estimate the growth rates.

In order to quantify the values for drug resistance, average growth rate measurements for each drug concentration were normalized by OD measurements without the drug, and the dose-response curve was then fit to a Hill function ($g(d) = (1 + (d/k)^h)^{-1}$), with d the drug concentration, k the IC_{50}, and h the Hill coefficient.

5.5 Supplemental Figures

For completeness, we include additional examples of adaptation experiments that supplement the figures in the main text.

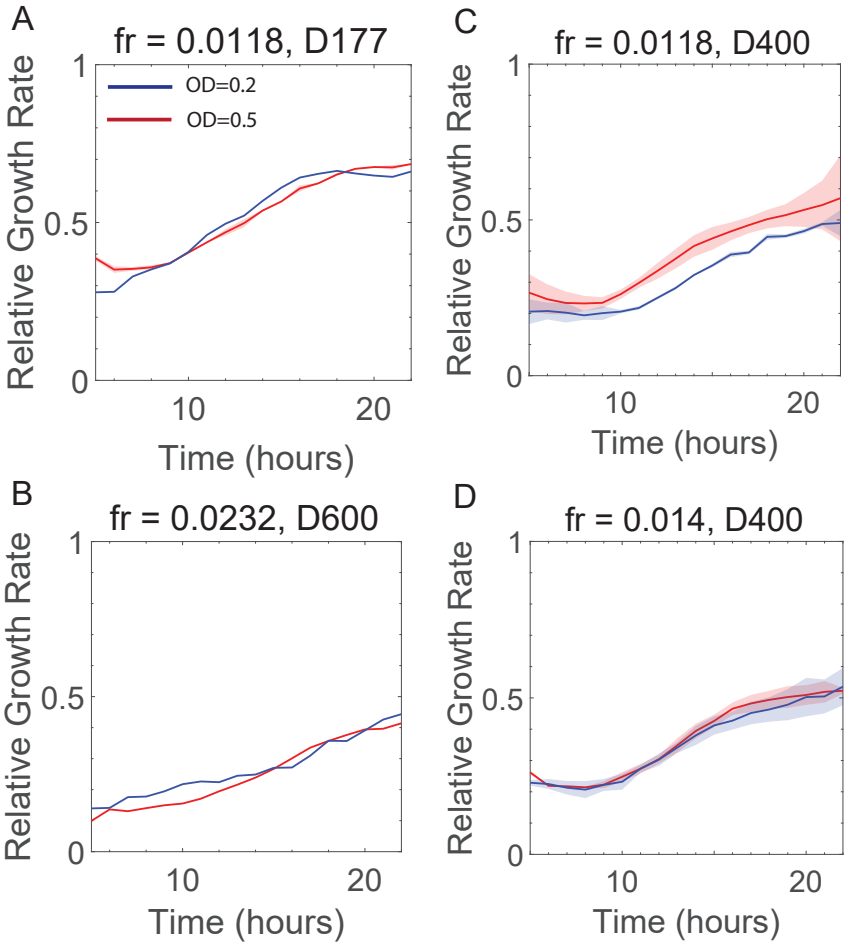

Figure 5.6: **Experiment starting with a known initial resistance**. A) The blue curves, which represent a mixed population of a fraction of resistant cells (fr) of 0.0118, were added to the sensitive population at a lower density (OD=0.2), while the red curves were at a higher population density (OD=0.5). Both populations were exposed to [Dox] = 177 ng/ml. B) Similarly, in the case of fr = 0.0232, [Dox] = 600 ng/ml. C) Case of fr = 0.0118, [Dox] = 400 ng/ml D) Case of fr = 0.014, [Dox] = 400 ng/m.

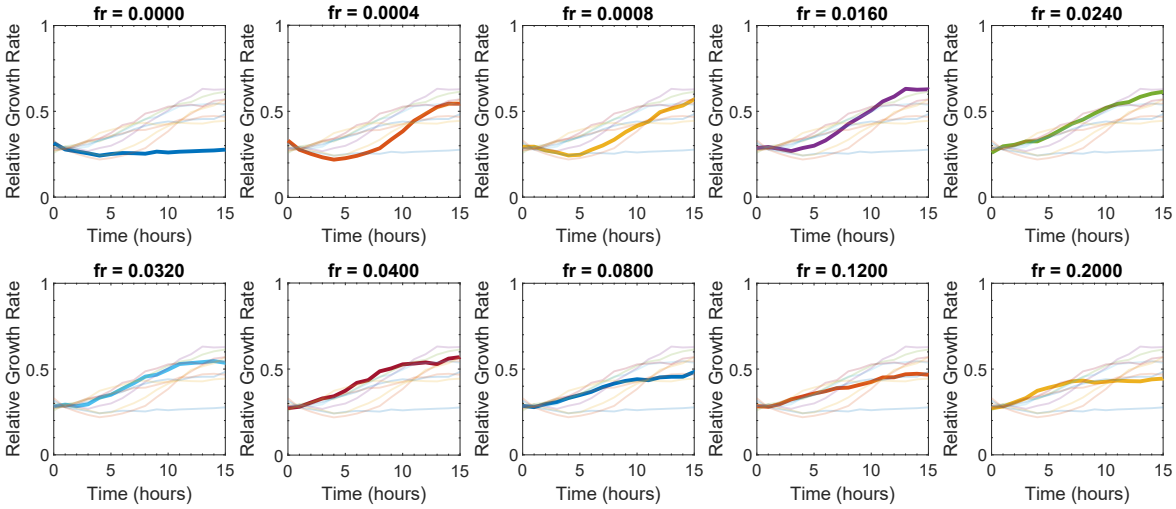

Figure 5.7: **Relative growth rate of mixed populations of sensitive and resistant cells measured with a turbidostat.** All the mixed populations were exposed to the same drug concentration (Dox = 400 ng/ml) and the population density was held at 0.5. Each plot shows the transparent curves for all 10 different initial fractions of resistance (fr), and one particular fr is highlighted in each figure (represented by thick colored curves). Please note that all curves are normalized to the curve with fr = 0.0004

CHAPTER 6

Conclusions and Future Directions

This thesis explores various evolution-based strategies for modulating the emergence of resistance in laboratory populations. We focused on two primary themes: the temporal dynamics of collateral sensitivity and the impact of spatial heterogeneity of drug distribution.

In Part I, we demonstrated that within individual drugs, the collateral effects over time vary. For some drugs, bacteria evolve at early stages favor collateral resistance and later stages collateral sensitivity. This suggests that depending on the drug treatment, there is an optimal time window during which drug switching can be the most effective treatment. However, in the case of Daptomycin, while mutants evolve in parallel under the same selection pressure, we observed collateral effects that differ substantially across the individual Daptomycin populations. Daptomycin resistances show different levels of resistance to CRO, and surprisingly, DNA sequencing reveals a surprisingly rich collection of different lineages. This finding highlights the complicated dynamic of the evolution of Daptomycin evolution, even in a controlled laboratory experiment. Daptomycin is considered one of the last-resorts to treat infections, and considering real life situations are considerably more complex, which emphasizes the challenges associated with designing and developing effective strategies using collateral effects. Future work may look into how these results change in other growth modalities–for example, in surface-associated biofilms, which is the most state of cells in natural environments.

Overall, our results from part II on spatial heterogeneity indicate that by balancing the heterogeneity of selection pressures with migration in metapopulations it may be possible to slow down evolution of resistance. Our studies involve large populations, but future work will aim to extend these approaches to smaller populations where effects of demographic noise and evolutionary stochasticicty are likely important. In future work, we also hope to investigate the effects of different connection topologies in the metacommunities, and to explore adaptation in communities with significantly smaller migration rates, where dynamics are predicted to be considerably different [20].

We incorporated several different experimental approaches to study evolution in the lab. In Chapters 2 and 3, evolution was accomplished via serial dilution in small test tubes. In Chapter

4, the experimental setup involved holding the population at the desired density by using the turbidostat under constant selection pressure, while in Chapter 5, we used optical density to provide feedback for drug dosing and therefore time-dependent selection pressures. Our preliminary results suggest that population size and drug delay time modulate the growth of mixed populations. As a whole, these varied approaches provide a framework for experimentally studying evolutionary adaptation in different limits–large and small populations, fixed and adaptive drug dosing–in the lab.

Overall, our research provides insights that contribute to an improved basic science understanding of resistance evolution that may one day lead to new strategies for the clinical management of infection. Our work serves as a reminder that even in the most controlled and simplistic scenarios in the lab, evolution is dynamic and complex.

BIBLIOGRAPHY

[1] Michelle R Scribner, Alfonso Santos-Lopez, Christopher W Marshall, Christopher Deitrick, and Vaughn S Cooper. Parallel evolution of tobramycin resistance across species and environments. *MBio*, 11(3):10–1128, 2020.

[2] Christopher Walsh et al. *Antibiotics: actions, origins, resistance.* American Society for Microbiology (ASM), 2003.

[3] Andrew F Read and Robert J Woods. Antibiotic resistance management. *Evolution, medicine, and public health*, 2014(1):147, 2014.

[4] Ramanan Laxminarayan. Antibiotic effectiveness: balancing conservation against innovation. *science*, 345(6202):1299–1301, 2014.

[5] Brad Spellberg and David N Gilbert. The future of antibiotics and resistance: a tribute to a career of leadership by john bartlett. *Clinical infectious diseases*, 59(suppl_2):S71–S75, 2014.

[6] Laura JV Piddock. The crisis of no new antibiotics—what is the way forward? *The Lancet infectious diseases*, 12(3):249–253, 2012.

[7] Saswati Sengupta, Madhab K Chattopadhyay, and Hans-Peter Grossart. The multifaceted roles of antibiotics and antibiotic resistance in nature. *Frontiers in microbiology*, 4:47, 2013.

[8] Carolyn Anne Michael, Dale Dominey-Howes, and Maurizio Labbate. The antimicrobial resistance crisis: causes, consequences, and management. *Frontiers in public health*, 2:145, 2014.

[9] Bilal Aslam, Wei Wang, Muhammad Imran Arshad, Mohsin Khurshid, Saima Muzammil, Muhammad Hidayat Rasool, Muhammad Atif Nisar, Ruman Farooq Alvi, Muhammad Aamir Aslam, Muhammad Usman Qamar, et al. Antibiotic resistance: a rundown of a global crisis. *Infection and drug resistance*, 11:1645, 2018.

[10] Nicholas A Church and John L McKillip. Antibiotic resistance crisis: Challenges and imperatives. *Biologia*, 76(5):1535–1550, 2021.

[11] Gitta De Wit, Luka Svet, Bram Lories, and Hans P Steenackers. Microbial interspecies interactions and their impact on the emergence and spread of antimicrobial resistance. *Annual Review of Microbiology*, 76:179–192, 2022.

[12] Michael J Bottery, Jonathan W Pitchford, and Ville-Petri Friman. Ecology and evolution of antimicrobial resistance in bacterial communities. *The ISME Journal*, 15(4):939–948, 2021.

[13] Marlis Denk-Lobnig and Kevin B Wood. Antibiotic resistance in bacterial communities. *Current Opinion in Microbiology*, 74:102306, 2023.

[14] Erwin M. Brown and Dilip Nathwani. Antibiotic cycling or rotation: a systematic review of the evidence of efficacy. *Journal of Antimicrobial Chemotherapy*, 55(1):6–9, 01 2005.

[15] Carl T. Bergstrom, Monique Lo, and Marc Lipsitch. Ecological theory suggests that antimicrobial cycling will not reduce antimicrobial resistance in hospitals. *Proceedings of the National Academy of Sciences*, 101(36):13285–13290, 2004.

[16] Daniel Nichol, Peter Jeavons, Alexander G Fletcher, Robert A Bonomo, Philip K Maini, Jerome L Paul, Robert A Gatenby, Alexander RA Anderson, and Jacob G Scott. Steering evolution with sequential therapy to prevent the emergence of bacterial antibiotic resistance. *PLoS Comput Biol*, 11(9):e1004493, 2015.

[17] Aditi Batra, Roderich Roemhild, Emilie Rousseau, Sören Franzenburg, Stefan Niemann, and Hinrich Schulenburg. High potency of sequential therapy with only β-lactam antibiotics. *Elife*, 10:e68876, 2021.

[18] Qiucen Zhang, Guillaume Lambert, David Liao, Hyunsung Kim, Kristelle Robin, Chihkuan Tung, Nader Pourmand, and Robert H Austin. Acceleration of emergence of bacterial antibiotic resistance in connected microenvironments. *Science*, 333(6050):1764–1767, 2011.

[19] Michael Baym, Tami D Lieberman, Eric D Kelsic, Remy Chait, Rotem Gross, Idan Yelin, and Roy Kishony. Spatiotemporal microbial evolution on antibiotic landscapes. *Science*, 353(6304):1147–1151, 2016.

[20] Maxwell G De Jong and Kevin B Wood. Tuning spatial profiles of selection pressure to modulate the evolution of drug resistance. *Physical review letters*, 120(23):238102, 2018.

[21] Alison F Feder, Kristin N Harper, Chanson J Brumme, and Pleuni S Pennings. Understanding patterns of hiv multi-drug resistance through models of temporal and spatial drug heterogeneity. *eLife*, 10:e69032, sep 2021.

[22] Eugene A Yurtsev, Hui Xiao Chao, Manoshi S Datta, Tatiana Artemova, and Jeff Gore. Bacterial cheating drives the population dynamics of cooperative antibiotic resistance plasmids. *Molecular systems biology*, 9(1):683, 2013.

[23] Hannah R Meredith, Allison J Lopatkin, Deverick J Anderson, and Lingchong You. Bacterial temporal dynamics enable optimal design of antibiotic treatment. *PLoS Comput Biol*, 11(4):e1004201, 2015.

[24] Hannah R Meredith, Jaydeep K Srimani, Anna J Lee, Allison J Lopatkin, and Lingchong You. Collective antibiotic tolerance: mechanisms, dynamics and intervention. *Nature chemical biology*, 11(3):182, 2015.

[25] Nathan Farrokhian, Jeff Maltas, Mina Dinh, Arda Durmaz, Patrick Ellsworth, Masahiro Hitomi, Erin McClure, Andriy Marusyk, Artem Kaznatcheev, and Jacob G Scott. Measuring competitive exclusion in non–small cell lung cancer. *Science Advances*, 8(26):eabm7212, 2022.

[26] Robert A Gatenby, Ariosto S Silva, Robert J Gillies, and B Roy Frieden. Adaptive therapy. *Cancer research*, 69(11):4894–4903, 2009.

[27] Jeffrey West, Li You, Jingsong Zhang, Robert A Gatenby, Joel S Brown, Paul K Newton, and Alexander RA Anderson. Towards multidrug adaptive therapy. *Cancer research*, 80(7):1578–1589, 2020.

[28] Elsa Hansen, Jason Karslake, Robert J Woods, Andrew F Read, and Kevin B Wood. Antibiotics can be used to contain drug-resistant bacteria by maintaining sufficiently large sensitive populations. *PLoS biology*, 18(5):e3000713, 2020.

[29] Anat Zimmer, Itay Katzir, Erez Dekel, Avraham E Mayo, and Uri Alon. Prediction of multidimensional drug dose responses based on measurements of drug pairs. *Proceedings of the National Academy of Sciences*, 113(37):10442–10447, 2016.

[30] Kevin Wood, Satoshi Nishida, Eduardo D Sontag, and Philippe Cluzel. Mechanism-independent method for predicting response to multidrug combinations in bacteria. *Proceedings of the National Academy of Sciences*, 109(30):12254–12259, 2012.

[31] Joseph Peter Torella, Remy Chait, and Roy Kishony. Optimal drug synergy in antimicrobial treatments. *PLoS Comput Biol*, 6(6):e1000796, 2010.

[32] Jean-Baptiste Michel, Pamela J Yeh, Remy Chait, Robert C Moellering, and Roy Kishony. Drug interactions modulate the potential for evolution of resistance. *Proceedings of the National Academy of Sciences*, 105(39):14918–14923, 2008.

[33] Ziah Dean, Jeff Maltas, and Kevin Wood. Antibiotic interactions shape short-term evolution of resistance in e. faecalis. *PLoS pathogens*, 16(3):e1008278, 2020.

[34] Leonie Johanna Jahn, Daniel Simon, Mia Jensen, Charles Bradshaw, Mostafa Mostafa Hashim Ellabaan, and Morten Otto Alexander Sommer. Compatibility of evolutionary responses to constituent antibiotics drive resistance evolution to drug pairs. *Molecular Biology and Evolution*, 2021.

[35] Elif Tekin, Casey Beppler, Cynthia White, Zhiyuan Mao, Van M Savage, and Pamela J Yeh. Enhanced identification of synergistic and antagonistic emergent interactions among three or more drugs. *Journal of The Royal Society Interface*, 13(119):20160332, 2016.

[36] Erida Gjini and Kevin B Wood. Price equation captures the role of drug interactions and collateral effects in the evolution of multidrug resistance. *Elife*, 10:e64851, 2021.

[37] Camilo Barbosa, Roderich Römhild, Philip Rosenstiel, and Hinrich Schulenburg. Evolutionary stability of collateral sensitivity to antibiotics in the model pathogen pseudomonas aeruginosa. *Elife*, 8:e51481, 2019.

[38] Jeff Maltas, Douglas M McNally, and Kevin B Wood. Evolution in alternating environments with tunable interlandscape correlations. *Evolution*, 75(1):10–24, 2021.

[39] Viktória Lázár, Gajinder Pal Singh, Réka Spohn, István Nagy, Balázs Horváth, Mónika Hrtyan, Róbert Busa-Fekete, Balázs Bogos, Orsolya Méhi, Bálint Csörgő, et al. Bacterial evolution of antibiotic hypersensitivity. *Molecular systems biology*, 9(1):700, 2013.

[40] Viktória Lázár, István Nagy, Réka Spohn, Bálint Csörgő, Ádám Györkei, Ákos Nyerges, Balázs Horváth, Andrea Vörös, Róbert Busa-Fekete, Mónika Hrtyan, et al. Genome-wide analysis captures the determinants of the antibiotic cross-resistance interaction network. *Nature communications*, 5(1):1–12, 2014.

[41] Lejla Imamovic and Morten OA Sommer. Use of collateral sensitivity networks to design drug cycling protocols that avoid resistance development. *Science translational medicine*, 5(204):204ra132–204ra132, 2013.

[42] Lejla Imamovic, Mostafa Mostafa Hashim Ellabaan, Ana Manuel Dantas Machado, Linda Citterio, Tune Wulff, Soren Molin, Helle Krogh Johansen, and Morten Otto Alexander Sommer. Drug-driven phenotypic convergence supports rational treatment strategies of chronic infections. *Cell*, 172(1-2):121–134, 2018.

[43] Roderich Roemhild, Marius Linkevicius, and Dan I Andersson. Molecular mechanisms of collateral sensitivity to the antibiotic nitrofurantoin. *PLoS biology*, 18(1):e3000612, 2020.

[44] Boyang Zhao, Joseph C Sedlak, Raja Srinivas, Pau Creixell, Justin R Pritchard, Bruce Tidor, Douglas A Lauffenburger, and Michael T Hemann. Exploiting temporal collateral sensitivity in tumor clonal evolution. *Cell*, 165(1):234–246, 2016.

[45] Sarah M Ardell and Sergey Kryazhimskiy. The population genetics of collateral resistance and sensitivity. *eLife*, 10:e73250, 2021.

[46] Cristina Herencias, Jerónimo Rodríguez-Beltrán, Ricardo León-Sampedro, Aida Alonso-del Valle, Jana Palkovičová, Rafael Cantón, and Álvaro San Millán. Collateral sensitivity associated with antibiotic resistance plasmids. *Elife*, 10:e65130, 2021.

[47] Michael Lässig, Ville Mustonen, and Armita Nourmohammad. Steering and controlling evolution—from bioengineering to fighting pathogens. *Nature Reviews Genetics*, pages 1–17, 2023.

[48] Michael S Gilmore, Don B Clewell, Yasuyoshi Ike, and Nathan Shankar. Enterococci: From commensals to leading causes of drug resistant infection [internet]. 2014.

[49] Cesar A Arias, German A Contreras, and Barbara E Murray. Management of multidrug-resistant enterococcal infections. *Clinical microbiology and infection*, 16(6):555–562, 2010.

[50] Yesim Cetinkaya, Pamela Falk, and C Glen Mayhall. Vancomycin-resistant enterococci. *Clinical microbiology reviews*, 13(4):686–707, 2000.

[51] Mark M Huycke, Daniel F Sahm, and Michael S Gilmore. Multiple-drug resistant enterococci: the nature of the problem and an agenda for the future. *Emerging infectious diseases*, 4(2):239, 1998.

[52] Kelli L Palmer, Anu Daniel, Crystal Hardy, Jared Silverman, and Michael S Gilmore. Genetic basis for daptomycin resistance in enterococci. *Antimicrobial agents and chemotherapy*, 55(7):3345–3356, 2011.

[53] Corwin Miller, Jiayi Kong, Truc T Tran, Cesar A Arias, Gerda Saxer, and Yousif Shamoo. Adaptation of enterococcus faecalis to daptomycin reveals an ordered progression to resistance. *Antimicrobial agents and chemotherapy*, 57(11):5373–5383, 2013.

[54] Kelli L Palmer, Veronica N Kos, and Michael S Gilmore. Horizontal gene transfer and the genomics of enterococcal antibiotic resistance. *Current opinion in microbiology*, 13(5):632–639, 2010.

[55] Robert Woods, Andrew F Read, Meghan Forstchen, Clare Kinnear, Jordan McKaig, Twisha Patel, Kevin Tracy, and Carol L Young. Rising daptomycin resistance in enterococcus faecium across a hospital system occurred via rampant recurrent evolution and occasional transmission between patients. *bioRxiv*, pages 2023–05, 2023.

[56] Jeff Maltas and Kevin B Wood. Pervasive and diverse collateral sensitivity profiles inform optimal strategies to limit antibiotic resistance. *PLoS biology*, 17(10):e3000515, 2019.

[57] Camilo Barbosa, Vincent Trebosc, Christian Kemmer, Philip Rosenstiel, Robert Beardmore, Hinrich Schulenburg, and Gunther Jansen. Alternative evolutionary paths to bacterial antibiotic resistance cause distinct collateral effects. *Molecular biology and evolution*, 34(9):2229–2244, 2017.

[58] Tugce Oz, Aysegul Guvenek, Sadik Yildiz, Enes Karaboga, Yusuf Talha Tamer, Nirva Mumcuyan, Vedat Burak Ozan, Gizem Hazal Senturk, Murat Cokol, Pamela Yeh, et al. Strength of selection pressure is an important parameter contributing to the complexity of antibiotic resistance evolution. *Molecular biology and evolution*, 31(9):2387–2401, 2014.

[59] Daniel Nichol, Joseph Rutter, Christopher Bryant, Andrea M Hujer, Sai Lek, Mark D Adams, Peter Jeavons, Alexander RA Anderson, Robert A Bonomo, and Jacob G Scott. Antibiotic collateral sensitivity is contingent on the repeatability of evolution. *Nature communications*, 10(1):1–10, 2019.

[60] Jeff Maltas, Brian Krasnick, and Kevin B Wood. Using selection by nonantibiotic stressors to sensitize bacteria to antibiotics. *Molecular biology and evolution*, 37(5):1394–1406, 2020.

[61] Pooja Bhardwaj, Amrita Hans, Kinnari Ruikar, Ziqiang Guan, and Kelli L Palmer. Reduced chlorhexidine and daptomycin susceptibility in vancomycin-resistant enterococcus faecium after serial chlorhexidine exposure. *Antimicrobial agents and chemotherapy*, 62(1), 2018.

[62] Viktória Lázár, Ana Martins, Réka Spohn, Lejla Daruka, Gábor Grézal, Gergely Fekete, Mónika Számel, Pramod K Jangir, Bálint Kintses, Bálint Csörgő, et al. Antibiotic-resistant bacteria show widespread collateral sensitivity to antimicrobial peptides. *Nature microbiology*, 3(6):718–731, 2018.

[63] Anna Knöppel, Joakim Näsvall, and Dan I Andersson. Evolution of antibiotic resistance without antibiotic exposure. *Antimicrobial agents and chemotherapy*, 61(11), 2017.

[64] Kaitlin E Creamer, Frederick S Ditmars, Preston J Basting, Karina S Kunka, Issam N Hamdallah, Sean P Bush, Zachary Scott, Amanda He, Stephanie R Penix, Alexandra S Gonzales, et al. Benzoate-and salicylate-tolerant strains of escherichia coli k-12 lose antibiotic resistance during laboratory evolution. *Applied and environmental microbiology*, 83(2):e02736–16, 2017.

[65] Jeremy P Moore, Haofan Li, Morgan L Engmann, Katarina M Bischof, Karina S Kunka, Mary E Harris, Anna C Tancredi, Frederick S Ditmars, Preston J Basting, Nadja S George, et al. Inverted regulation of multidrug efflux pumps, acid resistance, and porins in benzoate-evolved escherichia coli k-12. *Applied and environmental microbiology*, 85(16):e00966–19, 2019.

[66] Shamreen Iram, Emily Dolson, Joshua Chiel, Julia Pelesko, Nikhil Krishnan, Özenç Güngör, Benjamin Kuznets-Speck, Sebastian Deffner, Efe Ilker, Jacob G Scott, et al. Controlling the speed and trajectory of evolution with counterdiabatic driving. *Nature Physics*, pages 1–8, 2020.

[67] Roderich Roemhild and Dan I Andersson. Mechanisms and therapeutic potential of collateral sensitivity to antibiotics. *PLoS Pathogens*, 17(1):e1009172, 2021.

[68] Mari C Rodriguez de Evgrafov, Marius Faza, Konstantinos Asimakopoulos, and Morten OA Sommer. Systematic investigation of resistance evolution to common antibiotics reveals conserved collateral responses across common human pathogens. *Antimicrobial Agents and Chemotherapy*, 65(1), 2020.

[69] Andrew M Beckley and Erik S Wright. Identification of antibiotic pairs that evade concurrent resistance via a retrospective analysis of antimicrobial susceptibility test results. *The Lancet Microbe*, 2(10):e545–e554, 2021.

[70] Laura B Zwep, Yob Haakman, Kevin LW Duisters, Jacqueline J Meulman, Apostolos Liakopoulos, and JG Coen van Hasselt. Identification of antibiotic collateral sensitivity and resistance interactions in population surveillance data. *JAC-antimicrobial resistance*, 3(4):dlab175, 2021.

[71] Andrew Dhawan, Daniel Nichol, Fumi Kinose, Mohamed E Abazeed, Andriy Marusyk, Eric B Haura, and Jacob G Scott. Collateral sensitivity networks reveal evolutionary instability and novel treatment strategies in alk mutated non-small cell lung cancer. *Scientific reports*, 7(1):1–9, 2017.

[72] Kirill S Korolev, Mikkel Avlund, Oskar Hallatschek, and David R Nelson. Genetic demixing and evolution in linear stepping stone models. *Reviews of modern physics*, 82(2):1691, 2010.

[73] Kirill S Korolev. The fate of cooperation during range expansions. *PLoS Comput Biol*, 9(3):e1002994, 2013.

[74] Kirill S Korolev. Evolution arrests invasions of cooperative populations. *Physical review letters*, 115(20):208104, 2015.

[75] Michael A Brockhurst, Paul B Rainey, and Angus Buckling. The effect of spatial heterogeneity and parasites on the evolution of host diversity. *Proceedings of the Royal Society of London. Series B: Biological Sciences*, 271(1534):107–111, 2004.

[76] Paulo RA Campos, Pedro SCA Neto, Viviane M De Oliveira, and Isabel Gordo. Environmental heterogeneity enhances clonal interference. *Evolution: International Journal of Organic Evolution*, 62(6):1390–1399, 2008.

[77] Hélène Chabas, Sébastien Lion, Antoine Nicot, Sean Meaden, Stineke van Houte, Sylvain Moineau, Lindi M Wahl, Edze R Westra, and Sylvain Gandon. Evolutionary emergence of infectious diseases in heterogeneous host populations. *PLoS biology*, 16(9):e2006738, 2018.

[78] Rutger Hermsen and Terence Hwa. Sources and sinks: a stochastic model of evolution in heterogeneous environments. *Physical review letters*, 105(24):248104, 2010.

[79] Rutger Hermsen, J Barrett Deris, and Terence Hwa. On the rapidity of antibiotic resistance evolution facilitated by a concentration gradient. *Proceedings of the National Academy of Sciences*, 109(27):10775–10780, 2012.

[80] Thomas B Kepler and Alan S Perelson. Drug concentration heterogeneity facilitates the evolution of drug resistance. *Proceedings of the National Academy of Sciences*, 95(20):11514–11519, 1998.

[81] Stefany Moreno-Gamez, Alison L Hill, Daniel IS Rosenbloom, Dmitri A Petrov, Martin A Nowak, and Pleuni S Pennings. Imperfect drug penetration leads to spatial monotherapy and rapid evolution of multidrug resistance. *Proceedings of the National Academy of Sciences*, 112(22):E2874–E2883, 2015.

[82] Feng Fu, Martin A Nowak, and Sebastian Bonhoeffer. Spatial heterogeneity in drug concentrations can facilitate the emergence of resistance to cancer therapy. *PLoS Comput Biol*, 11(3):e1004142, 2015.

[83] Philip Greulich, Bartłomiej Waclaw, and Rosalind J Allen. Mutational pathway determines whether drug gradients accelerate evolution of drug-resistant cells. *Physical review letters*, 109(8):088101, 2012.

[84] Brandon H Schlomann, Travis J Wiles, Elena S Wall, Karen Guillemin, and Raghuveer Parthasarathy. Sublethal antibiotics collapse gut bacterial populations by enhancing aggregation and expulsion. *Proceedings of the National Academy of Sciences*, 116(43):21392–21400, 2019.

[85] Brandon H Schlomann and Raghuveer Parthasarathy. Gut bacterial aggregates as living gels. *Elife*, 10:e71105, 2021.

[86] Katherine Ramos Sarmiento, Alex Carr, Christian Diener, Kenneth J Locey, and Sean M Gibbons. Island biogeography theory and the gut: why taller people tend to harbor more diverse gut microbiomes. *bioRxiv*, 2023.

[87] Brandon G Wong, Christopher P Mancuso, Szilvia Kiriakov, Caleb J Bashor, and Ahmad S Khalil. Precise, automated control of conditions for high-throughput growth of yeast and bacteria with evolver. *Nature biotechnology*, 36(7):614–623, 2018.

[88] Jason Karslake, Jeff Maltas, Peter Brumm, and Kevin B Wood. Population density modulates drug inhibition and gives rise to potential bistability of treatment outcomes for bacterial infections. *PLoS computational biology*, 12(10):e1005098, 2016.

[89] Caroline Colijn and Ted Cohen. How competition governs whether moderate or aggressive treatment minimizes antibiotic resistance. *Elife*, 4:e10559, 2015.

[90] Elsa Hansen, Robert J Woods, and Andrew F Read. How to use a chemotherapeutic agent when resistance to it threatens the patient. *PLoS biology*, 15(2):e2001110, 2017.

[91] Jeffrey West, Fred Adler, Jill Gallaher, Maximilian Strobl, Renee Brady-Nicholls, Joel Brown, Mark Roberson-Tessi, Eunjung Kim, Robert Noble, Yannick Viossat, et al. A survey of open questions in adaptive therapy: Bridging mathematics and clinical translation. *Elife*, 12:e84263, 2023.

[92] Teemu Kuosmanen, Johannes Cairns, Robert Noble, Niko Beerenwinkel, Tommi Mononen, and Ville Mustonen. Drug-induced resistance evolution necessitates less aggressive treatment. *PLoS computational biology*, 17(9):e1009418, 2021.

[93] Clemente I Montero, Frida Stock, and Patrick R Murray. Mechanisms of resistance to daptomycin in enterococcus faecium. *Antimicrobial agents and chemotherapy*, 52(3):1167–1170, 2008.

[94] Joe Pogliano, Nicolas Pogliano, and Jared A Silverman. Daptomycin-mediated reorganization of membrane architecture causes mislocalization of essential cell division proteins. *Journal of bacteriology*, 194(17):4494–4504, 2012.

[95] Truc T Tran, Jose M Munita, and Cesar A Arias. Mechanisms of drug resistance: daptomycin resistance. *Annals of the New York Academy of Sciences*, 1354(1):32–53, 2015.

[96] Scott D Taylor and Michael Palmer. The action mechanism of daptomycin. *Bioorganic & medicinal chemistry*, 24(24):6253–6268, 2016.

[97] Jennifer M Streit, Ronald N Jones, and Helio S Sader. Daptomycin activity and spectrum: a worldwide sample of 6737 clinical gram-positive organisms. *Journal of Antimicrobial Chemotherapy*, 53(4):669–674, 2004.

[98] Judith N Steenbergen, Jeff Alder, Grace M Thorne, and Francis P Tally. Daptomycin: a lipopeptide antibiotic for the treatment of serious gram-positive infections. *Journal of antimicrobial Chemotherapy*, 55(3):283–288, 2005.

[99] Vance G Fowler Jr, Helen W Boucher, G Ralph Corey, Elias Abrutyn, Adolf W Karchmer, Mark E Rupp, Donald P Levine, Henry F Chambers, Francis P Tally, Gloria A Vigliani, et al. Daptomycin versus standard therapy for bacteremia and endocarditis caused by staphylococcus aureus. *New England Journal of Medicine*, 355(7):653–665, 2006.

[100] Juwon Yim, Jordan R Smith, and Michael J Rybak. Role of combination antimicrobial therapy for vancomycin-resistant enterococcus faecium infections: review of the current evidence. *Pharmacotherapy: The Journal of Human Pharmacology and Drug Therapy*, 37(5):579–592, 2017.

[101] Francisco Arnaiz de Las Revillas, Marta Fernandez-Sampedro, Ana María Arnaiz-García, Manuel Gutierrez-Cuadra, Carlos Armiñanzas, Ivana Pulitani, Alejandro Ponton, Valentin Tascon, Ivan García, and María Carmen Fariñas. Daptomycin treatment in gram-positive vascular graft infections. *International Journal of Infectious Diseases*, 68:69–73, 2018.

[102] Jeff Maltas and Kevin B Wood. Pervasive and diverse collateral sensitivity profiles inform optimal strategies to limit antibiotic resistance. *PLoS biology*, 17(10):e3000515, 2019.

[103] Jeff Maltas, Anh Huynh, and Kevin B Wood. Dynamic collateral sensitivity profiles highlight challenges and opportunities for optimizing antibiotic sequences. *bioRxiv*, 2021.

[104] William R Miller, Truc T Tran, Lorena Diaz, Rafael Rios, Ayesha Khan, Jinnethe Reyes, Amy G Prater, Diana Panesso, Yousif Shamoo, and Cesar A Arias. Liar-independent pathways to daptomycin resistance in enterococcus faecalis reveal a multilayer defense against cell envelope antibiotics. *Molecular microbiology*, 111(3):811–824, 2019.

[105] Michael Baym, Laura K Stone, and Roy Kishony. Multidrug evolutionary strategies to reverse antibiotic resistance. *Science*, 351(6268):aad3292, 2016.

[106] Lejla Imamovic and Morten OA Sommer. Use of collateral sensitivity networks to design drug cycling protocols that avoid resistance development. *Science translational medicine*, 5(204):204ra132–204ra132, 2013.

[107] Daniel Nichol, Joseph Rutter, Christopher Bryant, Andrea M Hujer, Sai Lek, Mark D Adams, Peter Jeavons, Alexander RA Anderson, Robert A Bonomo, and Jacob G Scott. Antibiotic collateral sensitivity is contingent on the repeatability of evolution. *Nature communications*, 10(1):334, 2019.

[108] Csaba Pál, Balázs Papp, and Viktória Lázár. Collateral sensitivity of antibiotic-resistant microbes. *Trends in microbiology*, 23(7):401–407, 2015.

[109] Tristan O'Driscoll and Christopher W Crank. Vancomycin-resistant enterococcal infections: epidemiology, clinical manifestations, and optimal management. *Infection and drug resistance*, 8:217, 2015.

[110] L Silvia Munoz-Price, Karen Lolans, and John P Quinn. Emergence of resistance to daptomycin during treatment of vancomycin-resistant enterococcus faecalis infection. *Clinical infectious diseases*, 41(4):565–566, 2005.

[111] Eleni P Balli, Chris A Venetis, and Spiros Miyakis. Systematic review and meta-analysis of linezolid versus daptomycin for treatment of vancomycin-resistant enterococcal bacteremia. *Antimicrobial agents and chemotherapy*, 58(2):734–739, 2014.

[112] Cressida Auckland, Louise Teare, Fiona Cooke, Mary E Kaufmann, Marina Warner, Graeme Jones, Kathy Bamford, Helen Ayles, and Alan P Johnson. Linezolid-resistant enterococci: report of the first isolates in the united kingdom. *Journal of Antimicrobial Chemotherapy*, 50(5):743–746, 2002.

[113] Theodoros Kelesidis, Romney Humphries, Daniel Z Uslan, and David A Pegues. Daptomycin nonsusceptible enterococci: an emerging challenge for clinicians. *Clinical Infectious Diseases*, 52(2):228–234, 2011.

[114] Dijun Du, Xuan Wang-Kan, Arthur Neuberger, Hendrik W van Veen, Klaas M Pos, Laura JV Piddock, and Ben F Luisi. Multidrug efflux pumps: structure, function and regulation. *Nature Reviews Microbiology*, 16(9):523–539, 2018.

[115] Brandie M Jonas, Barbara E Murray, and George M Weinstock. Characterization of emea, anora homolog and multidrug resistance efflux pump, in enterococcus faecalis. *Antimicrobial Agents and Chemotherapy*, 45(12):3574–3579, 2001.

[116] Eun-Woo Lee, M Nazmul Huda, Teruo Kuroda, Tohru Mizushima, and Tomofusa Tsuchiya. Efrab, an abc multidrug efflux pump in enterococcus faecalis. *Antimicrobial agents and chemotherapy*, 47(12):3733–3738, 2003.

[117] Valérie Duval and Ida M Lister. Mara, soxs and rob of escherichia coli–global regulators of multidrug resistance, virulence and stress response. *International journal of biotechnology for wellness industries*, 2(3):101, 2013.

[118] Mahadeo Sukhai and Micheline Piquette-Miller. Regulation of the multidrug resistance genes by stress signals. *J Pharm Pharm Sci*, 3(2):268–280, 2000.

[119] Kyle J Card, Thomas LaBar, Jasper B Gomez, and Richard E Lenski. Historical contingency in the evolution of antibiotic resistance after decades of relaxed selection. *PLoS biology*, 17(10):e3000397, 2019.

[120] Noémie Harmand, Romain Gallet, Roula Jabbour-Zahab, Guillaume Martin, and Thomas Lenormand. Fisher's geometrical model and the mutational patterns of antibiotic resistance across dose gradients. *Evolution*, 71(1):23–37, 2017.

[121] Yoann Anciaux, Luis-Miguel Chevin, Ophélie Ronce, and Guillaume Martin. Evolutionary rescue over a fitness landscape. *Genetics*, 209(1):265–279, 2018.

[122] Olga Lomovskaya, Mark S Warren, Angela Lee, Jorge Galazzo, Richard Fronko, MAY Lee, Johanne Blais, Deidre Cho, Suzanne Chamberland, TOM Renau, et al. Identification and characterization of inhibitors of multidrug resistance efflux pumps in pseudomonas aeruginosa: novel agents for combination therapy. *Antimicrobial agents and chemotherapy*, 45(1):105–116, 2001.

[123] Hiroshi Nikaido. Preventing drug access to targets: cell surface permeability barriers and active efflux in bacteria. In *Seminars in cell & developmental biology*, volume 12, pages 215–223. Elsevier, 2001.

[124] Hiroshi Nikaido and Yumiko Takatsuka. Mechanisms of rnd multidrug efflux pumps. *Biochimica et Biophysica Acta (BBA)-Proteins and Proteomics*, 1794(5):769–781, 2009.

[125] Katherine S Long and Birte Vester. Resistance to linezolid caused by modifications at its binding site on the ribosome. *Antimicrobial agents and chemotherapy*, 56(2):603–612, 2012.

[126] Shenshen Wang and Lei Dai. Evolving generalists in switching rugged landscapes. *PLoS computational biology*, 15(10):e1007320, 2019.

[127] Vedant Sachdeva, Kabir Husain, Jiming Sheng, Shenshen Wang, and Arvind Murugan. Tuning environmental timescales to evolve and maintain generalists. *Proceedings of the National Academy of Sciences*, 117(23):12693–12699, 2020.

[128] Yeping Ma and Song Lin Chua. No collateral antibiotic sensitivity by alternating antibiotic pairs. *The Lancet Microbe*, 3(1):e7, 2022.

[129] Alfonso Santos-Lopez, Christopher W Marshall, Michelle R Scribner, Daniel J Snyder, and Vaughn S Cooper. Evolutionary pathways to antibiotic resistance are dependent upon environmental structure and bacterial lifestyle. *Elife*, 8, 2019.

[130] Erdal Toprak, Adrian Veres, Jean-Baptiste Michel, Remy Chait, Daniel L Hartl, and Roy Kishony. Evolutionary paths to antibiotic resistance under dynamically sustained drug selection. *Nature genetics*, 44(1):101–105, 2012.

[131] Daniel F Sahm, Jessica Kissinger, Michael S Gilmore, Patrick R Murray, Ross Mulder, Joanne Solliday, and Barbara Clarke. In vitro susceptibility studies of vancomycin-resistant enterococcus faecalis. *Antimicrobial agents and chemotherapy*, 33(9):1588–1591, 1989.

[132] Mini Kamboj, Nina Cohen, Kathleen Gilhuley, N Esther Babady, Susan K Seo, and Kent A Sepkowitz. Emergence of daptomycin-resistant vre: experience of a single institution. *Infection Control & Hospital Epidemiology*, 32(4):391–394, 2011.

[133] Theodoros Kelesidis, Angela LP Chow, Romney Humphries, Daniel Z Uslan, and David Pegues. Case-control study comparing de novo and daptomycin-exposed daptomycin-nonsusceptible enterococcus infections. *Antimicrobial agents and chemotherapy*, 56(4):2150–2152, 2012.

[134] Romney M Humphries, Simon Pollett, and George Sakoulas. A current perspective on daptomycin for the clinical microbiologist. *Clinical microbiology reviews*, 26(4):759–780, 2013.

[135] William R Miller, Arnold S Bayer, and Cesar A Arias. Mechanism of action and resistance to daptomycin in staphylococcus aureus and enterococci. *Cold Spring Harbor perspectives in medicine*, 6(11):a026997, 2016.

[136] Clare L Kinnear, Twisha S Patel, Carol L Young, Vincent Marshall, Duane W Newton, Andrew F Read, and Robert J Woods. Impact of an antimicrobial stewardship intervention on within-and between-patient daptomycin resistance evolution in vancomycin-resistant enterococcus faecium. *Antimicrobial agents and chemotherapy*, 63(4):e01800–18, 2019.

[137] Clare L Kinnear, Elsa Hansen, Valerie J Morley, Kevin C Tracy, Meghan Forstchen, Andrew F Read, and Robert J Woods. Daptomycin treatment impacts resistance in off-target populations of vancomycin-resistant enterococcus faecium. *PLoS biology*, 18(12):e3000987, 2020.

[138] Cesar A Arias, Diana Panesso, Danielle M McGrath, Xiang Qin, Maria F Mojica, Corwin Miller, Lorena Diaz, Truc T Tran, Sandra Rincon, E Magda Barbu, et al. Genetic basis for in vivo daptomycin resistance in enterococci. *New England Journal of Medicine*, 365(10):892–900, 2011.

[139] Lorena Diaz, Truc T Tran, Jose M Munita, William R Miller, Sandra Rincon, Lina P Carvajal, Aye Wollam, Jinnethe Reyes, Diana Panesso, Natalia L Rojas, et al. Whole-genome analyses of enterococcus faecium isolates with diverse daptomycin mics. *Antimicrobial agents and chemotherapy*, 58(8):4527–4534, 2014.

[140] Truc T Tran, Diana Panesso, Nagendra N Mishra, Eugenia Mileykovskaya, Ziqianq Guan, Jose M Munita, Jinnethe Reyes, Lorena Diaz, George M Weinstock, Barbara E Murray, et al. Daptomycin-resistant enterococcus faecalis diverts the antibiotic molecule from the division septum and remodels cell membrane phospholipids. *MBio*, 4(4):e00281–13, 2013.

[141] Sandra Rincon, Diana Panesso, William R Miller, Kavindra V Singh, Melissa R Cruz, Ayesha Khan, An Q Dinh, Lorena Diaz, Rafael Rios, Yousif Shamoo, et al. Disrupting membrane adaptation restores in vivo efficacy of antibiotics against multidrug-resistant enterococci and potentiates killing by human neutrophils. *The Journal of Infectious Diseases*, 220(3):494–504, 2019.

[142] Ayesha Khan, Milya Davlieva, Diana Panesso, Sandra Rincon, William R Miller, Lorena Diaz, Jinnethe Reyes, Melissa R Cruz, Orville Pemberton, April H Nguyen, et al. Antimicrobial sensing coupled with cell membrane remodeling mediates antibiotic resistance and virulence in enterococcus faecalis. *Proceedings of the National Academy of Sciences*, 116(52):26925–26932, 2019.

[143] Yusuke Ota, Kazuki Furuhashi, Wataru Hayashi, Nachi Hirai, Jinko Ishikawa, Osanori Nagura, Katsumasa Yamanaka, Kazuto Katahashi, Kotaro Aoki, Noriyuki Nagano, et al. Daptomycin resistant enterococcus faecalis has a mutation in liax, which encodes a surface

protein that inhibits the liafsr systems and cell membrane remodeling. *Journal of Infection and Chemotherapy*, 27(1):90–93, 2021.

[144] Jinnethe Reyes, Diana Panesso, Truc T Tran, Nagendra N Mishra, Melissa R Cruz, Jose M Munita, Kavindra V Singh, Michael R Yeaman, Barbara E Murray, Yousif Shamoo, et al. A liar deletion restores susceptibility to daptomycin and antimicrobial peptides in multidrug-resistant enterococcus faecalis. *The Journal of infectious diseases*, 211(8):1317–1325, 2015.

[145] Krzysztof Sieradzki and Alexander Tomasz. Gradual alterations in cell wall structure and metabolism in vancomycin-resistant mutants of staphylococcus aureus. *Journal of Bacteriology*, 181(24):7566–7570, 1999.

[146] K Sieradzki, T Leski, J Dick, L Borio, and A Tomasz. Evolution of a vancomycin-intermediate staphylococcus aureus strain in vivo: multiple changes in the antibiotic resistance phenotypes of a single lineage of methicillin-resistant s. aureus under the impact of antibiotics administered for chemotherapy. *Journal of clinical microbiology*, 41(4):1687–1693, 2003.

[147] Soo-Jin Yang, Yan Q Xiong, Susan Boyle-Vavra, Robert Daum, Tiffanny Jones, and Arnold S Bayer. Daptomycin-oxacillin combinations in treatment of experimental endocarditis caused by daptomycin-nonsusceptible strains of methicillin-resistant staphylococcus aureus with evolving oxacillin susceptibility (the "seesaw effect"). *Antimicrobial agents and chemotherapy*, 54(8):3161–3169, 2010.

[148] Adriana Renzoni, William L Kelley, Roberto R Rosato, Maria P Martinez, Melanie Roch, Maryam Fatouraei, Daniel P Haeusser, William Margolin, Samuel Fenn, Robert D Turner, et al. Molecular bases determining daptomycin resistance-mediated resensitization to β-lactams (seesaw effect) in methicillin-resistant staphylococcus aureus. *Antimicrobial agents and chemotherapy*, 61(1):e01634–16, 2017.

[149] Katie E Barber, Cortney E Ireland, Natalia Bukavyn, and Michael J Rybak. Observation of "seesaw effect" with vancomycin, teicoplanin, daptomycin and ceftaroline in 150 unique mrsa strains. *Infectious Diseases and Therapy*, 3:35–43, 2014.

[150] George Sakoulas, Poochit Nonejuie, Victor Nizet, Joseph Pogliano, Nancy Crum-Cianflone, and Fadi Haddad. Treatment of high-level gentamicin-resistant enterococcus faecalis endocarditis with daptomycin plus ceftaroline. *Antimicrobial agents and chemotherapy*, 57(8):4042–4045, 2013.

[151] Seyedehameneh Jahanbakhsh, Nivedita B Singh, Juwon Yim, Razieh Kebriaei, Jordan R Smith, Katherine Lev, Truc T Tran, Warren E Rose, Cesar A Arias, and Michael J Rybak. Impact of daptomycin dose exposure alone or in combination with β-lactams or rifampin against vancomycin-resistant enterococci in an in vitro biofilm model. *Antimicrobial Agents and Chemotherapy*, 64(5):e02074–19, 2020.

[152] Ayesha Khan. Molecular mechanisms of antimicrobial resistance in multi-drug resistant enterococci. 2020.

[153] Ayesha Khan, April Nguyen, Diana Panesso, Heidi Vitrac, William R Miller, Truc T Tran, Yousif Shamoo, Michel Arthur, and Cesar A Arias. 903. resensitization to β-lactams in enterococci depends on penicillin-binding protein (pbp) mislocalization and is mediated by a single protein that modulates cell membrane (cm) adaptation to daptomycin (dap). In *Open Forum Infectious Diseases*, volume 6, pages S28–S29. Oxford University Press US, 2019.

[154] Truc T Tran, Nagendra N Mishra, Ravin Seepersaud, Lorena Diaz, Rafael Rios, An Q Dinh, Cristina Garcia-de-la Maria, Michael J Rybak, Jose M Miro, Samuel A Shelburne, et al. Mutations in cdsa and pgsa correlate with daptomycin resistance in streptococcus mitis and s. oralis. *Antimicrobial agents and chemotherapy*, 63(2):10–1128, 2019.

[155] Joshua M Kirsch, Shannon Ely, Madison E Stellfox, Karthik Hullahalli, Phat Luong, Kelli L Palmer, Daria Van Tyne, and Breck A Duerkop. Targeted is-element sequencing uncovers transposition dynamics during selective pressure in enterococci. *PLoS pathogens*, 19(6):e1011424, 2023.

[156] Weiliang Zeng, Luozhu Feng, Changrui Qian, Tao Chen, Sipei Wang, Ying Zhang, Xiangkuo Zheng, Lingbo Wang, Shixing Liu, Tieli Zhou, et al. Acquisition of daptomycin resistance by enterococcus faecium confers collateral sensitivity to glycopeptides. *Frontiers in Microbiology*, 13:815600, 2022.

[157] MH Zwietering, Il Jongenburger, FM Rombouts, and K Van't Riet. Modeling of the bacterial growth curve. *Appl. Environ. Microbiol.*, 56(6):1875–1881, 1990.

[158] Daniel E Deatherage and Jeffrey E Barrick. Identification of mutations in laboratory-evolved microbes from next-generation sequencing data using breseq. *Engineering and analyzing multicellular systems: methods and protocols*, pages 165–188, 2014.

[159] Jeffrey E Barrick, Geoffrey Colburn, Daniel E Deatherage, Charles C Traverse, Matthew D Strand, Jordan J Borges, David B Knoester, Aaron Reba, and Austin G Meyer. Identifying structural variation in haploid microbial genomes from short-read resequencing data using breseq. *BMC genomics*, 15:1–17, 2014.

[160] David Deamer, Mark Akeson, and Daniel Branton. Three decades of nanopore sequencing. *Nature biotechnology*, 34(5):518–524, 2016.

[161] Ad C Fluit, Maarten R Visser, and Franz-Josef Schmitz. Molecular detection of antimicrobial resistance. *Clinical microbiology reviews*, 14(4):836–871, 2001.

[162] DB Longley and PG Johnston. Molecular mechanisms of drug resistance. *The Journal of Pathology: A Journal of the Pathological Society of Great Britain and Ireland*, 205(2):275–292, 2005.

[163] Josephine Bryant, Claire Chewapreecha, and Stephen D Bentley. Developing insights into the mechanisms of evolution of bacterial pathogens from whole-genome sequences. *Future microbiology*, 7(11):1283–1296, 2012.

[164] Chrispin Chaguza, Jennifer E Cornick, and Dean B Everett. Mechanisms and impact of genetic recombination in the evolution of streptococcus pneumoniae. *Computational and structural biotechnology journal*, 13:241–247, 2015.

[165] Paul G Lane, Anton Hutter, Stephen G Oliver, and Philip R Butler. Selection of microbial mutants tolerant to extreme environmental stress using continuous culture- control design. *Biotechnology progress*, 15(6):1115–1124, 1999.

[166] Tadeusz J Kawecki, Richard E Lenski, Dieter Ebert, Brian Hollis, Isabelle Olivieri, and Michael C Whitlock. Experimental evolution. *Trends in ecology & evolution*, 27(10):547–560, 2012.

[167] Diarmaid Hughes and Dan I Andersson. Evolutionary trajectories to antibiotic resistance. *Annual Review of Microbiology*, 71:579–596, 2017.

[168] Ilkka Hanski. Metapopulation dynamics. *Nature*, 396(6706):41–49, 1998.

[169] Loring J Thomas, Peng Huang, Fan Yin, Xiaoshuang Iris Luo, Zack W Almquist, John R Hipp, and Carter T Butts. Spatial heterogeneity can lead to substantial local variations in covid-19 timing and severity. *Proceedings of the National Academy of Sciences*, 117(39):24180–24187, 2020.

[170] JF Silva, MR Fariñas, JM Felfili, and CA Klink. Spatial heterogeneity, land use and conservation in the cerrado region of brazil. *Journal of biogeography*, 33(3):536–548, 2006.

[171] Benjamin Allen, Gabor Lippner, Yu-Ting Chen, Babak Fotouhi, Naghmeh Momeni, Shing-Tung Yau, and Martin A Nowak. Evolutionary dynamics on any population structure. *Nature*, 544(7649):227–230, 2017.

[172] George WA Constable and Alan J McKane. Fast-mode elimination in stochastic metapopulation models. *Physical Review E*, 89(3):032141, 2014.

[173] Erez Lieberman, Christoph Hauert, and Martin A Nowak. Evolutionary dynamics on graphs. *Nature*, 433(7023):312–316, 2005.

[174] Jesse Kreger, Donovan Brown, Natalia L Komarova, Dominik Wodarz, and Justin Pritchard. The role of migration in mutant dynamics in fragmented populations. *Journal of Evolutionary Biology*, 36(2):444–460, 2023.

[175] Partha Pratim Chakraborty, Louis R Nemzer, and Rees Kassen. Experimental evidence that metapopulation structure can accelerate adaptive evolution. *bioRxiv*, 2021.

[176] Gerald W Tannock and Greg Cook. Enterococci as members of the intestinal microflora of humans. *The enterococci: pathogenesis, molecular biology, and antibiotic resistance*, pages 101–132, 2002.

[177] Philip Greulich, Matthew Scott, Martin R Evans, and Rosalind J Allen. Growth-dependent bacterial susceptibility to ribosome-targeting antibiotics. *Molecular systems biology*, 11(3):796, 2015.

[178] Philip Greulich, Jakub Doležal, Matthew Scott, Martin R Evans, and Rosalind J Allen. Predicting the dynamics of bacterial growth inhibition by ribosome-targeting antibiotics. *Physical biology*, 14(6):065005, 2017.

[179] Kelsey M Hallinen, Jason Karslake, and Kevin B Wood. Delayed antibiotic exposure induces population collapse in enterococcal communities with drug-resistant subpopulations. *Elife*, 9:e52813, 2020.

[180] Mohsen Heidary, Azar Dohkt Khosravi, Saeed Khoshnood, Mohammad Javad Nasiri, Saleh Soleimani, and Mehdi Goudarzi. Daptomycin. *Journal of Antimicrobial Chemotherapy*, 73(1):1–11, 2018.

[181] Nicole Cotroneo, Robert Harris, Nancy Perlmutter, Terry Beveridge, and Jared A Silverman. Daptomycin exerts bactericidal activity without lysis of staphylococcus aureus. *Antimicrobial Agents and Chemotherapy*, 52(6):2223–2225, 2008.

[182] Fernando Baquero, Maria-Cristina Negri, Maria-Isabel Morosini, and Jesús Blázquez. Antibiotic-selective environments. *Clinical infectious diseases*, 27(Supplement_1):S5–S11, 1998.

[183] Gary E Stein. Antimicrobial resistance in the hospital setting: impact, trends, and infection control measures. *Pharmacotherapy: The Journal of Human Pharmacology and Drug Therapy*, 25(10P2):44S–54S, 2005.

[184] Thilo Köhler, Mehri Michea-Hamzehpour, Patrick Plesiat, Anne-Lise Kahr, and Jean-Claude Pechere. Differential selection of multidrug efflux systems by quinolones in pseudomonas aeruginosa. *Antimicrobial agents and chemotherapy*, 41(11):2540–2543, 1997.

[185] Salvador E Luria and Max Delbrück. Mutations of bacteria from virus sensitivity to virus resistance. *Genetics*, 28(6):491, 1943.